Evaluating Agricultural Management Practices Benefiting the Monterey Bay: Reducing Nutrient Loads and Harmful Algal Bloom (HAB) Events

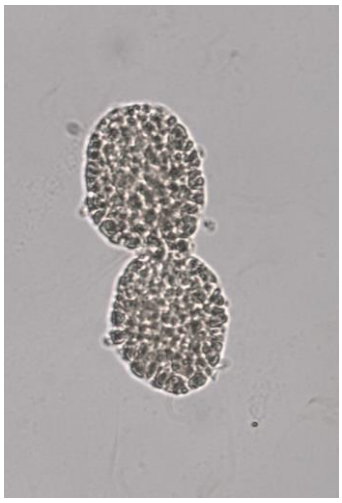

August 2025

Prepared for the Environmental Protection Agency
EPA Agreement Number: 84008301

Funded By:

Environmental Protection Agency

Suggested Citation:

Clark, R., Bowers, H., Berg, M., Fulkerson, B., Turner, J., Cunningham, S. 2025. Evaluating agricultural management practices benefiting the Monterey Bay: reducing nutrient loads and Harmful Algal Bloom (HAB) events. A report prepared for the Environmental Protection Agency for EPA Agreement #84008301.

SJSU SAN JOSÉ STATE UNIVERSITY

This report is dedicated to Ross P. Clark IV, our esteemed colleague, co-PI, and Director of the Central Coast Wetlands Group, whose leadership and vision shaped this project from the start. His unexpected passing during the course of this work is deeply felt, and we honor his lasting contributions to our research and community. We miss him deeply and carry forward his work with gratitude and respect.

EXECUTIVE SUMMARY

Objective of Research

Monterey Bay, California experiences high loadings of agriculturally derived nutrients and related seasonal links with harmful algal bloom (HAB) events that pose risks to marine life. Given the impacts on one of the world's most diverse marine ecosystems, our project had three overarching goals: 1) to gauge the efficacy of several different types of wetland treatment systems in removal of nitrogen-based nutrients from agricultural drainages, 2) to quantify loading of nitrogen from the agriculturally dominated watersheds and subwatersheds within Monterey Bay, and 3) to investigate the linkage between agriculturally derived nitrogen and HAB species responses.

California's Central Coast Irrigated Lands Regulatory Program (Ag Order) has been in place and updated for almost 20 years, yet biostimulatory response to nutrient loading within coastal receiving waters continues. Management practice adoption has led to significant changes in irrigation and nutrient application practices, leading to changes in flow and nutrient loading that are not fully understood or accounted for in regional monitoring programs and downstream treatment system design and operations. Our proposal investigated how watershed scale adoption of existing designs of agricultural management practices (already documented to reduce nitrate loading) could lead to reductions in offshore HAB events. The approach included complementary studies by team members focused on management practice effectiveness and HAB species response.

Summary of Findings

Below is a summary of our study findings, organized by research area. Each research area aligns with one of the three project goals and addresses the questions posed in the original proposal.

RESEARCH AREA 1: TREATMENT WETLAND EFFICACY	
Goal: Demonstrate the efficiency of different types of wetland treatment systems in reducing nitrogenous nutrients originating with agricultural run-off	
Research Question	**Results**
1a: How do various treatment systems (treatment wetlands, bioreactors, plants) affect concentrations of specific nitrogen substrates?	Eight treatment systems, including four wetlands and four bioreactors, were tested for their efficiency in removing nitrogen from nutrient-rich agricultural influent. Based on changes in concentrations of NO_3 between the inlet and outlet of the treatment systems, efficiencies of removal varied from 20-90% with an average removal efficiency of 68%.
	In experiments to test nitrogen removal efficiencies of specific treatment habitats (vegetated/unvegetated, shallow/deep, wetland/drainage channel) we found that the most efficient habitat with respect to nitrogen loss was a drainage channel. We also found that the addition of vegetation did not increase nitrogen loss from any of the tested habitats suggesting that sediment-associated microbial activity was primarily responsible for nitrogen loss from wetland habitats.
	Nitrate was the primary substrate in the agricultural effluents tested here, comprising 81-99% of the total dissolved nitrogen pool. Using agricultural effluent collected from the Castroville Slough added to a variety of wetland habitats, lower efficiencies of removal were observed for NH_4 and urea compared with NO_3. While NO_3 was removed with 41-77% efficiency, NH_4 was removed with 6-62% efficiency, and urea was removed with 20-57% efficiency by the various wetland treatment habitats.

RESEARCH AREA 2: WATERSHED NITROGEN LOADING	
Goal: Quantify loading of nitrogen from agriculturally dominated watersheds and sub-watersheds within the Monterey Bay region	
Research Questions	**Results**
1b: What are the relative contributions of groundwater, surface flows, and agricultural tile drains to nutrients entering Monterey Bay and how do contributions change with season and agricultural practices?	Data collected from the subwatershed-scale stations in the Pajaro River and Salinas River/Gabilan watershed demonstrated large variability in NO_3 loads with season and by year. Examining the variation in NO_3 concentrations and flow demonstrated that changes in flow rates contributed the most to the variability in loading estimates.
2a: Do watershed loading estimates from available models based solely on nitrate accurately represent total nitrogen load that may affect occurrence of HABs within receiving waters?	NO_3 was the primary source of nitrogen in all the sources of agricultural effluent tested here, comprising 81-99% of the total dissolved nitrogen pool. Only one source of effluent, collected from the Castroville Slough, contained measurable concentrations of NH_4 and urea, comprising close to 20% of the total nitrogen pool. For the other effluent sources, NO_3 comprised 94-99% of the total dissolved nitrogen pool suggesting that it is a safe assumption to base watershed loading calculations on NO_3 only.
2b: What are the total nitrate loads originating from the two primary agricultural watersheds into Monterey Bay?	Total NO_3 loads originating from the Pajaro River watershed, as estimated from station PR4 at Chittenden, varied from 770 kg d^{-1} in fall 2022, which was an average flow year, to 5700 kg d^{-1} in the fall of 2023 which was a high flow year. In comparison, loads of NO_3 from Tembladero Slough, a subset of the Salinas watershed, averaged 600-800 kg d^{-1} in the fall. Because flows were on average greater and more variable from the Pajaro River with year in the spring compared with Tembladero Slough, our estimates show that when averaging spring and fall loads, NO_3 loads from the Pajaro River were 4-fold higher in a low flow year and over 30-fold higher in high flow year compared with loads from Tembladero Slough.
4a: What is the scale of nutrient removal or treatment needed to reduce nearshore nutrient inputs to Monterey Bay?	We focused our investigation on the scale of nutrient treatment in the Gabilan watershed and on the Tembladero Slough for two main reasons. One, the flows in this region are primarily regulated by farm irrigation and pumping making the flows predictable and easy to “catch” for treatment purposes. Also, loads are concentrated which is beneficial for treatment purposes. By examining incoming loads along Tembladero Slough we identified the bottom 5.4 km region (between station SR1 and SR6) as the section receiving the most nitrogen discharge and therefore contributing disproportionately to the NO_3 load from the Slough and from the region. We then calculated that the acreage of treatment wetland needed to reduce the loads in this region would be on the order of 50-230 acres. This scale of reduction would make a large impact, on a similar order of reducing Pajaro River loads from the fall season in a low-flow year.
4b: How can we best integrate sub-watershed treatment systems within a watershed cooperative approach?	As demonstrated here for the Tembladero Slough region and Gabilan watershed, characterizing and pinpointing regions with greater loads can be very effective for the application of treatment wetlands and for reducing loads from the entire watershed. Therefore, receiving cooperation from farmers in a limited area can benefit whole-watershed nutrient load reductions. CCWG has drafted watershed plans for treating surface water in several subwatersheds in the Salinas Valley and is currently working with other industry partners and farmers to create a cooperative program that benefits multiple landowners.

RESEARCH AREA 3: LINKING HAB SPECIES RESPONSE TO AGRICULTURALLY DERIVED NITROGEN	
Goal: Investigate the linkage between agriculturally derived nitrogenous nutrients and HAB responses	
Research Question	**Results**
3a: How is the growth of different phytoplankton species affected by the different nitrogenous nutrients in agricultural run-off?	Our laboratory mesocosm experiments demonstrated that both treated and untreated agricultural effluent promoted growth of two toxin-producing HAB species, one diatom (*Pseudo-nitzschia*) and one dinoflagellate (*Alexandrium*). Both types of agricultural effluent promoted growth equally well compared with growth in a control containing pristine river water amended with nutrients. Growth was not impacted by the availability of different types of nitrogen as both species primarily utilized NO_3 during the exponential growth phase. The diatom grew 3-fold faster than the dinoflagellate due to intrinsic factors including a higher photosystem II photochemical efficiency. Production of domoic acid toxin by the diatom was triggered by nutrient limitation and increased with increasing limitation.
3b: What nitrogen sources in agricultural run-off promotes the growth of HAB phytoplankton species known to bloom in Monterey Bay?	Nitrate was the primary source of nitrogen for growth of both HAB species tested here. The diatom primarily utilized NO_3, and also NH_4 before it was depleted, during the exponential growth phase. The dinoflagellate used NO_3, and also NH_4 before it was depleted, during the exponential growth phase and did not utilize urea or NO_2 until after it became nitrogen-limited. Most experiments that demonstrate utilization of urea by HAB species supply urea as the sole source of nitrogen in culture. Here we demonstrated for two HAB species that when supplied several sources of nitrogen simultaneously, as found in agricultural effluent, urea was only utilized after cells go into nitrogen limitation and is not a preferred source of nitrogen.
3c: How is HAB response associated with nearshore nutrient input (2b: How does the loading, nitrogen constituent forms, and timing of discharges relate to offshore nutrient patterns and HAB occurrences?)	Monthly transect sampling in the nearshore region south and north of the Pajaro River discharge compared with the offshore region demonstrated that riverine nutrient inputs likely did not influence phytoplankton biomass accumulation and blooms in spring or summer. The primary source of nitrogen fueling both non-HAB and HAB responses in the nearshore region during this time was NO_3. Urea was a minor source of nitrogen in the nearshore, comprising 4% or less of the available nitrogen pool. During the fall season, the pattern of phytoplankton biomass accumulation changed and a bloom of the dinoflagellate HAB former *Cochlodinium* developed north of the Pajaro River discharge. Biomass of the bloom was up to 14-fold greater in the nearshore compared with the offshore region, and decreased in density south of the Pajaro River mouth. This phytoplankton distribution was consistent with a northerly current flow pattern carrying high-concentrations of nitrogen discharged from the Pajaro River sustaining the bloom. The primary source of nitrogen fueling the bloom was NO_3. Despite depletion of NO_3 by the end of the bloom, urea concentrations did not change (i.e. decrease) suggesting *Cochlodinium* did not utilize urea.

TABLE OF CONTENTS

Executive Summary iii
Table of Contents vi
List of Acronyms vii
Introduction 1
Regional Context 1
Agricultural Industry Standard 2
Research Area 1: Treatment System Efficacy 4
Existing Treatment Systems 5
Nitrogen Loss Experiments and Nitrogen Loss Efficiencies 10
Research Area 2: Watershed Nitrogen Loading 21
Subwatershed Drainages 21
OSMO Experiments 23
Long Term Monitoring Stations 31
High Resolution Loading Model 34
Tembladero Slough Nitrogen Loads and Wetlands Required to Treat Loads 42
Research Area 3: Linking HAB Species Response to Agriculturally Derived Nitrogen 45
Introduction 45
Laboratory Experiments 46
Offshore Transects 57
Synthesis 64
References 67
Presentations and Publications 71
Appendix A: Treatment System Efficiency A-1
Appendix B: Nitrogen Loss Experiment B-1
Appendix C: OSMO Experiment Results C-1
Appendix D: Monitoring Stations D-1

LIST OF ACRONYMS

ADP	Acoustic Doppler Profiler
ANOVA	Analysis of Variance
CCR	Coastal Conservation and Research
CCWG	Central Coast Wetlands Group
CCWQP	Central Coast Water Quality Preservation Inc.
CMP	Cooperative Monitoring Program
CW	Castroville Wetland
EBL	Environmental Biotechnology Laboratory
FIA	Flow Injection Analysis
HAB	Harmful Algal Blooms
HUC	Hydrologic Unit Code
MLML	Moss Landing Marine Laboratories
MT	Molera Triangle
OSMO	Osmotic Pump Sampler
OSR	Old Salinas River
PR	Pajaro River
PSU	Practical Salinity Unit
R19	Ranch 19
SUNA	Submersible Ultraviolet Nitrate Analyzer
SR	Salinas River
SWAT	Soil and Water Assessment Tool
TMDL	Total Maximum Daily Load
USGS	United States Geological Survey

INTRODUCTION

Regional Context

Monterey Bay, encompassing an area of approximately 1160 km^2 (449 square miles) on the California Central Coast, is part of the Monterey Bay National Marine Sanctuary, the largest national marine sanctuary on the west coast. It is known for its wide variety of habitats, including underwater canyons, rocky shores, and kelp forests that support a large diversity of marine life from plankton to blue whales (Office of National Marine Sanctuaries 2015). The primary nutrient sources to Monterey Bay are upwelling of nutrient rich bottom waters and internal tidal pumping from the Monterey Canyon (Rosenfeld et al. 1994, Shea and Broenkow 1982). These sources of nutrients support a high productivity of phytoplankton, primarily diatoms, during the upwelling season (Garrison 1979). When upwelling relaxes in the fall, water overlying the shallow shelf areas becomes stratified, surface water temperatures increase, and blooms of toxin-producing harmful algal blooms (HABs) may develop (Ryan et al. 2008). These blooms, which typically start in the fall at the beginning of the wet season, can reach concentrations of chlorophyll up to 500 µg L^{-1} and are of a size varying from 5-80 km^2 (Ryan et al. 2005, Ryan et al. 2008).

Fall events of HABs in Monterey Bay that develop during upwelling relaxation are thought to mainly be fueled by surface nutrient inputs from the Pajaro and Salinas Rivers, and the Elkhorn Slough estuary, which together drain large agricultural watersheds in the Monterey Bay region. Approximately 75% of the combined land areas of these watersheds, covering a total area of 14,197 km^2, with the Salinas River watershed being the largest at 10,600 km^2 followed by the Pajaro River watershed at 3394 km^2, are used for crop row farming of vegetables and berries (Los Huertos et al. 2001, Hunt et al. 2019). As a result of application of fertilizer to the farmed fields within the three watersheds, nitrogen run-off into Monterey Bay is substantial. For example, annual nitrogen load at Chittenden in the Pajaro River typically varies between 300-1,400 metric tons of nitrogen (300-1,400 x 10^3 kg) depending on whether it is a drier (low flow) or wetter (high flow) year (Los Huertos et al. 2001).

Intensification of irrigation in crop row fields during late summer and early fall delivers large loads of nitrogen to these rivers and the Slough. Subsequently, rainfall may carry water from these rivers into Monterey Bay where the plumes can fuel HAB events. For example, Kudela et al. (2014) demonstrated an increase in HAB occurrence and domoic acid production in surface water bracketing the mouth of the Pajaro River after a rainfall event compared with before the event. Plumes discharged from the rivers may be carried northward along the coast and concentrate nutrients (and pollutants) in the northern Monterey Bay shelf region. Several studies have found that this shallow shelf region acts as an incubator for potentially toxic HABs comprised of saxitoxin producing dinoflagellates as well as domoic acid producing *Pseudo-nitzschia* species (Ryan et al. 2008, Fischer et al. 2014, Schulien et al. 2017).

From bloom incubator loci, HABs can spread throughout Monterey Bay (Ryan et al. 2008). For example, multiple species of *Alexandrium* are common, and shellfish monitoring by the Dept. of Public Health documents annual elevated saxitoxin levels (Jester et al. 2009). Human health events are uncommon, however toxin bioaccumulation throughout the food web remains a persistent danger to higher trophic levels, from seafood resources to otters and whales (Lefebvre et al. 2002, Jester et al. 2009, Hawkins

2010, Rines et al. 2010). Multiple species of the dinoflagellate *Dinophysis* are commonly found within Monterey Bay and demonstrate a very low threshold for toxic bloom development (10^2 cells L^{-1}; reviewed in Reguera et al., 2012). Blooms of the chain-forming unarmored dinoflagellate *Cochlodinium fulvescens* is considered an emerging threat and toxic events include a 2004 bloom spanning 800 km of coastline that was linked to mass mussel mortalities (Curtiss et al. 2008), and a bloom in 2007 that was linked to loss of commercially farmed abalone (Howard et al. 2012). In addition, Monterey Bay experiences near-annual *Pseudo-nitzschia* blooms leading to extended bans on recreationally harvested mussels and Dungeness crab due to the persistent presence of domoic acid biotoxins. During a warm water event in 2015, toxin levels within Monterey Bay were the highest ever recorded (Bowers et al. 2018). This event resulted in a loss of more than $48 million for the California Dungeness crab fishery and led the state to request a federal fishery disaster declaration from the U.S. Department of Commerce (Federal relief funding did not materialize until 2019).

Given high loading of agriculturally derived nutrients and the seasonal link with HAB event risks to marine life in one of the world's most diverse marine ecosystems, our project had three overarching goals: 1) to gauge the efficacy of several different types of wetland treatment systems in removal of nitrogen-based nutrients from agricultural drainages, 2) to quantify loading of nitrogen from the agriculturally dominated watersheds and subwatersheds within Monterey Bay, and 3) to investigate the linkage between agriculturally derived nitrogen and HAB species responses. Each of these goals were associated with specific research questions, the answers to which would aid regional adoption of coordinated water management strategies under the most recent Central Coast Regional Water Quality Control Board (Regional Water Board) Irrigated Lands Waste Discharge Order. Our research aimed to lay the groundwork for providing design guidelines to aid selection of appropriate practices and treatment systems (wetlands and bioreactors) for site-specific nitrogen reductions, and to aid in the documentation of reductions in nitrogen loading at a resolution of subwatersheds as well as individual farms.

Agricultural Industry Standard

The current agriculture industry standard for monitoring water quality is carried out by Central Coast Water Quality Preservation Inc. (CCWQP) as part of the Cooperative Monitoring Program (CMP). This program was developed in 2004 when the Regional Water Board adopted a conditional waiver of waste discharge requirements for discharges from irrigated lands within the Central Coast Region. Due to the region's large size, growers formed a non-profit organization, CCWQP, to implement the CMP to perform surface water monitoring and reporting. The most recent update that the waiver and CMP have undergone is the General Waste Discharge Requirements for Discharges from Irrigated Lands, Order No. R3-2021-0040 (Ag Order 4.0), implemented in 2021.

The Regional Water Board has compiled substantial empirical data demonstrating that water quality conditions in agricultural areas of the region continue to be severely impaired or polluted by irrigated agricultural discharges. The main impacts from agricultural runoff include nitrate discharges to groundwater and associated drinking water impacts, nutrient discharges to surface water, pesticide discharges and associated toxicity, sediment discharges, and degradation of riparian and wetland areas and the associated impairment or loss of beneficial uses such as drinking water source or recreation (Ag

Order 4.0, 2021). The main objectives of this Order are to protect riparian and wetland habitats and decrease the nutrient, toxicity, and sediment discharges to surface and groundwater supplies. This requires that owners and operators of irrigated lands comply with the terms and conditions set forth in the Order not to exceed the total maximum daily load (TMDL) allowed for various nutrients by a specified date. Failure to comply may result in notices, financial penalties, increased inspections, or even legal action.

In order to track water quality improvements being made by owners and operators, monthly grab samples are taken as part of the CMP at specified locations throughout Central Coast subwatersheds. These grab samples are analyzed for nutrient concentrations, other water quality measurements, water discharge (i.e. flow), and toxicity measurements. These parameters and frequencies of measurements have constituted the industry standard since 2004. With respect to calculation of nutrient loads (i.e. concentration of nutrient multiplied by discharge of water in a waterway) these measurement frequencies have been statistically demonstrated to be adequate for the monitoring of water quality. However, with large reductions in nutrient concentrations and loads required in a short time frame by the Order, the question remains whether past measurement frequencies are adequate to track changes in nutrient loads in a highly modified landscape where flow is dominated by agricultural pumping and other infrastructure. As part of research area two, our goal was to quantify loading of nitrogen from subwatersheds within the agriculturally dominated Pajaro, Elkhorn Slough, and Salinas watersheds. To accomplish this goal, we sampled in close proximity to CMP sampling sites at relatively high resolution to determine any differences, if present, in the capture of changes in nutrient loading in the agriculturally influenced waterways and drainages.

In the sections below, data from these load measurements are used in combination with information and data on treatment system efficacies to determine potential sizes and locations of wetland treatment systems needed to reduce nitrogen loads within the Monterey Bay Region. In the second part of this report, agricultural run-off is tested as a source of nitrogen for fueling HAB species growth as well as the link between nearshore phytoplankton biomass and discharge from the Pajaro River watershed.

RESEARCH AREA 1: TREATMENT SYSTEM EFFICACY

One way to reduce water quality impacts from agricultural run-off is to install treatment wetland systems that promote conditions that reduce the nitrogen concentration in agricultural run-off before it enters streams and rivers (e.g. Blankenburg et al. 2008, O'Geen et al. 2010, Bruun et al. 2016, Vymazal et al. 2020). Typically, two processes reduce nitrogen in wetlands, one being uptake by wetland plants such as reeds and grasses, and the other being the conversion of fixed nitrogen to nitrogen gas via denitrifying bacteria. Uptake of nitrogen by plants is incorporated into plant biomass which can become available again when the plant material is decomposed and the nutrients remineralized. Denitrification is a microbially mediated process where nitrate (NO_3) is converted in a series of steps (often mediated by different types of bacteria) into gaseous nitrogen (N_2) that is released into the atmosphere and thereby lost from the system. This process requires low oxygen, or anaerobic conditions, as well as abundant electron donors primarily from organic carbon (Seitzinger et al. 2006). In addition, factors such as temperature play a key role in the rate of denitrification (Herrman et al. 2008, Zhang et al. 2023). Because denitrification occurs in tandem with a variety of nitrogen transformation processes in wetland sediments, including remineralization of ammonium (NH_4) from organic matter and nitrification (i.e. oxidation of NH_4 to nitrite (NO_2) and NO_3), and the interplay between these processes result in a reduction of fixed nitrogen in sediments as well as in the overlying water column, measuring changes in concentration of nitrogen species in the water is typically used as a proxy of sediment-associated nitrogen transformations including denitrification (e.g. Ruehl et al. 2007, Wankel et al. 2010).

Over a seasonal time-scale it is important to understand whether the loss of fixed nitrogen is principally through denitrification or plant uptake, and use that information to optimize the construction of wetlands to maximize the removal of nutrients, particularly nitrogen, in the agricultural run-off and drainages.

Here, we measured changes in nitrogen concentrations from water in a number of existing treatment wetlands and bioreactors in the Pajaro River, Elkhorn Slough, and Salinas watersheds with the aim of 1) characterizing their efficiency of nitrogen removal and 2) calculating the size of a treatment wetland needed for complete removal of the nitrogen given a certain of load of nitrogen to the wetland. Whether plant uptake or denitrification dominated the potential nitrogen loss was differentiated by comparing nitrogen concentrations over time in identical habitats with and without vegetation. It was hypothesized that the addition of vegetation would increase the amount of nitrogen loss and increase efficiency of nitrogen removal.

Included within the first goal of quantifying the efficiency of nitrogen removal was also to characterize features of the most efficient wetland treatment system in terms of habitat, not only including vegetation but also other features such as depth of water, and a ditch or channel habitat versus wetland habitat. Lastly, based on measured rates of nitrogen uptake (i.e nitrogen loss from the water) we created a wetland size calculator. This calculator gives the wetland size needed to completely remove nitrogen from water based on a certain loading and on a certain set of assumptions. Conversely, if there is a size restriction on the wetland, the size can be entered into the calculator and the nitrogen removal efficiency given a certain nitrogen loading rate can be calculated.

Existing Treatment Systems

Several treatment systems already exist in the Pajaro, Elkhorn Slough, and Salinas watersheds as part of previous or current projects to reduce nitrogen loading (Figure 1). All of these systems were created through or in partnership with the Central Coast Wetlands Group (CCWG) and Coastal Conservation and Research (CCR). These systems include wetlands and bioreactors, both of which are nature-based solutions that utilize natural processes to remove pollutants from the water, as described in the section above. Each of these systems are nestled within agricultural land and most exist on parcels that are no longer farmable due to frequent flooding. The parcels used for treatment projects were designed to have multiple benefits including, but not limited to 1) minimize the potential for flooding outside of the project area, 2) support multiple hydraulic conditions that are resilient to changes in climate and farming operations, 3) establish a variety of native vegetation communities, 4) minimize food safety concerns for nearby farmers, and 5) decrease nutrient loads that are entering waterways and flowing into the Monterey Bay.

Below we describe eight existing treatment projects, consisting of four treatment wetlands and four bioreactors, and identify their locations.

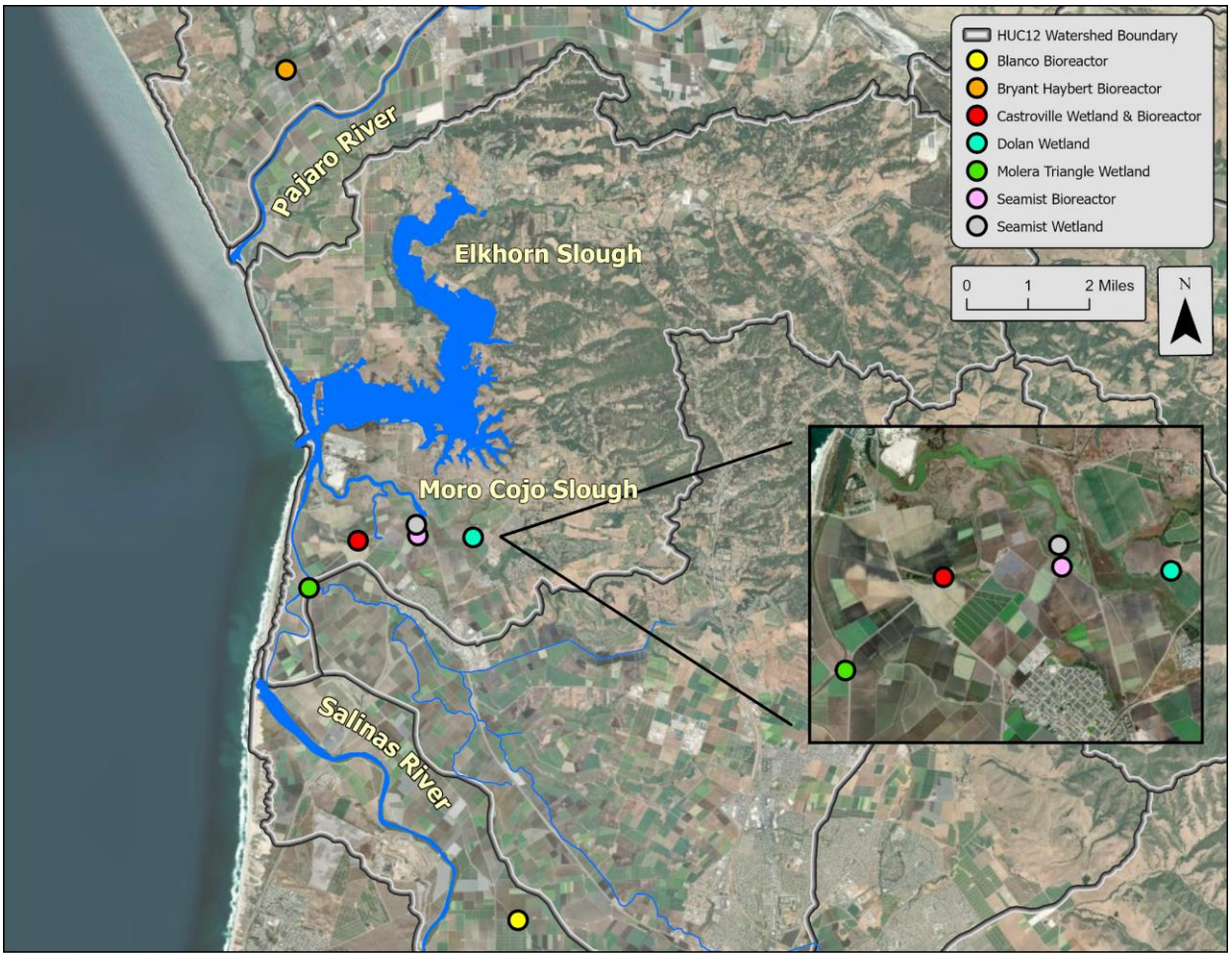

Figure 1. Locations of existing treatment systems.

Blanco Bioreactor

The Blanco Bioreactor is a 0.13 acre woodchip bioreactor that was brought online in early 2022 to help reduce nitrogen loading in the Blanco drainage area. Water is pumped from the Blanco Drain, a main tributary of the Salinas River, and is stored in three large tanks. That water enters the bioreactor from a pipe at the bottom of the woodchip filled pit, approximately 6 ft deep. The bioreactor is a straight system, but because the water is pumped into the bottom of the bioreactor, there is horizontal water flow along with upflow. This reduces short-circuiting, increases contact time with the wood chips, and potentially enhances NO_3 removal.

Bryant Haybert Bioreactor

The Bryant Haybert Bioreactor is a woodchip bioreactor that was built in 2017 to help reduce nitrogen loading from agricultural tile drains to the Watsonville Slough. This project was constructed on farm land that was purchased by the Land Trust of Santa Cruz County to treat tile drain runoff from 60 acres of surrounding farmland. A 1500 gallon tank was installed to collect tile drain water piped to the site from neighboring farms which then pumps water through the woodchip bioreactor (150 feet long, 55 feet wide, 440 cubic yards of wood chips). The treated water then flows through a broad, shallow, vegetated swale before discharging back into the Watsonville Slough.

Castroville Wetland & Multichannel Bioreactor

The Castroville Slough Treatment Wetland was built in 2016 and covers 12 acres of land in the Moro Cojo watershed. Inlet water is pumped from the Castroville Ditch which drains approximately 1000 acres of farmland. Water is first pumped into a sediment basin then gravity fed into a multichannel bioreactor with 12 parallel channels of different substrate including wood chips, heated wood chips, wetland plants, and control channels with no substrate. Water then flows through a 1.25 km wetland channel with built in depressions and ponds that support wetland plants and habitats, leading to substantial nitrogen losses from the agricultural influent water. Water then flows back into the Castroville Slough about 200 m downstream of the inlet. In 2023, the channels were removed and the bioreactor was converted to a solely woodchip system due to a lack of maintenance funds. The bioreactor still serves the same purpose and pretreats the water before it enters the wetland.

Dolan Wetland

Constructed in 2009, this project established a set of buffers between agricultural land uses and downstream slough habitat. The project included the construction of a sediment catchment basin and the restoration of wetland habitat treating 185 acres of agricultural land.

Molera Triangle Wetland

The Molera Triangle treatment wetland contains two sections, a 1.3 acre channelized upper zone and the 1.7 acre lower wetland zone. It was constructed in 2005 as an experimental treatment wetland to study the pollution removal potential. Molera Triangle is located at the confluence of the Tembladero Slough and the Old Salinas River near Castroville. Water from the Tembladero Slough is continuously pumped

into the top of the wetland which first flows through a sinuous channel then a wide flat wetland before draining back into the slough downstream of the intake pump.

Sea Mist Wetland and Bioreactor

The 21 acre Sea Mist treatment wetland was built in 2006 while the one third-acre bioreactor was built in 2016. Located in the center of the Moro Cojo watershed, it treats the drainage from 155 acres of farmland. Three agricultural ditches converge at the inlet pump location which then flows through a sinuous woodchip bioreactor before being pumped into the treatment wetland. The wetland consists of three ponds with connecting channels, creating 21 acres of shallow freshwater habitat. This project was designed to remove sediment, nutrients, and pesticide contaminants before the water drains into the main Moro Cojo Slough. Construction designs for this wetland and bioreactor are depicted in Figure 2.

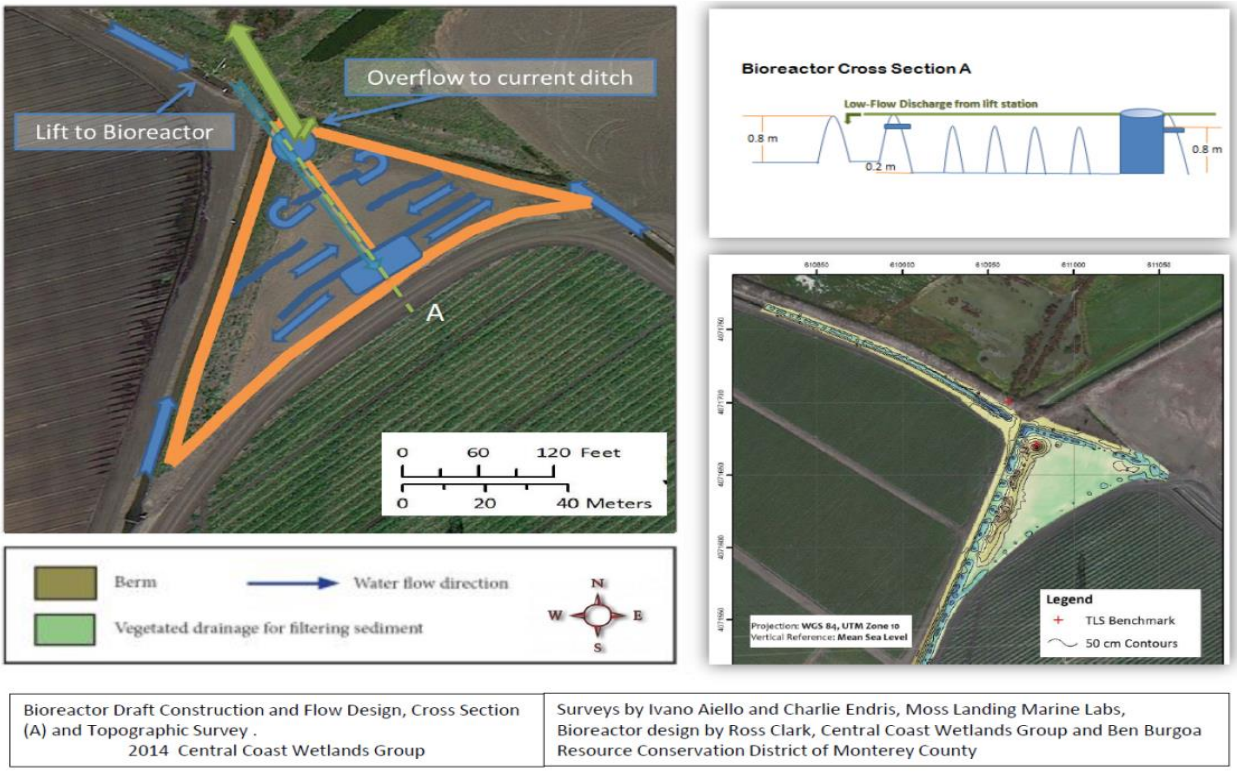

Figure 2. Sea Mist Wetland and Bioreactor design plans.

A summary of each treatment system's parameters is shown in Table 1. In order to measure the effectiveness with respect to nitrogen removal of each of these systems, we collected grab samples of the influent agricultural water, and the water draining from the treatment systems. Several grab samples were collected from each system over a varied period of time. The grab samples were analyzed by the Moss Landing Marine Laboratories Analytical Nutrient Laboratory (MLML Nutrient Lab) for concentrations of NO_3, NO_2, ortho-phosphate (PO_4), NH_4, and urea. All nitrogen species were in concentration of N (i.e. NO_3-N, NH_4-N, urea-N) and PO_4 in concentration of P. The removal efficiency of the nutrient source by the treatment system was calculated as the change in concentration (delta) of the nutrient (initial - final

concentration) relative to the initial concentration. Data collected from each system was averaged before efficiencies were calculated.

Table 1. Summary of CCWG's existing treatment systems and their parameters.

Name	Year of Installation	Area (acres)	Residence Time (days)
Blanco Bioreactor	2022	0.13	4
Bryant Haybert Bioreactor	2017	0.19	6
Castroville Bioreactor	2016	0.19	1
Castroville Wetland	2016	12	3
Dolan Wetland	2009	2	NA
Molera Triangle Wetland	2005	2	NA
Sea Mist Bioreactor	2016	0.35	NA
Sea Mist Wetland	2006	21	NA

The main source of nitrogen in the agricultural run-off, as evidenced by nutrient concentrations in the inlet to the treatment systems, was NO_3. Because irrigation and fertilization practices in the Monterey County region has evolved and diversified over time, with increased adoption of liquid urea based fertilization ("fertigation"), it was of interest in the current study to examine the prevalence of nitrogen substrate other than NO_3 such as urea and NH_4 in the agricultural run-off, and also to examine the efficiency of removal of various types of nitrogen substrates by the treatment systems.

Our results demonstrated that NO_3 was the principal source of nitrogen in the agricultural run-off comprising 87-99 % of the total nitrogen measured in the influent, i.e. initial concentrations presented in Table 2. One exception was the Castroville Wetland which received a greater proportion of NH_4 in its influent compared with the other treatment systems. The proportion of NO_3 as a percent of the total nitrogen pool was only 81% in this system (Table 2). Despite increased adoption of fertigation practices in the Monterey Region, urea composed a minor fraction of the total nitrogen pool in all the agricultural run-off sources measured here (Table 2). The finding that NO_3 comprises the main source of nitrogen in agricultural run-off is consistent with a number of other studies (Powlson and Addiscott 2005).

Because concentrations of PO_4, NH_4, and urea were so low in the agricultural run-off, concentrations in the water draining the treatment systems were difficult to measure (i.e. below detection limits in many cases) and therefore we could not easily calculate removal efficiencies. However, with respect to NO_3 we could calculate removal efficiencies for all the treatment systems.

Table 2. Mean nutrient concentrations in the treatment system inlet (initial concentration) and mean removal efficiencies in the existing treatment systems. For annual reduction estimates see Appendix A.

Site	Initial Concentrations (mg/L)					Removal Efficiencies (%)				
	NO_3	NO_2	PO_4	NH_4	Urea	NO_3	NO_2	PO_4	NH_4	Urea
Blanco Bioreactor	41.5	0.4	0.6	0.2	NA	85.5	24.7	BDL	BLD	NA
Bryant Haybert Bioreactor	13.2	0.1	1.1	0.05	0.02	73.3	BDL	9.1	BDL	12.3
Castroville Wetland	14.2	0.6	1.2	2.7	0.10	93.1	85.7	75.9	82.3	5.8
Castroville Bioreactor*	20.8	0.6	0.8	1.7	0.3	69.8	27.1	BDL	72.9	BDL
Dolan Wetland	13.4	0.2	NA	0.2	NA	60.5	38.0	NA	BDL	NA
Molera Triangle Wetland	23.9	0.1	0.6	0.2	0.1	90.3	17.2	98.2	80.6	88.9
Sea Mist Wetland	26.2	0.5	0.2	0.2	0.02	52.7	78.3	40.0	BDL	BDL
Sea Mist Bioreactor	46.5	0.3	0.5	0.5	0.05	20.6	BDL	11.5	34.5	1.1

*The bioreactor was converted from a multi-channel system to a pond bioreactor with only woodchips, therefore only data from the woodchip treatment channels was used in calculating estimates. For a breakdown of the reduction within each channel type refer to Appendix A.

Here we found that each of these systems demonstrated to be effective at reducing nitrogen in agricultural runoff, with NO_3 removal efficiencies varying from 21-93%. For example, the Castroville Wetland had the highest NO_3 removal efficiency, followed by Molera Triangle Wetland. Size could be a factor in removal of NO_3 but there was a 6-fold difference in the size between these two wetlands and the Sea Mist wetland was greater than both of them and had a lower NO_3 removal efficiency (Table 2). Age could be a factor for efficiency, with older systems possibly having a more complex microbial community to aid in denitrification and nitrogen loss. However, the Blanco Bioreactor had one of the highest removal efficiencies but is only three years old. This supports the idea that different designs have different NO_3 reduction potentials. In addition, each of these systems requires a varied level of maintenance to make sure that water is not leaking into or out of the system, that the flow rate is appropriate, and all other parameters are functioning properly. For a period of time, the Sea Mist Bioreactor was not functioning properly and agricultural drainage was leaking into the system, causing the outlet concentration to be higher than the inlet, which is likely why its reduction efficiency is the lowest.

Overall, each of these systems are unique and it was evident that measurements of nitrogen in the inlet and outlet from the system was not enough to characterize the components of the systems that were most effective in removal of the NO_3. In particular, we wanted to examine how efficiently NO_3 was removed by different types of sediments in the treatment wetlands, and what influence vegetation had on the nitrogen removal efficiencies. Below we discuss controlled experiments designed to measure the NO_3 reduction potential of several specific wetlands and drainage ditches to aid our ability to calculate the size of a wetland needed to remove a certain amount of NO_3.

Nitrogen Loss Experiments and Nitrogen Loss Efficiencies

A series of seasonal experiments were performed to determine the overall nitrogen reduction in different treatment wetlands and habitats. The sites included three treatment wetlands and two agricultural drainage ditches. The treatment wetlands consisted of the Castroville Wetland (CW), the Molera Triangle Wetland (MT), and the Ranch 19 Pond (R19). The latter pond was recently established and therefore was not included in the treatment systems discussed above. One of the agricultural drainage ditches was located along Beach Road and drained into the Pajaro River (PR). The other ditch was located upstream from and led directly into the Castroville Bioreactor and Wetland. Each site had multiple stations in different habitats including vegetated, non-vegetated, deep, and shallow water (Figure 3). The specific habitat for each station is described in Table 3. In order to determine the nitrogen reduction potential of the different habitats, the water column above the sediments was isolated to prevent dilution and the concentration of nitrogen was followed over a two-day period. These experiments were conducted in spring and fall of 2022 and 2023 (Table 3).

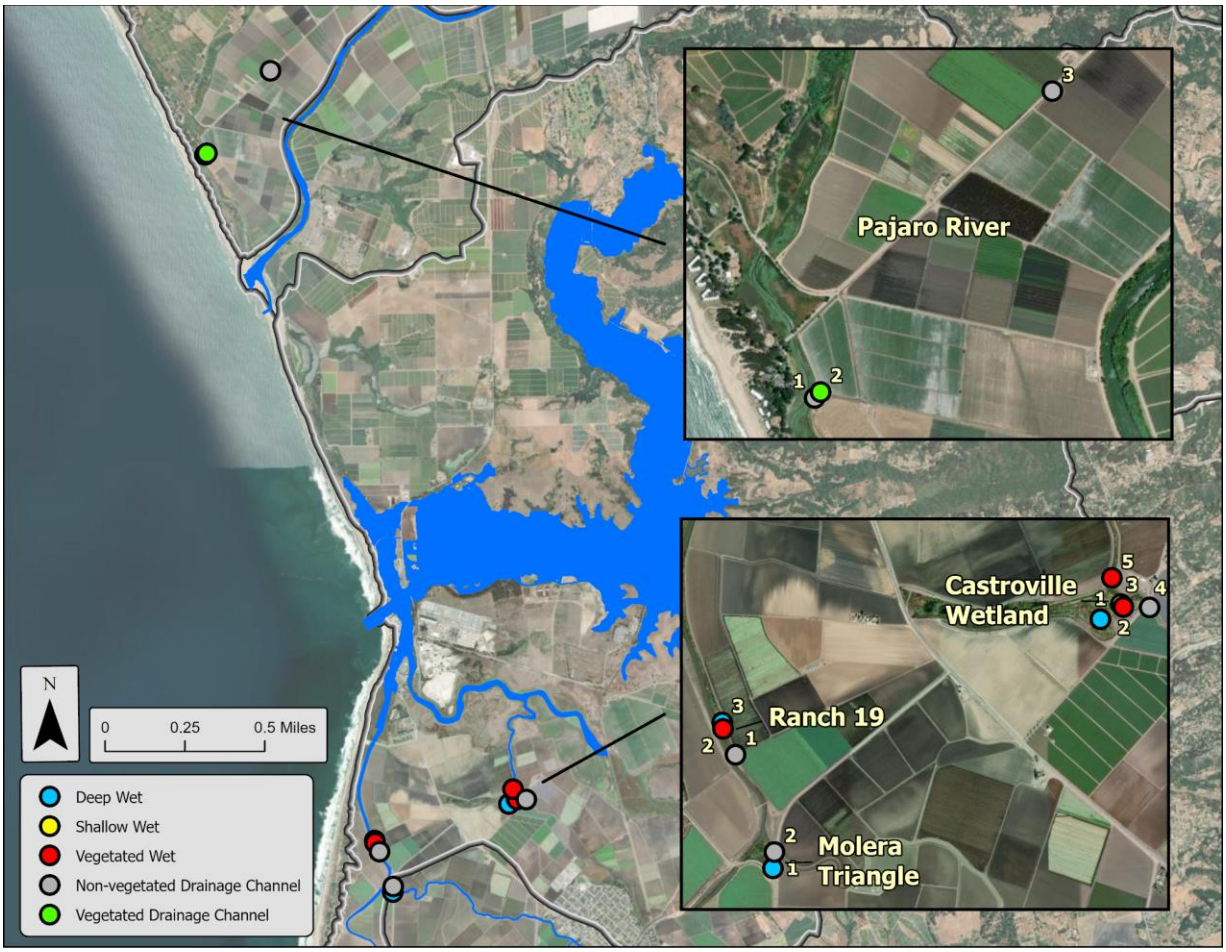

Figure 3. Locations of treatment wetlands used for nitrogen loss experiments.

Table 3. Nitrogen loss experiment treatment wetland sites including habitats sampled within each site, source water added to experimental rings at site, and months sampled at each site. Source waters were from sloughs feeding into treatment systems.

Site	Station	Habitat	Source Water	Months Sampled
Castroville Wetland	1	Deep Wetland	Castroville Slough	May, June, Aug, Sept
Castroville Wetland	2	Vegetated Wetland	Castroville Slough	May, June, Aug
Castroville Wetland	3	Shallow Wetland	Castroville Slough	May, June, Aug, Sept
Castroville Wetland	4	Non-vegetated Drainage Channel	Castroville Slough	May, June, Aug, Sept
Castroville Wetland	5	Vegetated Wetland	Castroville Slough	May, June, Sept
Molera Triangle	1	Deep Wetland	Tembladero Slough	June, July, Sept, Oct, Nov
Molera Triangle	2	Non-vegetated Drainage Channel	Tembladero Slough	June, July, Sept
Ranch 19	1	Non-vegetated Drainage Channel	Tembladero Slough	July, Sept, Oct, Nov
Ranch 19	2	Vegetated Wetland	Tembladero Slough	July, Sept, Oct, Nov
Ranch 19	3	Deep Wetland	Tembladero Slough	July, Sept, Oct, Nov
Ranch 19	4	Deep Wetland	Tembladero Slough	Sept, Oct, Nov
Ranch 19	5	Vegetated Wetland	Tembladero Slough	Sept, Oct, Nov
Pajaro River	1	Non-vegetated Drainage Channel	Watsonville Slough	Aug, Nov
Pajaro River	2	Vegetated Drainage Channel	Watsonville Slough	Aug, Nov
Pajaro River	3	Non-vegetated Drainage Channel	Watsonville Slough	Aug, Nov

In order to isolate the water column above the sediments for measurements of nitrogen concentrations, 55 gallon plastic drums were cut into rings with the top and bottom open. These rings were hammered into the sediments far enough to prevent water leaking in or out of the ring. The surface area of sediments isolated with the ring was 0.26 m^2. Each site contained multiple stations, and each station had 3 rings spaced at least 1 m apart (Figure 4). Once the rings were placed into the sediments, water was

completely removed using a hand bilge pump and nutrient-rich agricultural runoff from treatment system inlets was poured into each ring. The final amount of water pumped into each ring was determined by the depth of water outside the ring in order to prevent leaking.

Figure 4. Rings placed in a non-vegetated agricultural drainage channel. The sediment surface area isolated by each ring was 0.26 m2.

Once the rings had been filled, they were left to settle for a few hours before sampling. During sampling, temperature and DO were taken in situ from each ring. A temperature logger (HOBO, Pendant MX Temp) was left in the center ring at the surface for the duration of each experiment. DO was collected using a YSI (YSI, Professional Plus) at all of the rings. A 50 mL unfiltered water sample was taken from each ring to be analyzed by a Submersible Ultraviolet Nitrate Analyzer (SUNA) sampler (Seabird Scientific, V2). Field-filtered grab samples were collected from the middle ring for full nutrient analyte analysis, including NO_3, NO_2, PO_4, NH_4, and urea by the MLML Nutrient Lab. In addition, each ring had three depth measurements taken using a meter stick and a cast iron plate. Since the substrate at most sites was soft mud, the plate was placed on the substrate before taking the measurements to “flatten” the bottom and prevent the meter stick from sinking into the mud when recording depth. The mean water depth across all the rings was 0.20 $\pm$ 0.1 m. All of these measurements were collected at t = 0, 24, and 48 hours. Grab sample results are summarized in Table 4 and reductions over time are shown in Figure 5. Results from SUNA samples can be found in Appendix B.

Table 4. Summary of nitrogen species removal efficiency during experiments. Negative efficiency rates indicate an increase in concentration (mg/L) over the duration of the experiment.

Site	Treatment	Avg Temp (C°)	Avg Volume (L)	Nitrate + Nitrite			Ammonium			Urea		
				mg/L 0 Hrs	mg/L 48 Hrs	Removal Efficiency %	mg/L 0 Hrs	mg/L 48 Hrs	Removal Efficiency %	mg/L 0 Hrs	mg/L 48 Hrs	Removal Efficiency %
CW	Deep Wet	18.2	63.4	19.7	11.7	47.6	1.7	1.2	-32.7	0.5	0.4	37.2
CW	Shallow Wet	18.5	22.1	25.6	5.9	80.3	2.6	1.0	67.9	0.7	0.3	53.0
CW	Vegetated Wet	17.0	32.0	23.7	12.1	47.9	1.1	0.8	-56.1	0.6	0.3	31.1
CW	Non-vegetated Drainage Channel	18.4	59.0	27.7	10.6	64.9	3.4	3.2	-141.9	0.7	0.5	8.4
MT	Deep Wet	17.1	94.5	16.5	17.5	-21.6	0.2	0.3	-35.0	0.1	0.1	-135.2
MT	Non-vegetated Drainage Channel	19.8	66.7	21.1	20.1	27.1	0.2	0.1	19.0	0.1	0.1	14.6
R19	Deep Wet	18.1	45.0	18.6	11.8	57.2	0.1	0.1	-90.6	0.1	0.1	-183.7
R19	Vegetated Wet	17.2	42.3	15.5	4.3	70.8	0.3	0.3	-50.2	0.1	0.2	-304.3
R19	Non-vegetated Drainage Channel	17.9	94.9	21.6	23.8	-30.3	0.1	0.2	-4.2	0.1	0.2	-57.3
PR	Non-vegetated Drainage Channel	16.1	60.4	9.9	5.6	46.4	0.5	0.7	-19.5	0.0	0.1	-103.0
PR	Vegetated Drainage Channel	18.0	56.4	8.9	3.7	64.9	0.2	0.4	-90.3	0.0	0.1	-82.0

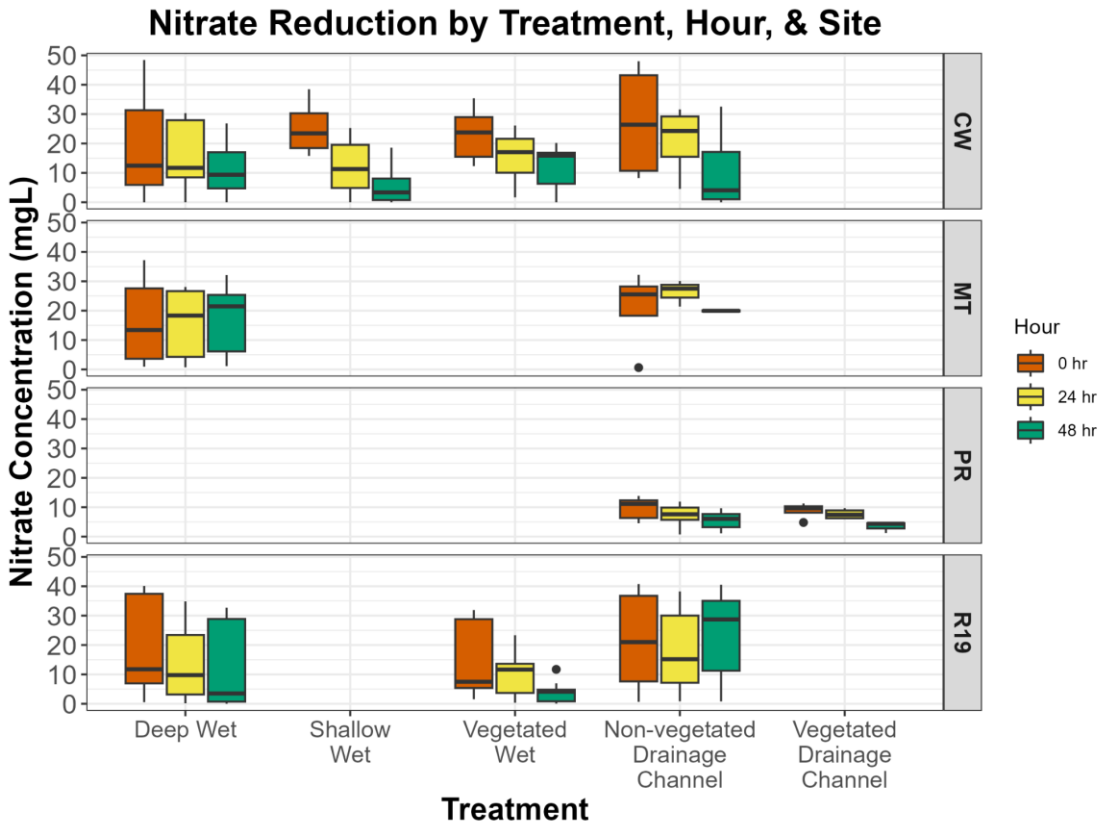

Figure 5. Box plots of NO_3 concentrations at t=0 hours, 24 hours, and 48 hours in the five different treatment habitats within each of four sites. Data being shown represents all measurements taken from each habitat across all seasons. Line within box represents the median of measurements; box represents the interquartile range (IQR); whiskers represent the maximum over minimum values <1.5 IQR above/below box; and circles represent outliers.

As discussed above, the principal source of nitrogen in the agricultural effluents added to these experiments was NO_3, comprising 87-99% of the total nitrogen pool. Based on our measurements, it appeared that nitrogen removal efficiencies varied by wetland site rather than habitat (Table 4). The highest removal efficiencies were measured at the Castroville wetland site where NO_3 removal varied from 41-77%, NH_4 removal varied from 6-62%, and urea removal from 20-57% (Table 4). The Castroville Slough agricultural run-off had the greatest concentrations of NH_4 and urea in the influent, and the Castroville Wetland treatment habitats were the only ones that we were able to measure changes in these two nitrogen sources over time (Table 4). In the other wetlands, the change in NH_4 or urea after 2 days was on the same order as the standard error of the measurements (i.e. on the order of 0.1 mg L^{-1}; (Table 4) and the percent change over time was not meaningful.

The least efficient site tested here was R19 where concentrations increased a number of times producing negative results for NO_3 removal efficiencies (Table 4). This could be related to the system's very recent establishment (i.e. only one year prior to measurements being taken) and therefore it has not had enough time for the microbial community responsible for performing the nitrogen transformations in the sediments to become established. An increase in NO_3 could also be due water leaking into the rings through the substrate.

One surprising finding in our results was that when comparing treatment habitats, NO_3 removal was not markedly greater, and in some instances notably less, in vegetated compared with unvegetated treatment habitats (Table 4). The implication of this is that most of the work of removing nitrogen rests with the microbial community in the sediments. Our results are consistent with other researchers that have directly compared vegetated and unvegetated wetland habitats and found that vegetation does not increase nitrogen removal (Vymazal et al. 2020). Ruehl et al. (2007) also determined that microbial activity, rather than plant uptake, was responsible for NO_3 removal. It may be possible that after establishment of the microbial community, plant uptake comprises a small fraction relative to removal in the sediments. In the section below, we delve into rates of NO_3 removal with treatment habitat and with season in further detail.

Calculation of Nitrogen Loss Rates and Application to Sizing of Treatment Wetlands

Introduction

Based on the data available on change in nitrogen concentrations over time from the four treatment wetlands described in the sections above, rates of nitrogen removal (i.e. nitrogen loss) by the wetlands were calculated. The four treatment wetlands included the R19 pond, the Castroville Wetland (CW), the Molera Triangle (MT) wetland, and the Pajaro River (PR) drainage channels. Within each of these systems different wetland habitats were sampled. For example, for the CW site, four different habitats were sampled including deep wetland, shallow wetland, vegetated wetland, and a drainage channel. Not all the habitats were found at each wetland site. The treatment habitats were sampled in different months to estimate the seasonal impact on nitrogen removal. Table 3 from the section above provides a matrix of treatment wetlands, habitats, and months the sites were sampled for changes in nitrogen concentration. As noted above, the most recently constructed of these wetland sites, and therefore the most inefficient in removing nitrogen, was the R19 wetland pond. As a consequence, this wetland was not representative of a mature wetland and was not used to calculate nitrogen loss rates.

Based on the calculated rates of nitrogen loss, we examined variation in rates with habitat, month, and season. We also qualitatively examined variation in rates with temperature and daylength hours. Using seasonal nitrogen losses, rates were then calculated for the size of a wetland needed to remove nitrogen in the influent. This calculation was the basis of a wetland size calculator application that was developed using the Shiny package in R. This calculator gives the wetland size needed to completely remove nitrogen from water based on a certain loading and on a certain set of assumptions. Conversely, if there is a size restriction on the wetland, the size can be entered into the calculator by reducing the efficiency until the desired size is reached, giving the nitrogen removal efficiency for a particular size and a nitrogen loading rate.

Approach

Below we describe the approach to generate the nitrogen removal rates from a number of treatment systems based on data generated from the nitrogen loss experiments described above.

Nitrogen Measurements

Samples for determination of NO_3 concentrations were collected from the experimental systems as described in the section above. Briefly, a ring with rigid walls made of plastic material, encompassing an area of 0.26 m^2, was pushed into the sediments. The water isolated by the ring was pumped out and nutrient-rich agricultural effluent was added to the ring. The water inside the ring was sampled three times over a 2-day period and the concentration of NO_3 was measured both via grab samples and via a SUNA flow through system. Several replicate measurements were taken over 2-day periods from each treatment habitat across multiple months.

Nitrogen Loss Rate Calculations

Nitrogen loss rates were calculated by performing linear regressions of dissolved inorganic nitrogen mass (mg N) as a function of time (i.e. over 48 hours). The slope of the regression, in mg N h^{-1}, represented the nitrogen loss rate. These hourly rates were converted to areal rates in units of mg N m^{-2} d^{-1} by adjusting to the number of hours in a day and the area of the ring (0.26 m^2).

Results

Nitrogen loss rates (mg N m^{-2} d^{-1}) varied greatly across treatments and months (Figure 6). A two-way analysis of variance (ANOVA) demonstrated that there was no significant relationship for either treatment habitat or month, or their interaction, with respect to nitrogen loss rate (not shown). The same was true when performing a one-way ANOVA for each parameter separately. In addition to relatively large variations in nitrogen loss rates with respect to treatment habitats, there was variation in rates with month due in part to a smaller number of samples collected in certain months such as July and October, and also potentially due to a decrease in rates with fall and winter months (Figure 6). Uneven sample sizes lead to insufficient data to estimate within-group variance and likely resulted in the lack of significance when performing the ANOVAs.

Despite this variation, when averaging nitrogen loss rates by treatment habitat, the fastest rates were observed in the unvegetated agricultural drainage channels (Figure 7). This habitat also had the greatest starting nitrogen concentrations raising the possibility that the high rates were concentration dependent. In a study comparing nitrogen loss from different wetland treatment habitats, Deng et al. (2020) found that ditch habitats had the greatest abundance of denitrifying bacteria, the highest rates of denitrification, and the greatest rates of nitrogen loss among the wetland habitats tested. It is possible that the bacterial assemblage in ditch and channel soil environments are pre-conditioned to high nitrogen concentrations, contain higher abundances of denitrifying bacteria, and are therefore primed to process and denitrify nitrogen.

In addition to different treatment habitats, we also assessed the influence of wetland vegetation on nitrogen loss rates. Our starting hypothesis was that vegetation, through uptake of nitrogen from the soil, would increase the rate of nitrogen loss from the wetland systems. Direct comparison of vegetated and unvegetated treatment wetlands demonstrated that there was no significant difference in the mean nitrogen loss rate (Figure 7). With respect to the drainage channel habitat, higher loss rates were observed for the unvegetated compared to vegetated channels (Figure 7). Based on our measurements we conclude that the bacterial assemblages residing in the wetland soils are responsible for most of the

nitrogen loss from wetland systems, rather than the vegetation in the wetland. As mentioned above, this is consistent with what other studies have found (Ruehl et al. 2007, Vymazal et al. 2020)

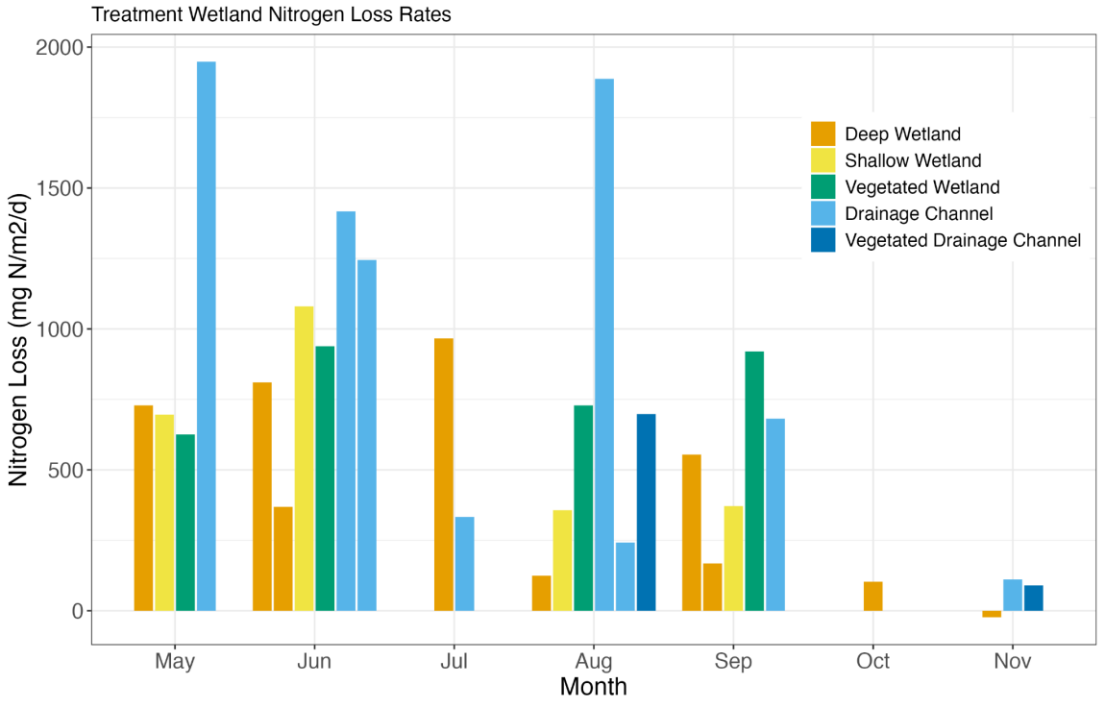

Figure 6. Areal nitrogen loss rates (mg N m^{-2} d^{-1}) derived from regressions of nitrogen concentration as a function of time across five different treatment habitats sampled over seven months.

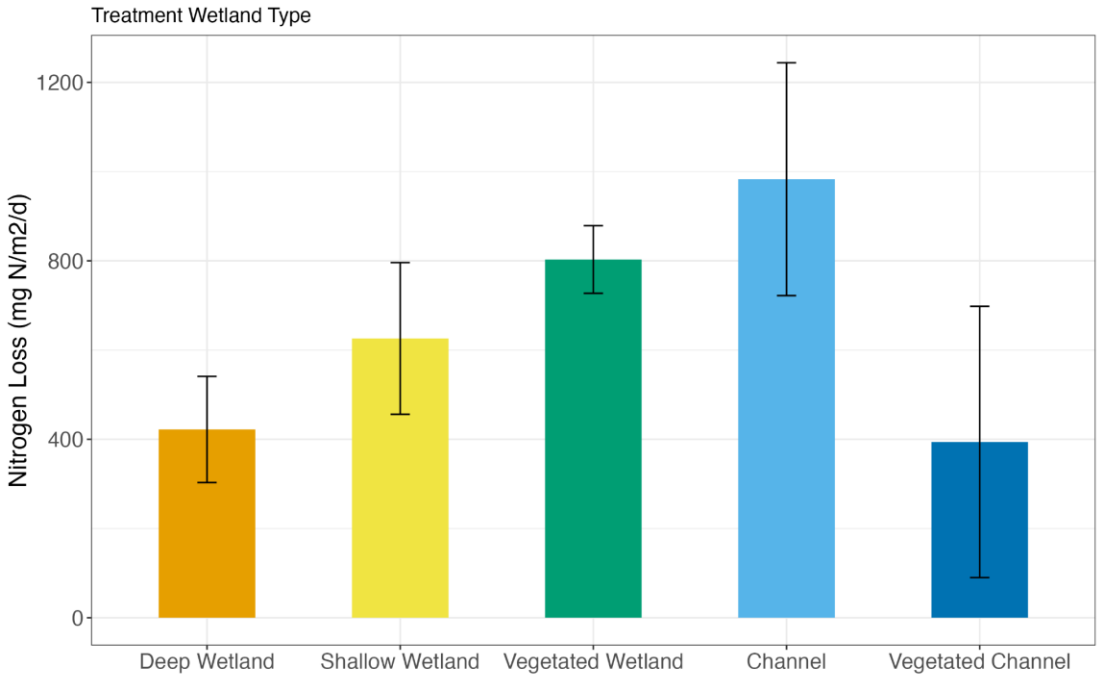

Figure 7. Nitrogen loss rates (mg N m^{-2} d^{-1}) averaged across treatment habitats. Error bars represent +/- the standard error of the mean.

Although variation in nitrogen loss rates with month was not significant due to the high variation in rates within each month, the decrease in rates with fall and winter months suggested that temperature could play a role in change of rates with month and with season. This has been shown to be an important factor in bioreactor nitrogen removal rate (Krone et al. 2022). Averaging nitrogen loss rates by month and comparing to mean monthly water temperatures measured for the treatment wetlands demonstrated interesting differences in the timing of maxima of nitrogen loss versus that of water temperature (Figure 8). The highest nitrogen loss rates were observed in May and June whereas the highest wetland water temperatures were observed in August (Figure 8). This suggested that temperature was not the sole driver of bacterial assemblage activity. Comparing the monthly nitrogen loss rates to daylength hours demonstrated that maximum daylength hours, occurring in May and June, coincided with maximum nitrogen loss rates from the wetlands (Figure 8). This could indicate that daylength hours, corresponding with another factor such as primary productivity and carbon supply, could be regulating bacterial assemblages in addition to temperature. This is consistent with studies that have found that sediment carbon supply is one of the prime determinants of denitrification rate, therefore nitrogen loss (Ashby et al. 1998, Yan et al. 2023).

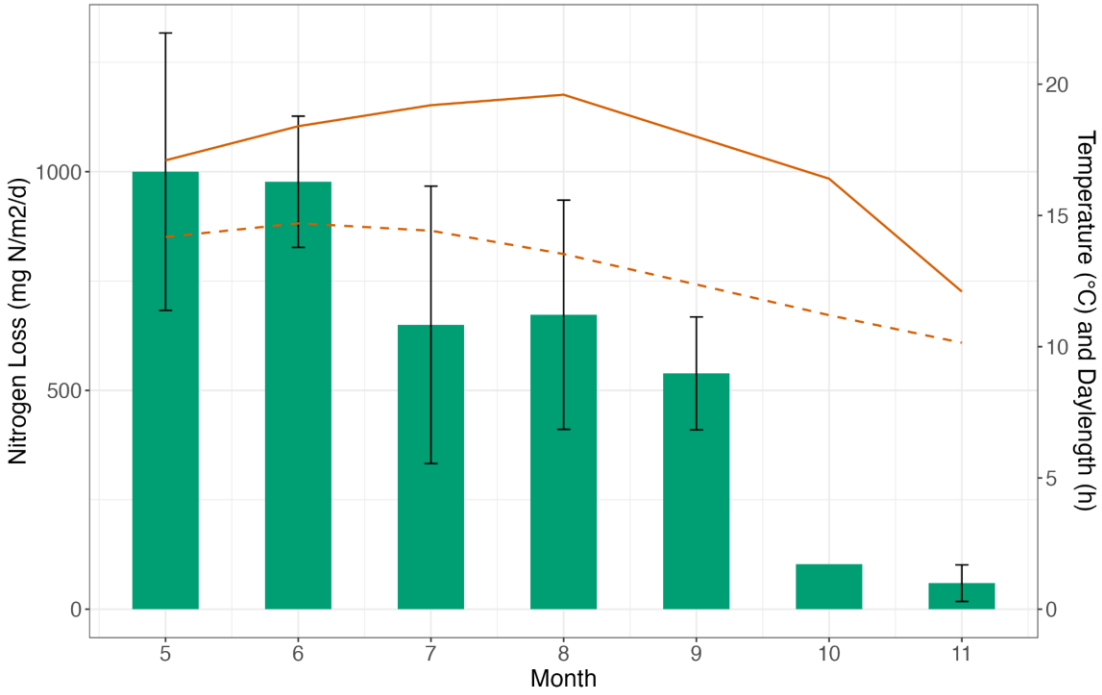

Figure 8. A) Green bars represent nitrogen loss rates (mg N m^{-2} d^{-1}) averaged by month across all treatment habitats. The red solid line represents mean monthly water temperature (°C) measured in the treatment wetlands and the red dashed line represents monthly daylength hours in Monterey County. Day-light hours by month in Santa Cruz and Monterey Counties

For the purpose of comparing to previously published rates in the literature, the rates measured here were averaged by season. Our data showed that nitrogen loss was greatest in summer and least in winter (Table 5). Rates of nitrogen loss determined here were comparable and on the same scale as rates previously published in the literature. For example, based on changes in NO_3 concentrations, Ruehl et al. (2007) found average nitrogen loss rates of 302 mg m^{-2} d^{-1} in the relatively fast-flowing Pajaro River.

Wankel et al. (2010) measured NO_3 loss rates of 84-504 mg m^{-2} d^{-1} in Elkhorn Slough sediments. In their experiments, rates of denitrification measured simultaneously represented approximately 30% of the total NO_3 loss rates. They postulated multiple nitrogen transformations occurring simultaneously, including nitrification (Wankel et al. 2010). Schmidt et al. (2011), measured average nitrogen loss rates of 700 mg m^{-2} d^{-1} in recharge ponds, close to the rate we measured during the summer season (i.e. 844 mg m^{-2} d^{-1}) across different treatment habitats (Table 5).

Table 5. Mean nitrogen loss rates averaged across treatment sites, habitats, and seasons.

Season	Nitrogen Loss Rate (mg N m^{-2} d^{-1})	Temperature Range (°C)
Summer	844 ± 123	16-22
Fall	466 ± 128	156-19
Winter	60 ± 42	8-15

Treatment Wetland Size Calculator

Using the mean seasonal nitrogen loss rates from Table 5, the size of a treatment wetland needed to remove nitrogen from agricultural run-off was calculated. The calculation derives the size of the wetland from the load of nitrogen, estimated from the inflow of water and the concentration of nitrogen in the water, over the nitrogen loss rate in summer as follows:

Size (m^2) = Inflow (L d^{-1}) x NO_3 concentration (mg L^{-1})/N loss rate (mg N m^{-2} d^{-1})

This calculation assumes that depth of water in the treatment wetland will be no more than 0.2 m. A deeper water column would have a higher water volume-to-sediment surface area ratio; therefore nitrogen loss would not be as efficient as demonstrated here. The average water depth in our experimental systems was 0.20 ± 0.1 m and our results pertain to systems with this average water depth. In addition to water depth, the nitrogen loss efficiencies demonstrated for specific seasons would only be valid above certain water temperature thresholds, i.e. above 16°C in summer, 15°C in fall, and above 8°C in winter (Table 5). In addition to temperature, nitrogen removal in a wetland also depends on the residence time of the water as it flows through the wetland. Within limits, residence time can be varied by extending the path length that water travels through the wetland to a certain degree. Here we chose to vary residence time from 1 to 5 days. Another constraint that is important to keep in mind when calculating the size of a treatment wetland is that given a maximum water depth of 0.2 m, there is a minimum area of wetland needed to hold a specific water volume for a given rate of water inflow. This minimum water volume “holding” area needs to be included in the wetland sizing calculation. Taking into account the constraints mentioned here including maximum water depth, minimum water volume area, and variation in residence time, we developed a wetland size calculator using the R interface ShinyApp (Figure 9) that produces the size of a treatment wetland needed to remove all the nitrogen from the water using two different seasonal nitrogen loss rates, the fall rate and the summer rate (Table 5). The features of this application include the ability to set the rate of inflow of water, the initial nitrogen concentration in the water, the residence time of water within a narrow range representing the ability to extend the path of

water through the wetland, and the nitrogen removal efficiency of the wetland, in obtaining the size of a treatment wetland (Figure 9). In addition, if a limited area of land is available for constructing a wetland and it is of interest to know, given this certain area, what the nitrogen removal efficiency would be, this can be obtained by toggling the nitrogen removal efficiency setting until the desired wetland size is obtained.

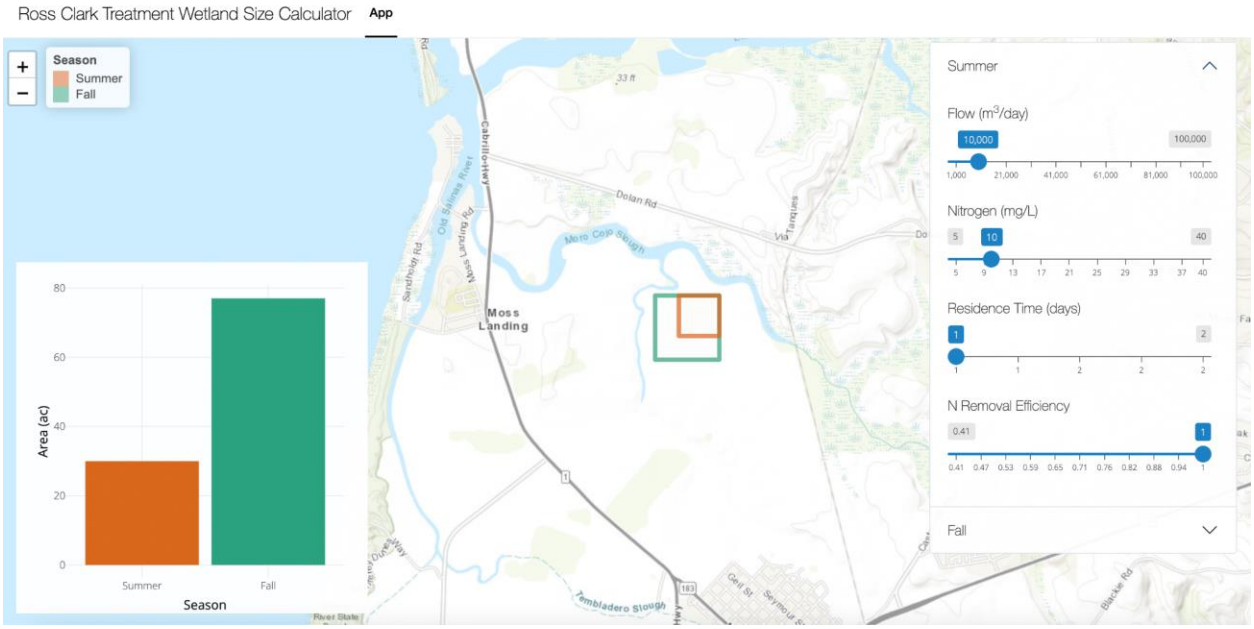

Figure 9. Wetland Size calculator available at: https://esassoc.shinyapps.io/ross-clark-treatment-wetland-size-calculator/

Industry Participation

As previously mentioned, the Regional Water Board has implemented Ag Order 4.0 which requires farmers and landowners to reduce the amount of nitrogen runoff they are producing with irrigation and fertilization practices. Farmers have the option to limit or contain their tailwater to prevent TMDL exceedances. However, if farmers cannot contain their tailwater, they must treat it before it reaches a CMP monitoring station in order to be compliant with Ag Order 4.0. CCWG is currently working with CCWQP to offer farmers and landowners the opportunity to reduce their nutrient runoff by building treatment wetlands on small sections of their land. This process has proved to be challenging because some farmers do not want to give up their land or invest money in a treatment system even though they are at risk of being fined by the Regional Water Board. The results from this study coupled with the Wetland Size calculator will help to bridge the gap between farmers and organizations like CCWG with proof of concept and a simple way to visualize the area and reduction potential of an on-farm treatment wetland. In recent months, landowners working with CCWG have shown interest in installing a treatment system to reduce their nitrogen loads and this tool will be used to determine the appropriate wetland size. Overall, this tool will aid the farming community with Ag Order 4.0 compliance.

RESEARCH AREA 2: WATERSHED NITROGEN LOADING

Subwatershed Drainages

The two watersheds at the focus of our study, the Pajaro River and the Salinas River watersheds, are highly modified landscapes with spatially and seasonally varying nutrient loads. Dividing the watershed into a finer scale allowed us to directly address water quality impairments at their source, ultimately enabling the application of more targeted conservation strategies.

The United States Geological Survey (USGS) developed the Hydrologic Unit Code (HUC) system as a standardized method of delineating watershed size, with the subwatersheds size referred to as HUC-12. At the larger scale, water movement and nutrient loads are primarily regulated by natural processes but at the subwatershed scale, particularly in an environment with heavy agricultural operations, water movement and nutrient loads may be dominated by artificial drainage systems such as ditches and tile drains that are primarily controlled by pumps managed by landowners and farmers. While originally intending to use a modeling tool such as the Soil and Water Assessment Tool (SWAT) to describe watershed loadings, we found it was not suitable for this project due to the need for detailed data on land management and farming practices (e.g. crop rotation, tillage practices, fertilizer application rates, irrigation timing, soil composition, etc.). As a result, we focused on fine scale measurements of nitrogen and flow over different seasons at the HUC-12 scale to inform our strategy. The HUC-12 scale is a workable size for identifying and prioritizing projects, engaging local stakeholders, and understanding the hydrologic processes in these highly modified landscapes (ACPF n.d.).

For our characterization of subwatershed NO_3 loadings into the Pajaro River watershed, we focused our sampling on three agricultural discharges into the Pajaro River. These discharges included the Anzar Ditch sampled at station PR5, The Salsipuedes Creek sampled at stations PR3, and the Beach Road Ditch sampled at station PR1. We also characterized the load in the Pajaro River at the USGS Chittenden station which we labeled PR4 (Figure 10). With respect to the Salinas River watershed, we focused our characterization of NO_3 loading into Tembladero Slough in the Gabilan subwatershed. Tembladero Slough is a 303(d) listed waterway and is strongly impaired for water quality constituents including nutrients and Chl-a. The tributaries we sampled included Alisal Creek sampled at station SR4, Carr Lake sampled at station SR3, Espinosa sampled at station SR2, and Alisal Slough sampled at station SR5. We sampled the middle of Tembladero Slough at station SR1 (Figure 10).

In addition to the subwatershed sampling stations, CCWG has three long-term monitoring stations installed in the Elkhorn Slough (Moro Cojo) and Salinas River watersheds that also allows for loads of NO_3 to be estimated. Data from these long-term stations were used in combination with data from the subwatershed scale to gauge where the largest loads of NO_3 originated. For the Pajaro River watershed, load values from PR4 are used to estimate the total watershed load into the Monterey Bay. Due to flooding and theft, the Pajaro River continuous monitoring array was not installed as originally intended. In the following sections we describe our approach for measuring NO_3 loads at various points throughout the two subwatersheds.

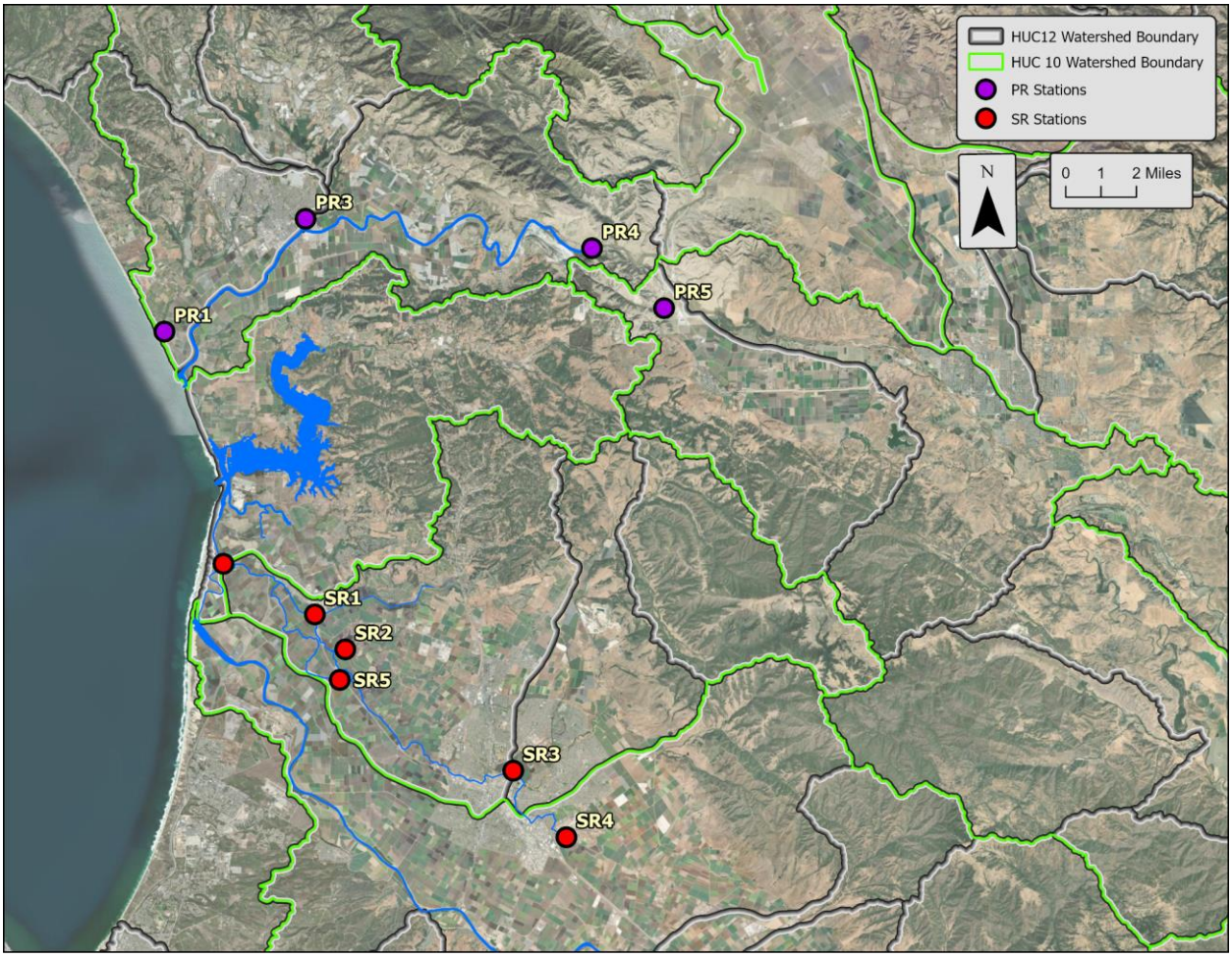

Figure 10. HUC-10 and HUC-12 boundaries in the study area.

OSMO Experiments

Water quality and flow samples were collected for one-month periods in the spring and fall to monitor seasonal loads in agriculturally influenced systems. The sites in both watersheds were chosen to be near the monthly water quality and flow samples taken as a part of the CMP, implemented by CCWQP (Figure 11, Figure 12). The main goals of this monitoring were to see if the current monthly monitoring standard is frequent enough to accurately capture the loading in these watersheds, and to identify potential locations to install a treatment system that could help bring these waterways into compliance with the Ag Order 4.0.

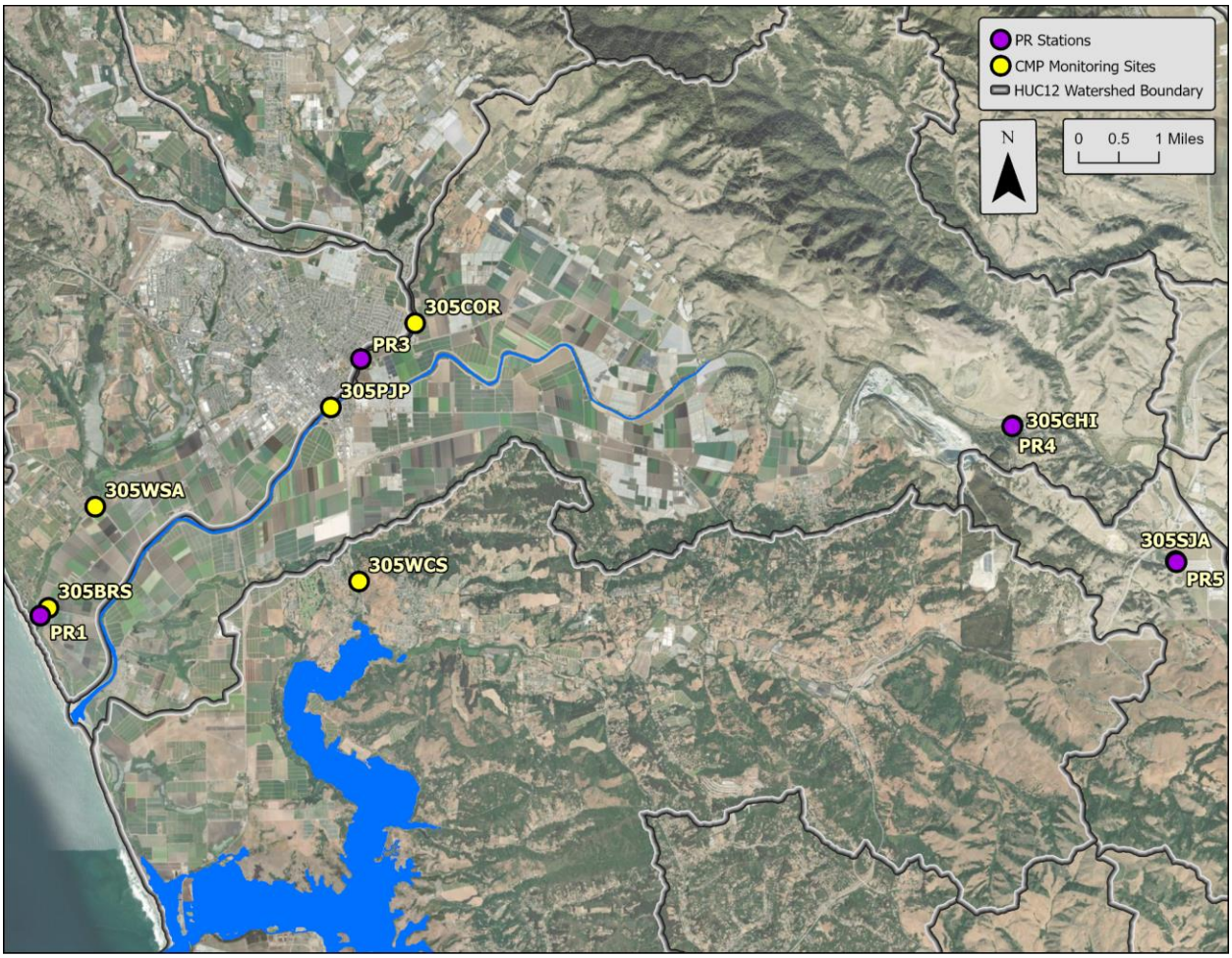

Figure 11. Pajaro River Watershed OSMO sampling sites and existing CMP monitoring sites.

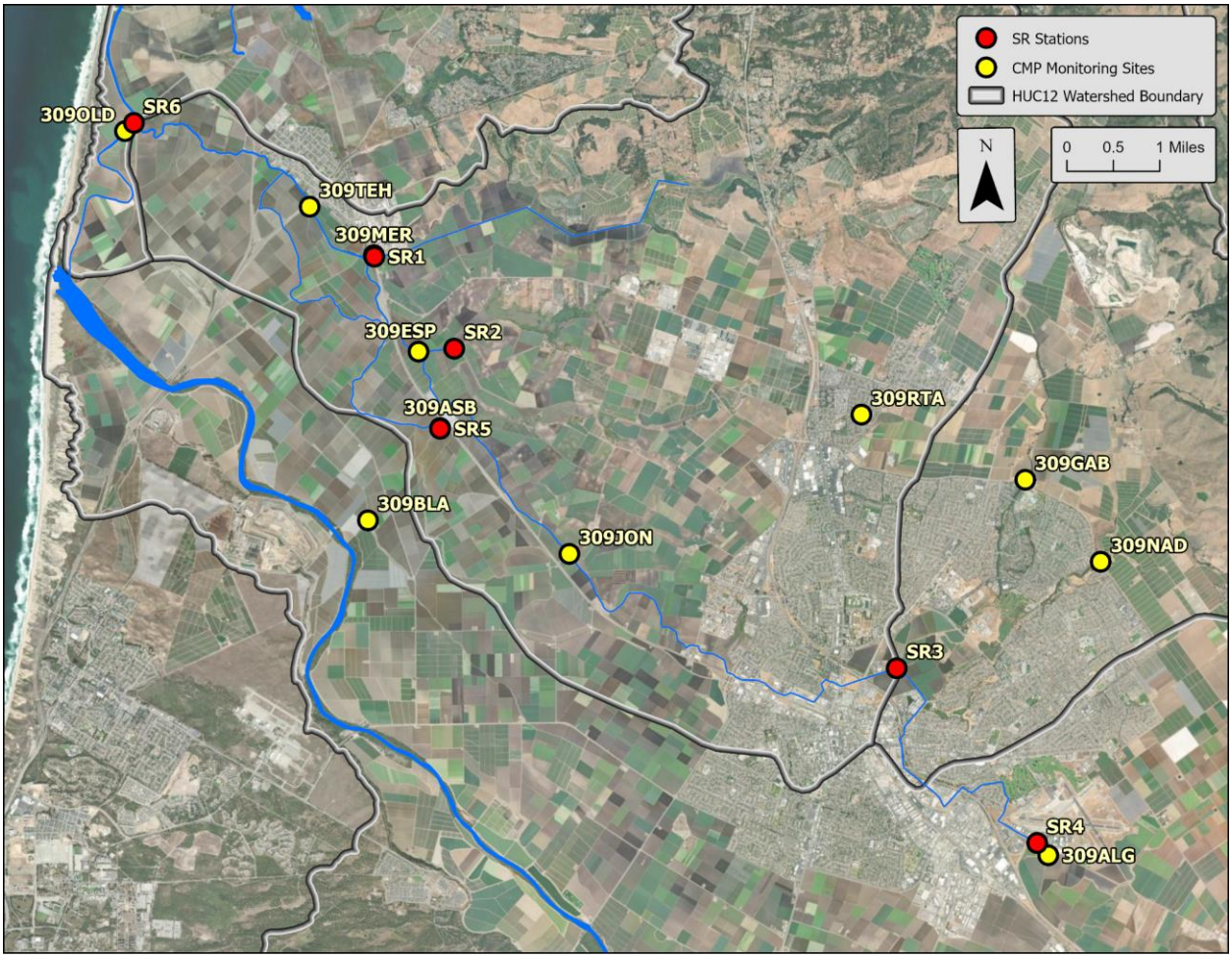

Figure 12. Salinas River/Gabilan Watershed OSMO sampling sites and existing CMP monitoring sites.

Nutrients

For nutrient collection at each site, an Osmotic Pump Sampler (OSMO) was deployed with 50 m of 0.07" OD FEP tubing to collect around 1.5 mL of water per day (Figure 13). The OSMO sampler collects continuous, small volume water samples over extended periods of time. The main chamber of the OSMO is filled with salt and when submerged in water, the higher concentration of solutes within the pump creates a pressure gradient and the tubing draws in water from the outside. The OSMOs were placed inside a box before being installed at each station to contain the equipment and prevent it from sinking into the mud. The boxes were zip tied to a T-stake in the center of the channel if possible, some sites required the boxes to be hidden along the side of the channel due to theft. The OSMOs were deployed for approximately one month. During this time, weekly nutrient grab samples were taken at the OSMO site starting at deployment and ending at retrieval. These samples were analyzed for PO_4, NO_2, NO_3, NH_4, and urea at the MLML Nutrient Lab. Once the OSMOs were collected, the tubing was cut into 1 m sections to extract the water within. Water from 4-6 days was combined into a composite sample in order to have enough volume to be analyzed in the lab.

Figure 13. OSMO sampler with 50 m of tubing attached to collect water over a month's time.

QA/QC

Additional coils of tubing were placed inside the OSMO box at predetermined sites. Source water was pumped into the coils at the site using a syringe and the coils were secured inside the box using a zip tie. Each week, coils were removed and added to have samples of water at different periods of time throughout the sampling month to test for bacterial activity within the OSMO tubing.

Flow

Flow was also sampled for this experiment using two methods. First, the submersible sensor of a Portable Area Velocity Flow Meter (Greyline Instruments, Manta Ray) was placed in the center of the channel upstream of the OSMO to eliminate flow interference from the OSMO box. This was attached to the main box with a long cord which was hidden as much as possible and the box was buried to avoid theft. The flow meters measure instantaneous velocity (m/s) and depth (m) every 15 minutes over the time they are deployed. The flow meters were deployed for one month during the spring and fall seasons.

The flow meters assume a uniform channel, so to acquire accurate discharge for the whole channel, flow transect measurements were collected using methods employed by the USGS (USGS, n.d.). Weekly flow

transects were taken at each site using an OTT HydroMet MF Pro © electromagnetic flow meter with approximately 20 shots per transect at equal distances from right edge of water to left edge of water measuring depth (m) and velocity (m/s) at each shot. Using the flow transect measurements, we calculated the change in velocity and depth at each shot from the center of the channel where the flow meter was located. With those changes known, we could combine the flow meter data with the flow transect measurements to calculate the instantaneous velocity and depth at each shot in order to get the total discharge for the whole channel (Figure 14).

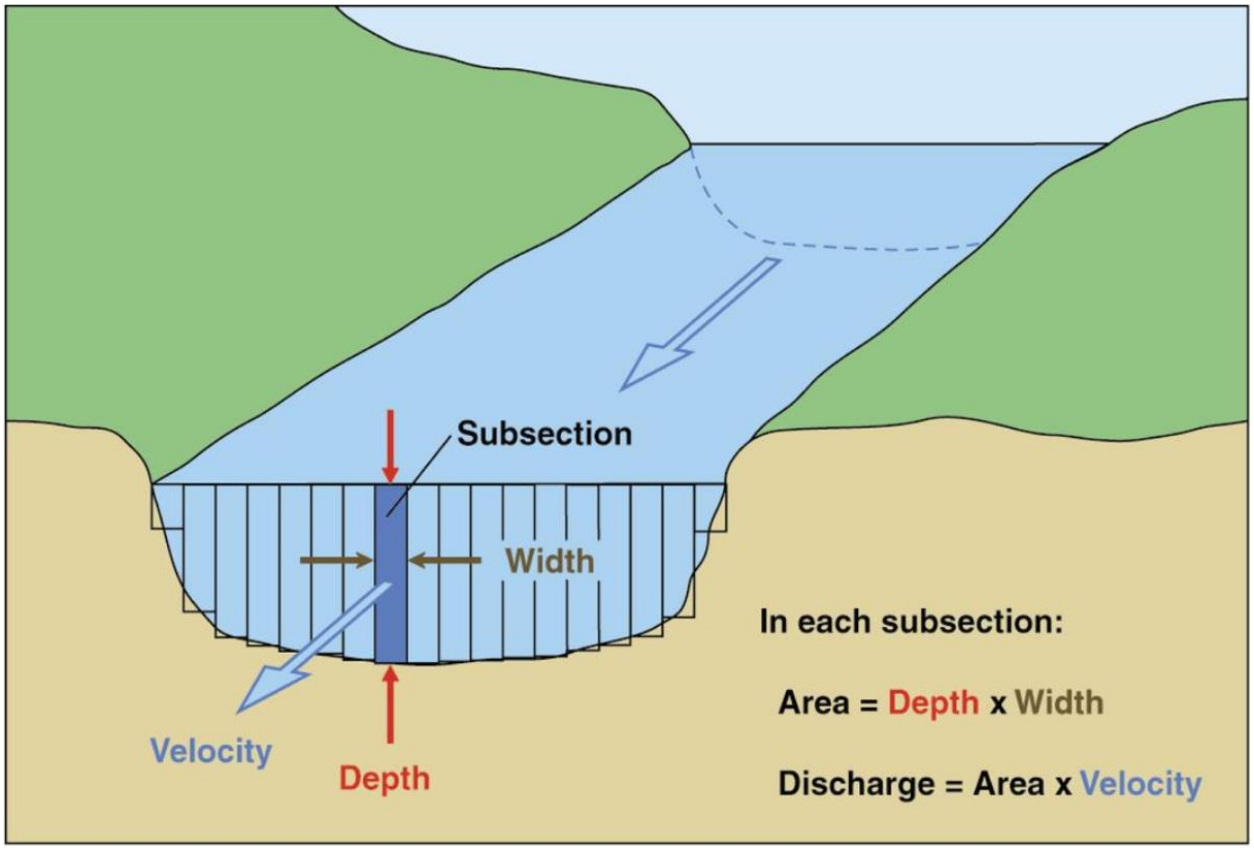

Figure 14. Example of how to calculate total discharge using a flow transect. Credit USGS.

At each site, we compared the OSMO composite NO_3 samples to grab samples taken by CCWG and CCWQP, as well as continuous flow to flow transects taken by CCWG and CCWQP. Several examples from both the Pajaro and Salinas River watersheds are shown in Figure 15 and Figure 16. At the Chittenden station, USGS stream gage data were used in the Spring 2022 and Fall 2023 seasons due to equipment failure, as well as in Spring 2023 where high flows prevented CCWG equipment from being deployed (USGS 2024). Two stations from each watershed are shown below, the remaining station figures can be found in Appendix C.

A.

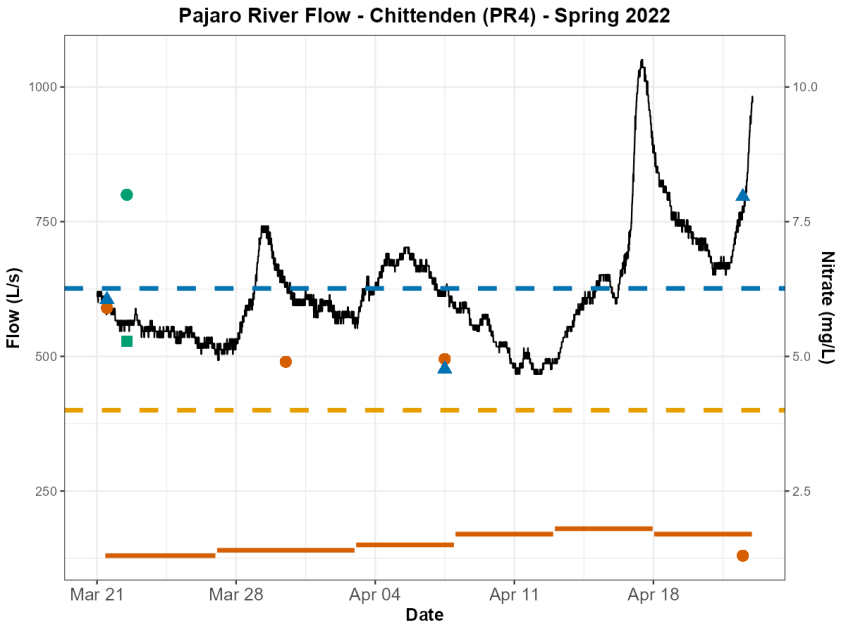

B.

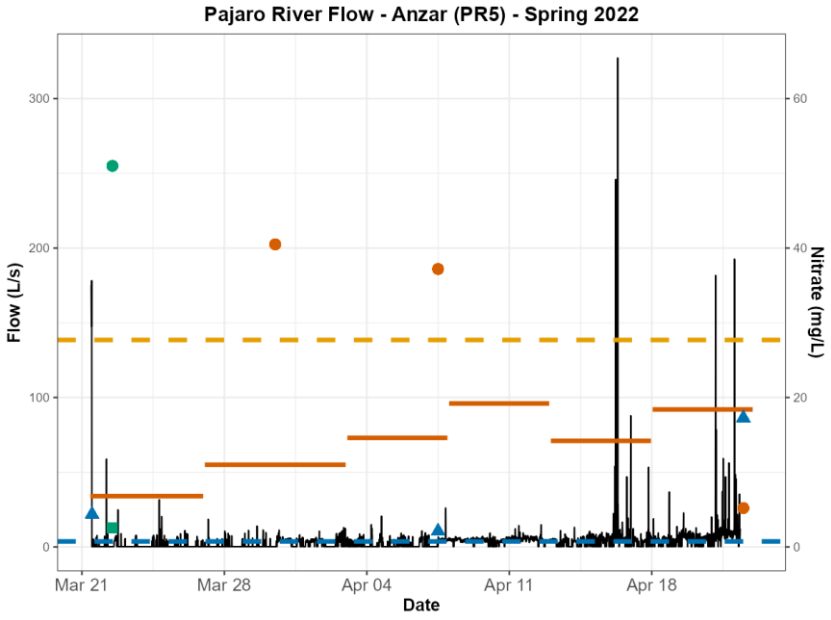

Figure 15. Comparison of two sites in the Pajaro River watershed in Spring 2022. A) Station PR4, USGS station Chittenden and B) Station PR5, Anzar Ditch. Flow measurements (primary Y-axis): black lines represent instantaneous continuous flow, dashed blue lines represent average continuous flow, blue triangles represent flow transect measurements, and the green square represents the CMP flow measurement. NO_3 concentrations (secondary Y-axis): orange lines represent OSMO NO_3 concentrations, orange circles represent grab NO_3 concentrations, the dashed orange line represents the average of the grab NO_3 concentrations, and the green circle represents the CMP grab NO_3 concentration.

A.

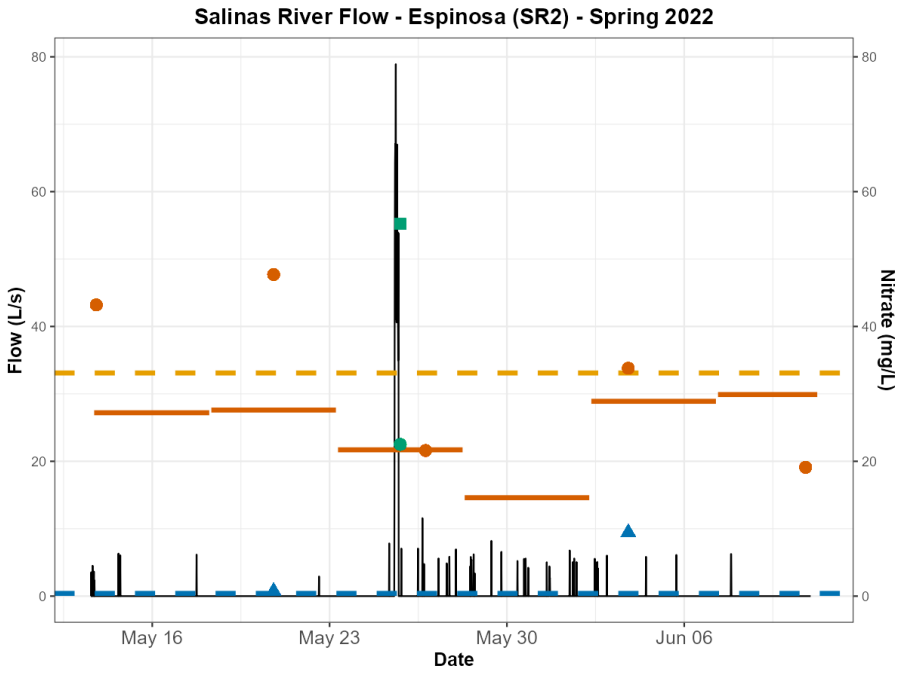

B.

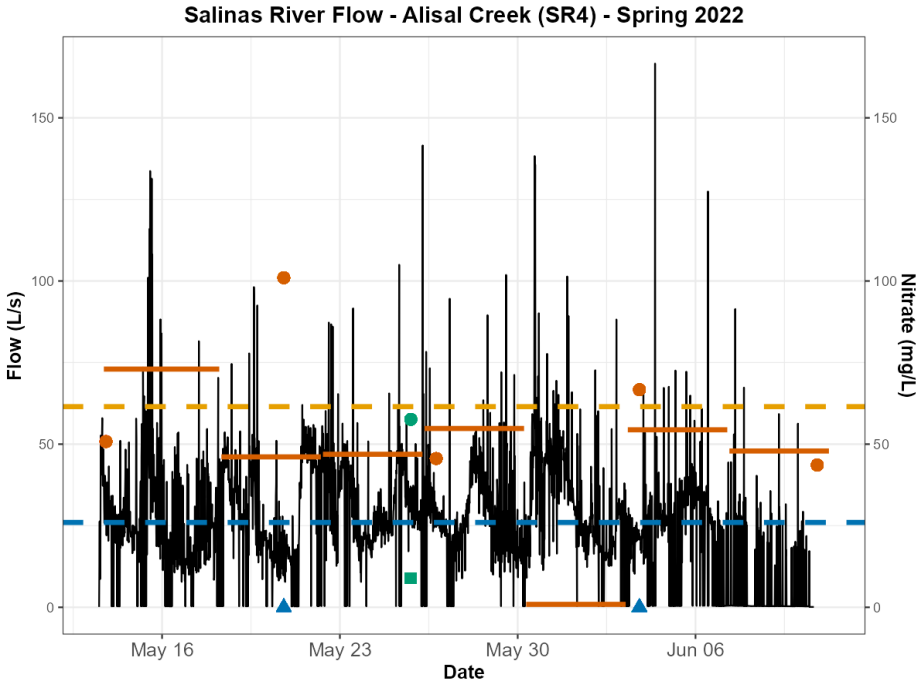

Figure 16. Comparison of two sites in the Salinas River watershed in Spring 2022. A) Station SR2 at Espinosa, and B) Station SR4 at Alisal Creek. Axes, lines, and symbols as in Figure 15.

Flow data was averaged for each month then multiplied by the average grab sample NO_3 concentration to obtain monthly load. Continuous flow data was used for sites where it was available (n=2500-3000), sites that did not have continuous flow utilized the flow transects to get the monthly average (n=2-5). When averaging the flow transects, negative flow values were excluded. Total monthly load for each of these sites was representative of the season it was collected in (Table 6). The fall and spring seasons were distinguished due to more fertilization and plant rotation occurring in the summer and fall months following cold and rainy weather in the winter. Additional site specific tables comparing all CCWG sampling efforts to CMP data are found in Appendix B.

Table 6. CCWG loading estimates within the Salinas and Pajaro Watersheds. NO_3 and flow are monthly averages. Sites with no available continuous data have flow transect averages shown instead, these are denoted by an asterisk.

Site	Site Name	Year	Season	NO_3 (mg/L)	Flow (L/s)	Load (kg/mo)
PR1	Beach Road	2022	Spring	17.8	5.6*	262
PR1	Beach Road	2022	Fall	11.3	0.02	0.5
PR3	Salsipuedes Creek	2022	Spring	0.6	833.2*	1314
PR3	Salsipuedes Creek	2022	Fall	0.0	17.5	0.4
PR4	Chittenden Creek	2022	Spring	3.0	622.0	4836.7
PR4	Chittenden Creek	2022	Fall	10.7	27.4	770
PR5	Anzar Ditch	2022	Spring	22.5	3.8	223
PR5	Anzar Ditch	2022	Fall	9.3	21.7	530
SR1	Tembladero Slough	2022	Spring	22.6	0.0*	NA
SR1	Tembladero Slough	2022	Fall	18.6	198.5	9708
SR2	Espinosa	2022	Spring	32.9	0.4	31.1
SR2	Espinosa	2022	Fall	8.2	114.0*	2458
SR3	Carr Lake	2022	Spring	41.7	4.6*	500
SR3	Carr Lake	2022	Fall	14.5	33.8*	1287
SR4	Alisal Creek	2022	Spring	68.7	44.5	8043
SR4	Alisal Creek	2022	Fall	26.5	47.5*	3307
SR5	Alisal Slough	2022	Spring	35.1	NA	NA
SR5	Alisal Slough	2022	Fall	25.9	NA	NA
PR1	Beach Road	2023	Spring	18.4	NA	NA
PR1	Beach Road	2023	Fall	9.9	NA	NA
PR3	Salsipuedes Creek	2023	Spring	1.0	NA	NA

Site	Site Name	Year	Season	NO_3 (mg/L)	Flow (L/s)	Load (kg/mo)
PR3	Salsipuedes Creek	2023	Fall	4.0	867.0*	9120
PR4	Chittenden Creek	2023	Spring	3.9	3336.4	34221
PR4	Chittenden Creek	2023	Fall	5.1	427.7	5736
PR5	Anzar Ditch	2023	Spring	30.2	60.2*	4782
PR5	Anzar Ditch	2023	Fall	21.7	42.9	2447
SR1	Tembladero Slough	2023	Spring	19.3	7.1*	359
SR1	Tembladero Slough	2023	Fall	13.1	8.8*	301
SR2	Espinosa	2023	Spring	11.4	16.3*	488
SR2	Espinosa	2023	Fall	21.3	0.3*	15
SR3	Carr Lake	2023	Spring	21.4	99.8	5614
SR3	Carr Lake	2023	Fall	4.7	32.3	398
SR4	Alisal Creek	2023	Spring	28.7	5.5*	416
SR4	Alisal Creek	2023	Fall	0.3	4.9	3.87
SR5	Alisal Slough	2023	Spring	29.8	NA	NA
SR5	Alisal Slough	2023	Fall	25.9	NA	NA
SR6	OSR/Tembladero	2023	Spring	36.3	208.2	19877
SR6	OSR/Tembladero	2023	Fall	0.8	95.7	201

Discussion

Our QA/QC experiments determined that the nutrient concentration data collected by the OSMOs were unreliable due to increased bioactivity in the tubing. In particular we noted intermittently high concentrations of NH_4. This was likely due to the warm conditions and high nutrients in the systems the OSMOs were placed in. As a result, nutrient concentrations from the weekly grab samples were used for all loading estimates.

Throughout the course of this experiment, several flow meters were lost to either theft or damage, including water damage and being run over by large farm equipment. This resulted in a loss of all data for that particular site and season. With the loss of equipment and addition of sites as the experiment progressed, continuous flow was not measured at all sites for all seasons. The flow transect measurements were also used in tandem with the flow meters to calculate total discharge from the sites with continuous data. Where continuous flow data was lacking, flow measured during the flow transects were averaged and used to calculate loads.

Flows varied substantially with season and with site. Some sites were dominated by pumping associated with irrigation while others experienced more natural water flow. For example, from the figures above,

Chittenden (PR4) shows more natural flows as expected for the middle of the Pajaro River while Anzar Ditch (PR5) experienced flow spikes from agricultural pumps (Figure 15). Alisal Creek (SR4) showed a more natural flow with some pump driven peaks while Espinosa (SR2) experienced little to no flow unless a pump was turned on (Figure 16). While flows varied by approximately 100-fold between pumps being turned on and off, and due to natural flow variations, concentrations of NO_3 varied much less, on the order of 2-4-fold within a single sampling month (Figure 15, Figure 16).

As evident from Table 6, the load of NO_3 varied substantially between seasons and between years for each site and station. The winter of 2022/2023 and spring of 2023 was particularly rainy which impacted loading of NO_3 and our ability to sample in the spring of 2023. However, when comparing the variability in NO_3 concentrations versus variability in water flow rates, we found that the variability in water flow was much greater and had an outsized influence on the load estimate.

When comparing data collection methods we found that, while throughout the month individual NO_3 measurements varied, in most cases the average monthly grab sample values collected by CCWG were not significantly different from CMP's singular monthly sample. However, monthly loading estimates varied greatly. This is likely due to the fact that flow at most of these sites is driven by farm pump activity (e.g. Espinosa, Anzar Ditch, Beach Road), so depending on the time of the sampling event the flow may be significantly different than any other given time during the month. This is also reflected in the flow averages from continuous vs transect methods. Flow data collected with the flow meters have many samples with each site logging approximately 2,500-3,000 flow measurements, while the transects have 2-5 samples per month. This results in sites where only transect data is available to potentially over or under estimate the total flow coming from any given site. Consequently, we recommend that continuous flow monitoring systems be used in specific locations to increase the accuracy of load estimates in these two watersheds to accurately track changes in on-farm activities.

Long Term Monitoring Stations

CCWG has three long term monitoring stations installed in the Elkhorn Slough (i.e. Moro Cojo) and Salinas River watersheds (Figure 17). Here, both NO_3 concentration data and flow data from these long-term stations was modeled in order to fill data gaps. This allowed high resolution loads to be calculated throughout the year and then compared with 1) the subwatershed scale data that was collected (described above), and 2) the CMP data. Below we describe the location of the long-term monitoring stations, the development of the data-gap filling modeling, and lastly, comparison of loads calculated using long-term monitoring data with loads calculated using the CMP data.

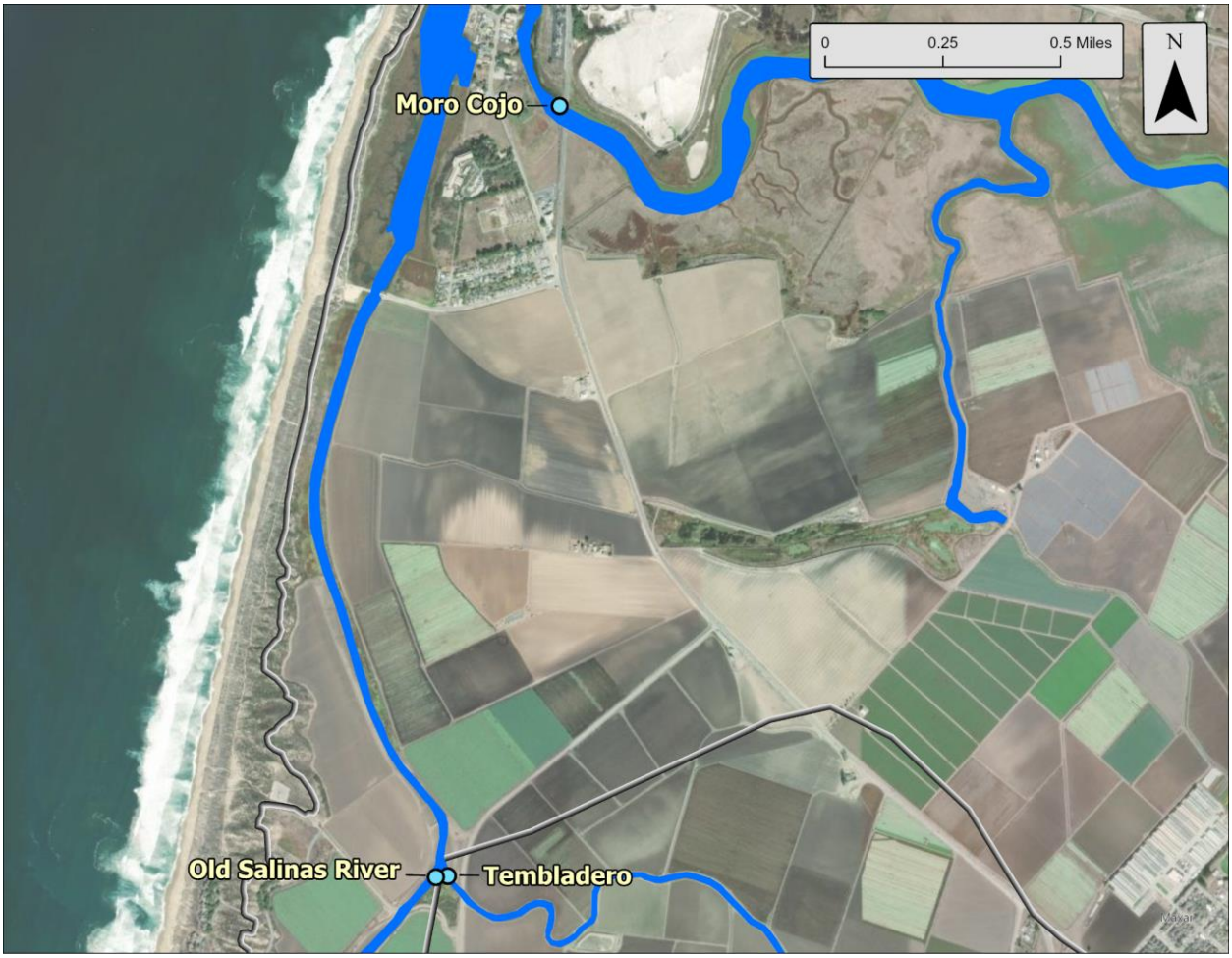

Figure 17. Locations of the existing monitoring stations. Precise GPS points of each system can be found in Appendix D.

Station Design

The long-term monitoring stations are maintained by MLML staff and real-time data is available for the public. A full list of equipment used at each site can be found in Appendix D.

Moro Cojo

The Moro Cojo station is located on the east side of HWY 1 near the culvert. Both the YSI EXO1 and the Seabird Scientific SUNA V2 are positioned on a floating platform 3 m downstream from the culvert for nutrient sampling, while the Acoustic Doppler Profiler (ADP) is placed directly in front of the culvert to measure flow. Data was collected every 20 minutes from the sensors and stored on a Raspberry Pi equipped with a cell modem. The data were then uploaded to a database at MLML for analysis.

Old Salinas River (OSR)

The station used a diaphragm pump, with ⅝” ID black vinyl tubing reaching about 30 m upstream of the convergence with Tembladaro Slough. The tubing was attached to a float on a post in the center of the waterway to ensure surface water sampling, representing freshwater agricultural runoff, rather than the

dense tidal saline water intrusion. The cross-sectional topography of each waterway was mapped every meter and loaded into the Sontek software to calculate the theoretical volume of flow every 20 minutes. Water was pumped through flowcells of a YSI 600 and SUNA V2 for nutrient sampling, then through a flow meter to ensure sample presence before discharge. A 3-minute flushing period was implemented to clear any residual water before taking new data. Samples were taken every 20 minutes. Data were stored on a Raspberry Pi equipped with a cell modem and then uploaded to a database at MLML for analysis.

Tembladero

Tembladero station used two diaphragm pumps with ⅝" ID black vinyl tubing reaching about 30 meters upstream from the convergence with the OSR. The tubing was attached to a float on a post in the center of the waterway to ensure surface water sampling, representing freshwater agricultural runoff, rather than the dense tidal saline water intrusion. The station was equipped with a Sontek IQ. The cross-sectional topography of each waterway was mapped every meter and loaded into the Sontek software to calculate the theoretical volume of flow every 20 minutes. Water was pumped through flowcells of a YSI 600 and SUNA V2 for nutrient sampling, then through a flow meter to ensure sample presence before discharge. A 3-minute flushing period was implemented to clear any residual water before taking new data. Samples were taken every 20 minutes. Data was stored on a Raspberry Pi equipped with a cell modem and then uploaded to a database at MLML for analysis.

Maintenance and Calibration

All YSI and SUNA sondes were cleaned and tested for accuracy, then calibrated monthly. Grab samples were collected every 3 months and processed for NO_3 using Flow Injection Analysis (FIA) to check for matrix effects affecting the SUNA's output. The ADPs were removed from the water, calibrated for pressure, cleaned, and redeployed.

The data from the sondes were reliable, with no drift exceeding 10%. The primary challenges for these stations arose from storm flooding, salinity changes, and sediment loads. Moro Cojo transitioned from hypersaline conditions (PSU > 40) to brackish (PSU ~20). The SUNA V2 has settings to adjust for deployment in saltwater or freshwater environments, adapting to the refractive index. To mitigate the impact of salinity fluctuations, only NO_3 points collected during low tide were used. Doing so also eliminated secondary NO_3 load from other water bodies, as high tide introduced water from other areas, such as Elkhorn Slough and Moss Landing Harbor, which could skew the results.

Sediment posed additional challenges, particularly at the OSR station, where clogging from mud occurred. Both stations also experienced high turbidity, which caused the SUNA V2 to return a "-1" value when the spectrogram could not be produced. These data points were filtered out during analysis.

Heavy rains further complicated data collection. In some instances, flooding was so severe that the ADP was unable to estimate discharge as water levels rose above the riverbank. At other times, equipment needed to be pulled out or powered down to prevent damage from flooding.

These issues, along with the maintenance downtime and clogging, resulted in an incomplete dataset. To address these gaps, modeling efforts were employed to best estimate the missing data and calculate NO_3 load.

High Resolution Loading Model

Nitrate Load Model Development

The nitrate load model was developed using data collected from monitoring stations, tide data from NOAA station 9413450, rainfall data from the Central and Northern California Ocean Observing System (CeNCOOS) weather station at Moss Landing Marine Labs, and USGS station height data. The incorporation of USGS height data provided an essential proxy for flow, particularly during heavy rain and flooding events when field stations were either inaccessible or flooded.

The following steps outline the methodology used in the development and training of the model:

Data Collection and Preparation

The modeling process began by collecting a year's worth of data from the monitoring stations, as well as other predictive inputs such as measured flow, NO_3, rainfall, tide data, and USGS station height data. These data were used to train the flow model. Specifically:

- Old Salinas River (OSR): USGS station 11151700 SALINAS R A SOLEDAD CA was used, with gage height data (parameter ID: 00065).
- Tembladero and Moro Cojo stations: USGS station 11152650 RECLAMATION DITCH NR SALINAS CA (parameter ID: 00065) provided the necessary gage height data.

Model Inputs

The model was trained using several input features that were critical in influencing flow predictions. These inputs include rainfall, tide data, and USGS gage height data, each of which had corresponding lag variables to account for delayed effects.

- **Rainfall**: The amount of precipitation was considered over the past 24 hours (Rain_24h) and 3 hours (Rain_3h) as well as realtime rainfall as critical inputs since rainfall directly affects flow rates by increasing water volume in rivers and streams.
- **Tide**: Tide levels, especially in areas near tidal influences like Moro Cojo and Tembladero, were included as inputs. The model utilized a Tide Lag, which accounts for the delayed effect of the previous 20-minute tide on flow, reflecting the fact that tide fluctuations have a lagged impact on discharge, influencing flow behavior in the next time step.
- **USGS Gage Height**: The USGS gage height data, representing the water level at specific sites, was used as a proxy for flow, particularly when direct measurements of flow were unavailable due to flooding or extreme conditions. The model included a USGS Lag, which captures the delayed effect of the water level change in the previous 20-minute period on the flow, allowing the model to predict flow based on past water level measurements.

Filling in Missing Data for Nitrate Concentrations

For NO_3 concentration data, SUNA V2 measurements during the low tide period were used as the most accurate representation of upstream NO_3 concentrations. To fill gaps in the NO_3 data where measurements were missing, a spline interpolation technique was applied. Specifically, the

UnivariateSpline function from the SciPy library was used to interpolate missing NO_3 data points based on time:

This method ensured that missing NO_3 concentrations were filled with values that preserved the smooth fluctuations typically seen in agricultural runoff, preventing any abrupt transitions in the data.

Flow and Nitrate Load Calculation

After filling and interpolating the data, the NO3 load for each time period was calculated by multiplying the interpolated NO_3 concentrations by the corresponding discharge values. This allowed for the estimation of annual and monthly NO3 loads.

Model Validation

To validate the performance of the model, the predicted discharge values were compared to observed values. Two key performance metrics were used to assess the model's accuracy:

- R^2 (Coefficient of Determination): The R^2 value quantifies how much of the flow variance in the observed data is explained by the model.
- RMSE (Root Mean Squared Error): The RMSE quantifies the average difference between the predicted and observed flow measurements, with lower RMSE values indicating better model performance.

Results

Tembladero

In 2021, the modeled NO_3 load was 358.9 metric tons, which increased to 395.7 metric tons in 2022, and further rose to 672.4 metric tons in 2023. These increases in NO_3 loading are mainly attributed to the higher flow observed, particularly in 2023, driven by heavy rainfall and flooding (Figure 18). The total flow values for each year also reflect these changes. In 2021, the total flow was 12,480,067 m^3, which increased to 16,551,178 m^3 in 2022, and significantly rose to 35,899,056 m^3 in 2023. The substantial increase in flow in 2023, compared to the previous years, aligns with the notable rise in NO_3 loading, indicating that the two are closely related (Appendix D, Table D-1). This connection suggests that the primary driver of NO_3 load fluctuations is the variation in flow.

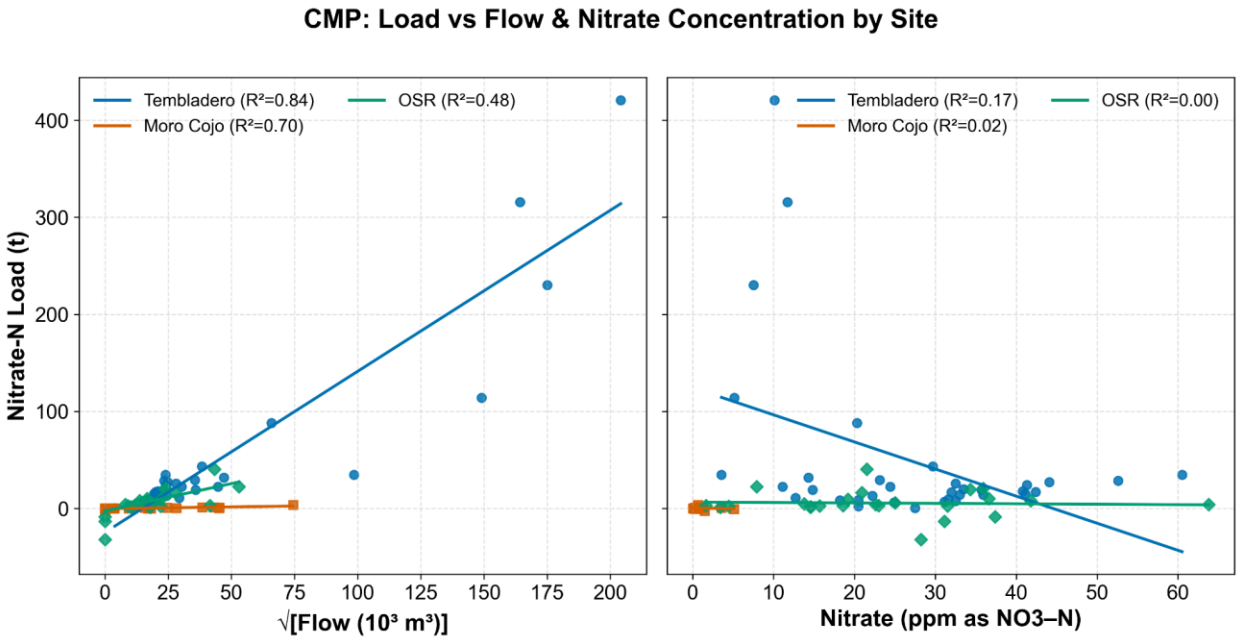

Figure 18. Relationship between NO_3 load (t) and flow (√[Flow, 10^3 m^3]) (left panel), and NO3 concentration (ppm as NO_3) (right panel) at CMP monitoring sites (2022-2023). Data points represent site-specific measurements, with linear regression lines fit to each site's data. Coefficients of determination (R^2) are reported in the legends. The stronger relationship between load and flow highlights that flow volume is the primary driver of NO_3 loading.

Nitrate samples taken from 2021 to 2023 are as follows: 3,031 samples in 2021, 13,718 samples in 2022, and 12,972 samples in 2023. These measured samples were complemented by modeled data, which filled gaps where measurements were unavailable. Modeled NO_3 samples for the same years are as follows: 23,249 samples in 2021, 12,586 samples in 2022, and 13,332 samples in 2023.

Comparison of Modeled Nitrate Loads with CMP Data

The yearly NO_3 loads for Tembladero from modeled data and CMP data are summarized below (Figure 19):

- 2021: High resolution station load = 358.8 metric tons, CMP load = 835.5 metric tons
- 2022: High resolution station load = 395.7 metric tons, CMP load = 511 metric tons
- 2023: High resolution station load = 672.5 metric tons, CMP load = 377.7 metric tons

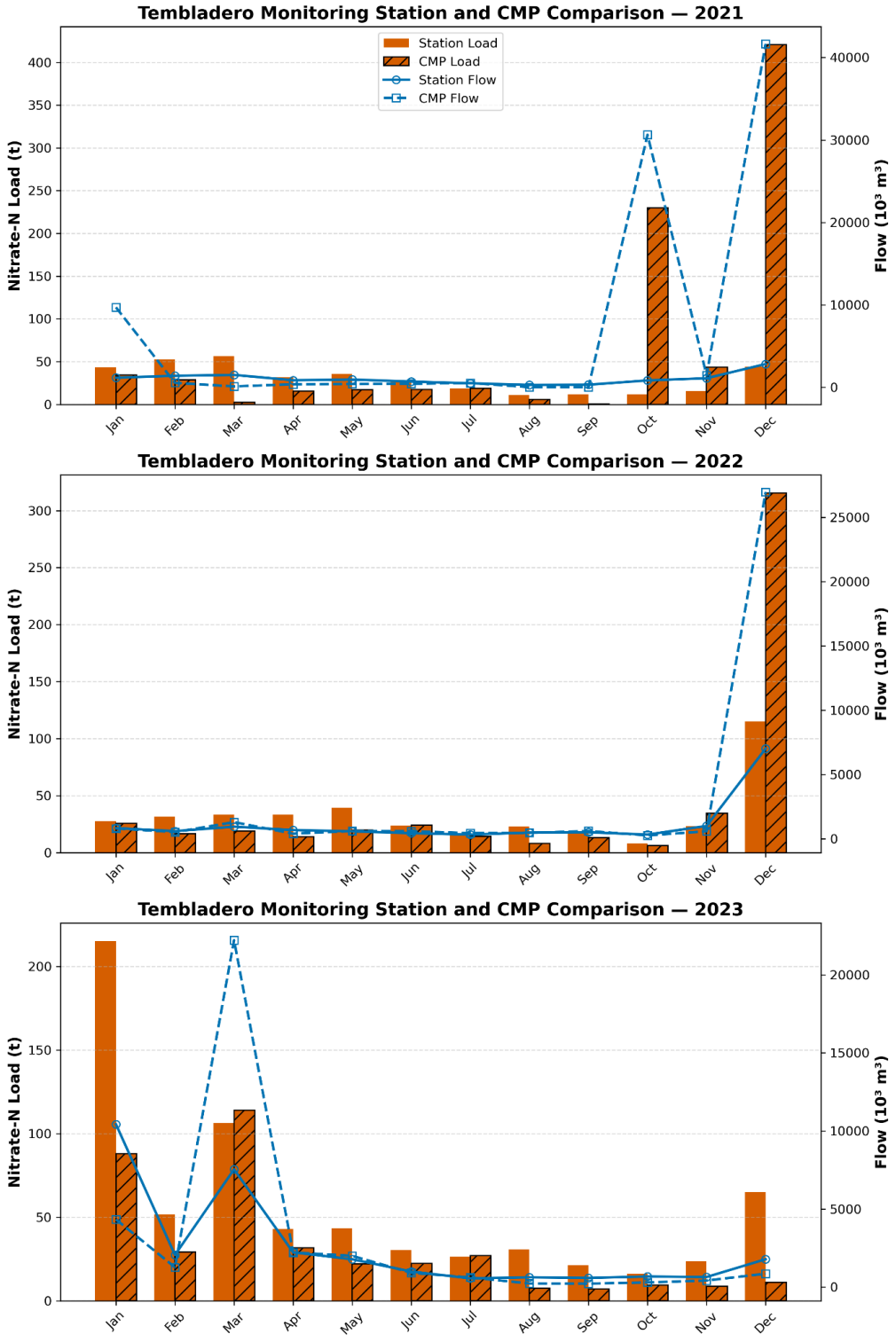

Figure 19. Comparison of NO_3 load (t) and water flow volume (103 m^3) estimated from high frequency station and CMP monitoring of the Tembladero from 2021 -2023. Values are total per month estimates.

Old Salinas River (OSR)

In 2022, the modeled NO_3 load was 92.3 metric tons, which increased to 138.8 metric tons in 2023. These increases in NO_3 loading are primarily driven by higher flow, particularly in 2023, influenced by heavy rainfall. The total flow values for each year are:

- 2022: 3,196 10^3 m^3
- 2023: 6,879 10^3 m^3

These values, reflecting the increase in flow, are detailed in Appendix D, where flow and loading comparisons across the years are presented. The substantial increase in flow in 2023, compared to the previous year, aligns with the rise in NO_3 loading, indicating that flow is the primary driver of NO_3 load fluctuations.

Nitrate samples taken from 2022 to 2023 are as follows: 13,245 and 13,829 samples respectively. These measured samples were complemented by modeled data, which filled gaps where measurements were unavailable. Modeled NO_3 samples for the same years are as follows: 13,059 and 2022 samples respectively.

Comparison of Modeled Nitrate Loads with CMP Data

The yearly NO_3 loads for Old Salinas River (OSR) from modeled data and CMP data are summarized below:

- 2022: High resolution station load = 92.3 metric tons, CMP load = 72.8 metric tons
- 2023: High resolution station load = 138.8 metric tons, CMP load = 112.1 metric tons

In 2022, the modeled NO_3 load of 92.3 metric tons was higher than the CMP estimate of 72.8 metric tons. In 2023, the modeled NO_3 load of 138.8 metric tons was also higher than the CMP estimate of 112.1 metric tons. Over the two years, CMP data had 3 months where flows were negative, and they defaulted to zero load for those months, which could account for the lower values compared to the monitoring stations (Figure 20).

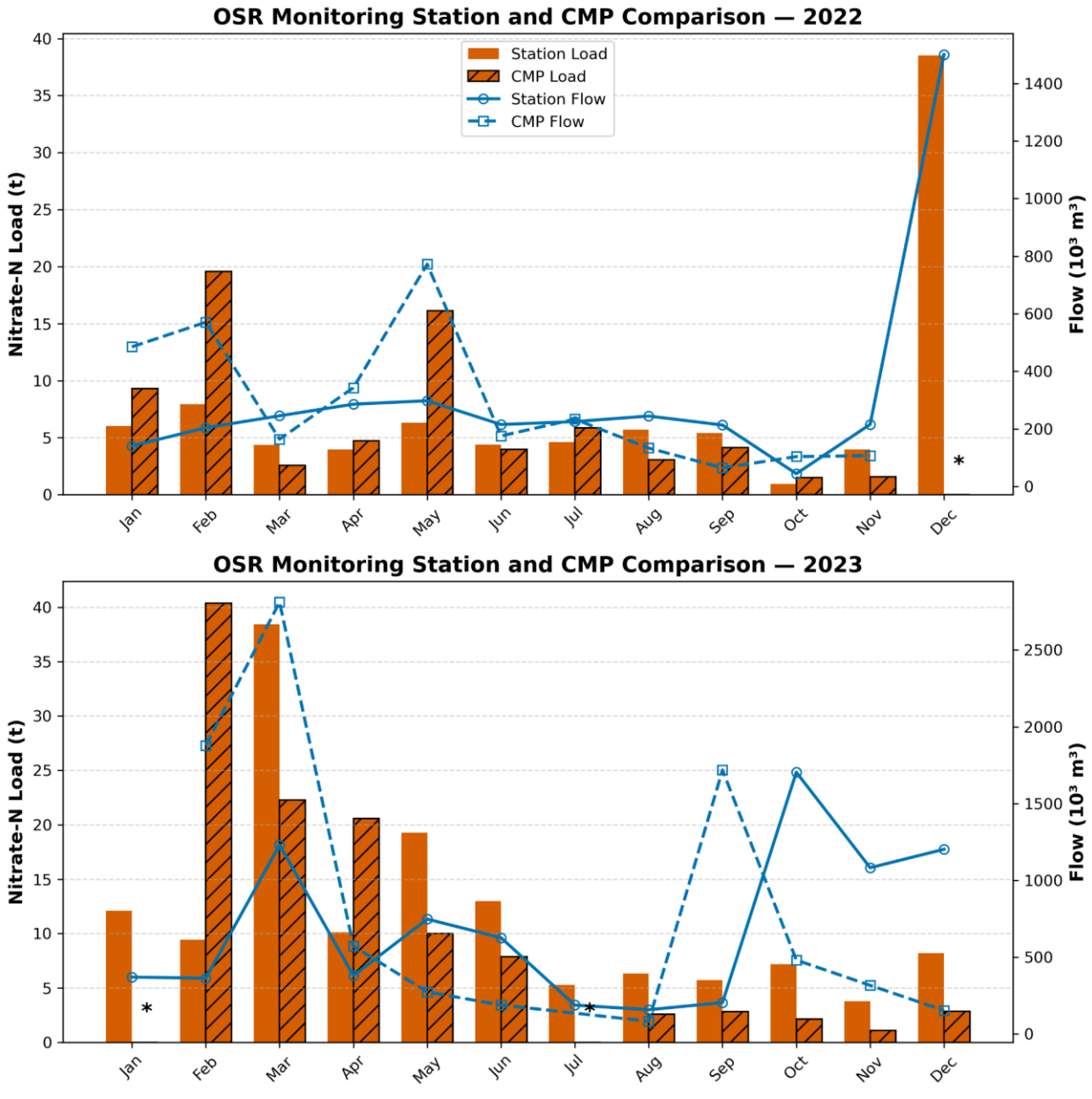

Figure 20. Comparison of NO_3 load (t) and water flow volume (10^3 m^3) estimated from high frequency station and CMP monitoring of the old Salinas river (OSR) from 2022-2023. Values are total per month estimates. Months marked with an asterisk indicate months where CMP flow values were recorded as negative, which were then translated to zero load estimates.

Moro Cojo

In 2022, the modeled NO_3 load was 0.7 metric tons, which increased to 9.3 metric tons in 2023. These increases in NO_3 loading are primarily driven by higher flow, particularly in 2023, influenced by heavy rainfall. The total flow values for each year are as follows:

- 2022: 659 10^3 m^3
- 2023: 4,008 10^3 m^3

These values reflect the increase in flow which is detailed in Appendix D, where flow and loading comparisons across the years are presented. The significant rise in flow in 2023, compared to 2022, aligns with the increase in NO_3 loading, indicating that flow is the primary driver of NO_3 load fluctuations.

Nitrate samples taken from 2022 to 2023 are as follows: 3,507 samples in 2022 and 8,898 samples in 2023. These measured samples were complemented by modeled data, which filled gaps where measurements were unavailable. Modeled NO_3 samples for the same years are as follows: 22,773 samples in 2022 and 17,382 samples in 2023.

Comparison of Modeled Nitrate Loads with CMP Data

The yearly NO_3 loads for Moro Cojo from modeled data and CMP data are summarized below:

- 2022: High-resolution station load = 0.7 metric tons, CMP load = 0.9 metric tons
- 2023: High-resolution station load = 9.3 metric tons, CMP load = 3.8 metric tons

In 2022, the modeled NO_3 load of 0.7 metric tons was lower, but relatively close to the CMP estimate of 0.9 metric tons. However, in 2023, the modeled NO_3 load of 9.3 metric tons was substantially higher than the CMP estimate of 3.8 metric tons. In 2023 CMP had 6 months where flow was recorded as a negative value which is counted as zero NO_3 load for the entire month. These zeros in the data account for some of the discrepancy coupled with high variation in flow values (Figure 21).

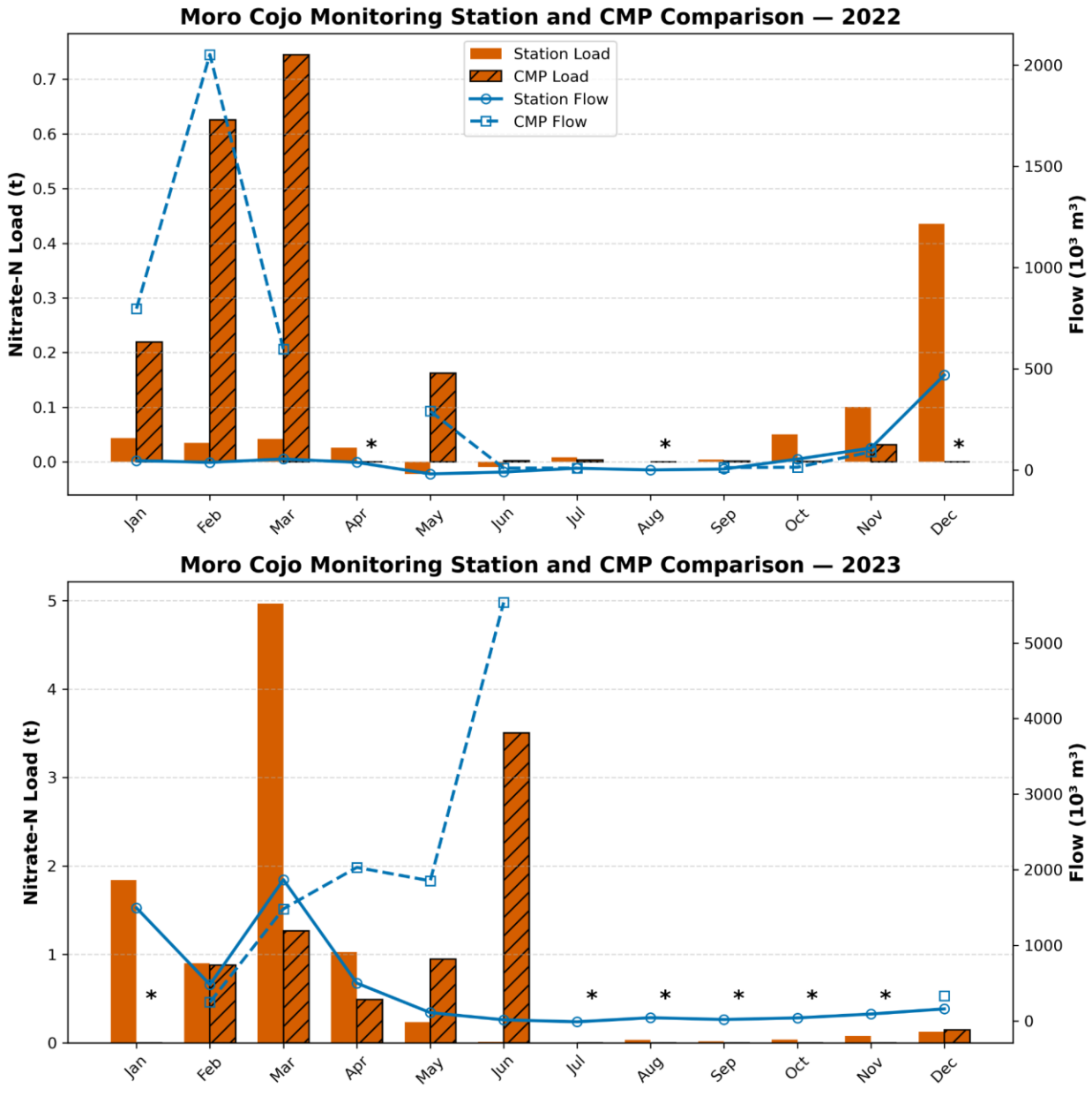

Figure 21. Comparison of NO_3 load (t) and water flow volume (10^3 m^3) estimated from high-frequency station and CMP monitoring of Moro Cojo Slough from 2022-2023. Values are total per month estimates. Months marked with an asterisk indicate months where CMP flow values were recorded as negative, which were then translated to zero load estimates.

Conclusion

The comparison between high-frequency station monitoring and CMP's low-frequency sampling highlights a critical limitation in the latter's data collection method. CMP's sparse sampling, with only 12 data points per year, leads to false zeros for entire months, particularly when flow values are recorded as negative and subsequently set to zero. Flow volume, being the primary driver of NO_3 loading, underscores the importance of accurate and continuous measurements. When flow is estimated using a single

measurement and extrapolated for an entire month, it introduces considerable variability, resulting in exaggerated spikes and troughs in NO_3 load estimates. While the overall trends in NO_3 loading from CMP data show relative alignment with high-frequency station data, the fluctuations in CMP flow estimates are more pronounced, highlighting the critical role of high-resolution data for accurate modeling.

Tembladero Slough Nitrogen Loads and Wetlands Required to Treat Loads

As mentioned above, the Tembladero Slough, stretching from the City of Salinas to the confluence of the Old Salinas River, meanders through a region of intensively farmed agricultural crop fields and is heavily impacted by agricultural discharges from tile drains and smaller tributaries. Due to the high nitrogen concentrations measured in the Slough, it is of interest to determine where along the Slough would be the best regions to place treatment wetlands in terms of mitigating nitrogen that drains into the slough and is discharged into Moss Landing Harbor through Old Salinas River.

Combining the subwatershed load data for Tembladero Slough from stations SR3 through SR6 with the high resolution load data from the Tembladero Slough long-term monitoring station, demonstrated that loads were highly variable with section and with season (Figure 22). In 2022, loads were greater in the fall season which was expected as fertilization and irrigation throughout summer results in greater discharges into the fall compared with the spring. However, in 2023, spring discharges were dominated by the winter 2023 storms which had saturated soils with water and loads were greater in spring compared with fall (Figure 22). While NO_3 loads in the middle section were variable, they were more consistent in the top section and the bottom section of the Tembladero Slough (Figure 22). We calculated sizes of treatment wetlands needed to remove nitrogen loads based on fall season loading data from the top and bottom sections of Tembladero Slough.

Nitrogen loads varied from 13 to 43 kg NO_3 d^{-1} in the fall in the top section around station SR3 (Figure 22). The size of wetland needed to treat and remove nitrogen from this magnitude of load would be 4 to 13 acres in size given a residence time of one day, determined by entering the loading into the wetland calculator (https://esassoc.shinyapps.io/ross-clark-treatment-wetland-size-calculator/). With a winter/spring storm, as in 2023, a combined wetland area of 13 acres in this region would be approximately 25% efficient in removing the nitrogen from the load measured for spring of 2023 (i.e. 187 kg NO_3 d^{-1}, Figure 22).

The largest NO_3 loads accumulated in the bottom of the Tembladero Slough, between stations SR1 and SR6. Going from above station SR1 to below station SR1, the Tembladero Slough increases in volume by approximately 2 to 10-fold by station SR6 depending on season (Table 7). This increase in water volume suggests that there are a number of agricultural drainages into this section of the slough that increase the load of nitrogen. Compared with the top section of the Slough, loads are close to 30-fold greater into this bottom section of the slough in an average-flow year in the fall. Interestingly, NO_3 loads into the bottom section of the Slough were similarly high in the fall and spring seasons (Figure 22). The total acreage of wetland needed to treat the NO_3 load coming into the bottom section of Tembladero Slough would be on the order of approximately 230 acres given a residence time of one day. However, if the path length and thereby residence time in the treatment wetlands were increased to four days (which is a reasonable

length of time) then the total area of treatment wetland needed would decrease 4-fold to approximately 50 acres.

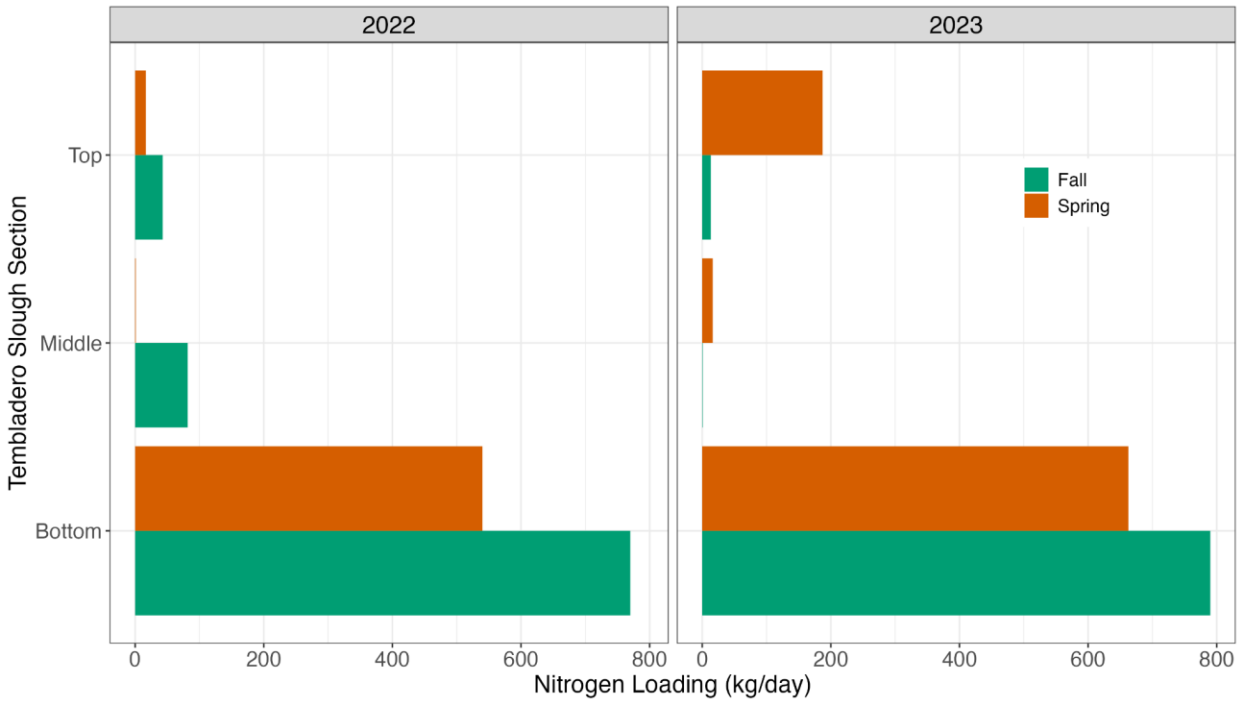

Figure 22. Nitrogen loads (kg d^{-1}) by season in sections of the Tembladero slough going from Salinas to its confluence with the Old Salinas River. Top section=station SR3 to station 309JON, section distance 0-6605 m; Middle section=station 309JON to SR1, section distance 6605-13255 m; Bottom section=station SR1 to station SR6, section distance 13255-18672 m.

Table 7. Tembladero Slough geometry and flow speed in three sections between stations SR3 to SR6 as determined in fall (November) and summer (July) of 2023.

Section Location	Total Distance (m)	Section Distance (m)	Section Volume (m^3)	Bottom Area (m^2)	Flow speed (m/d)
Fall					
SR3-309JON	6605	6605	12334.8	23117.5	509.6
309JON-SR1	13255	6650	8408.9	21612.5	604.8
SR1-SR6	18672	5417	14655.7	37919.0	786.2
Summer					
SR3-309JON	6605	6605	9035.6	23117.5	2246.4
309JON-SR1	13255	6650	2889.4	19950.0	2764.8
SR1-SR6	18672	5417	25725.3	65004.0	3611.5

In summary, total NO_3 loads originating from the Pajaro River watershed, as estimated from station PR4 at Chittenden, varied from 770 kg d^{-1} in the fall 2022, which was an average flow year, to 5700 kg d^{-1} in the fall of 2023, which was a high flow year. In comparison, loads of NO_3 from Tembladero Slough, a subset of the Salinas watershed, consistently averaged 600-800 kg d^{-1} in the fall. Because spring-time flows were on average greater and more variable by year from the Pajaro River compared with Tembladero Slough, our estimates show that when averaging spring and fall loads, NO_3 loads from the Pajaro River were 4-fold higher in a low flow year and over 30-fold higher in high flow year compared with loads from Tembladero Slough.

We focused our investigation on the scale of nutrient treatment in the Gabilan watershed and on the Tembladero Slough for two main reasons. One, the flows in this region are really regulated by farm irrigation and pumping making the flows predictable and easy to “catch” for treatment purposes. Also, loads are concentrated which is beneficial for treatment purposes. By examining incoming loads along Tembladero Slough we identified the bottom 5.4 km region (between station SR1 and SR6) as the section receiving the most nitrogen discharge and therefore contributing disproportionately to the NO_3 load from the Slough and from the region. We then calculated that the acreage of treatment wetland needed to reduce the loads in this region would be on the order of 50-230 acres depending on the residence time within the treatment wetlands. This scale of reduction would be on a similar order of magnitude to reducing Pajaro River loads from the fall season in a low-flow year, and make a large impact to overall reduction in loads from the Salinas watershed.

RESEARCH AREA 3: LINKING HAB SPECIES RESPONSE TO AGRICULTURALLY DERIVED NITROGEN

Introduction

Examining the HAB phytoplankton species response to nitrogen derived from agricultural run-off can be performed over two different scales. At the physiological level, utilization of different forms of nitrogen (i.e. reduced or oxidized, organic or inorganic) and their rates of uptake can be followed in individual HAB phytoplankton species. In addition to their nitrogen physiology, intrinsic growth rates of each phytoplankton species, given certain temperature and light conditions, can also be characterized to give species-level insight into the competitiveness of various HAB species in the natural environment (e.g. Collos and Harrison 2014, Berg et al. 2017, Thessen et al. 2009). On the other end of the scale, at the landscape scale, nitrogen derived from agricultural run-off that accumulates in the nearshore region can be quantified in relation to growth of phytoplankton communities, comprised of both HAB and non-HAB species, to potentially characterize and distinguish their respective responses.

Here we performed studies at both the physiological and landscape-scales to gain insight into HAB dynamics in relation to agricultural inputs. For the physiological studies we grew monocultures of the HAB phytoplankton species *Pseudo-nitzschia multiseries* and *Alexandrium catenella* with agricultural effluent as the sole source of nitrogen in mesocosms housed in the Environmental Biotechnology Laboratory (EBL) at MLML. These experiments were designed to examine the nitrogen utilization patterns of each phytoplankton species and to characterize how different types of agricultural runoff would impact their growth. The two HAB species were chosen based on their frequency of occurrence in Monterey Bay. As demonstrated by phytoplankton enumeration at the Monterey Wharf weekly monitoring site, both HAB species occur year-round in Monterey Bay and commonly form blooms at various times over the growing season (Bowers *unpublished*).

For the landscape-scale investigations, stations located parallel to shore in the nearshore region where the Pajaro River discharges were sampled monthly over the course of a year. Discharge from the Pajaro River was monitored both by characterizing nitrogen loading from several locations in the Pajaro mainstem and its tributaries (see sections above), and by measuring surface water nutrient concentrations in the nearshore. In addition to nutrient concentrations, HAB species responses were assessed via measurements of chlorophyll concentrations, toxin (domoic acid and saxitoxin) concentrations, and phytoplankton species enumeration, either microscopically or via qPCR primers designed for HAB species. Comparisons of the HAB abundances and biomass in seasons where agricultural run-off dominated riverine discharges were performed. These comparisons as well as the laboratory experiments are described in the two sections below.

Laboratory Experiments

Approach

Two large-scale laboratory-based mesocosm experiments were conducted to observe the response of *P. multiseries* and *A. catenella* to agricultural effluent (i.e. run-off) collected from the inlet and the outlet of the Sea Mist bioreactor. As described above, the 0.3 acre Sea Mist woodchip bioreactor acts as a pre-treatment for the 21-acre Sea Mist treatment wetland and receives the drainage from three agricultural ditches. Located in the center of the Moro Cojo watershed, it treats the drainage from approximately 155 acres of farmland. Here we collected water from the inlet to the bioreactor representing raw, untreated agricultural effluent (PRE). We also collected water from the outlet of the bioreactor representing treated effluent (POST). Final nitrogen concentrations in both these treatments, and in the control (CONT) which contained riverine freshwater, were adjusted to be similar so that differences in growth and utilization patterns would principally be related to the quality of the nitrogen pool (and possibly other factors including agricultural byproducts) and not the absolute quantity of nitrogen. The experimental design was made to 'mimic' a 15%-20% dilution of these nutrient-rich freshwater agricultural inputs into Monterey Bay. A comprehensive panel of measurements allowed us to monitor indicators of phytoplankton cell health and growth, nutrient uptake, and toxin production over the course of the exponential growth phase of the batch cultures. Growth and nitrogen uptake responses in the PRE and POST mesocosms were compared to growth responses in the CONT mesocosms which utilized nutrients derived from a commercial media kit and filtered freshwater from a local low-nutrient river source.

Stock Culture Isolation and Maintenance

P. multiseries was isolated as a single chain from a net tow sample collected 11/24/21 from Monterey Municipal Wharf (MWII; 36.60368 N, 121.889 W). Species identification was confirmed via Sanger sequencing of the large ribosomal rRNA subunit 28S (LSU) and deposited to GenBank under accession number PV817784. The culture was designated as EBL-27 and maintained in the EBL culture collection. *A. catenella* was isolated as a single cell from the same location on 10/27/21. Sanger sequencing of the LSU locus confirmed species identification (deposited to GenBank under accession number PV817788, and the strain was added to the EBL culture collection as EBL-44. The *P. multiseries* culture was acclimated to experimental conditions, which included f/4 final nutrient concentrations, using the NCMA f/2 medium kit (cat. MKf250L; NCMA, Bigelow, Maine) developed according to the recipe of Guillard (1975), in a base of 80% seawater + 20% freshwater (all source waters were 0.22 micron filtered). The cultures were grown in a non-climate controlled room with a day-time temperature of approximately 22°C with an average irradiance of 175 µmol photons m^{-2} s^{-1} on a 14:10 (light:dark) cycle. The *A. catenella* culture was acclimated to the same conditions, with the exception that L1/2 final nutrient concentrations, using the L1 culture media kit (MKL150L; NCMA, Bigelow, Maine), was used with a source water base of 85% seawater + 15% freshwater. The salinities of the *P. multiseries* (80%) and *A. catenella* (85%) stock cultures were the same as those used for the mesocosm experiments (described below).

Mesocosm Configuration

A plywood frame was constructed to hold nine, 6 mil (0.1524 mm) poly-tubing (Uline) bags supplied with constant aeration via a 4" aquarium airstone secured to silicon tubing (Figure 23). Treatments and

controls were randomly assigned to each mesocosm bag within the plywood frame. Experiments were conducted in a non-climate controlled room with an average daytime temperature of 22°C with an average irradiance of 175 µmol photons m^{-2} s^{-1} on a 14:10 (light:dark) cycle.

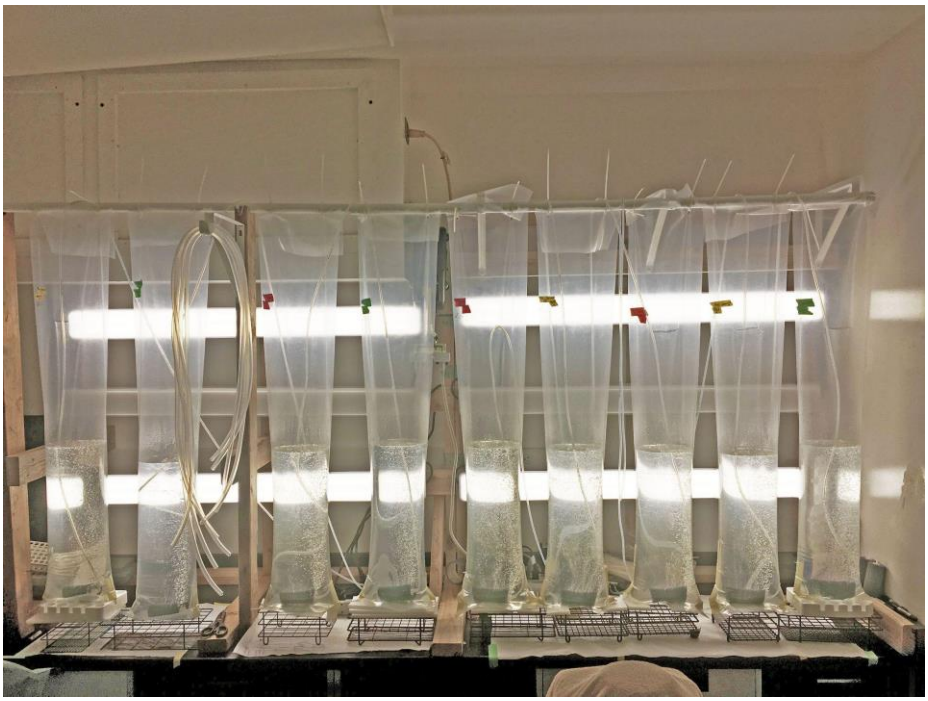

Figure 23. Mesocosm configuration for the single species experiments, Pseudo-nitzschia multiseries and Alexandrium catenella.

Preparation of culture media

For the *P. multiseries* experiment (performed July 2022), nine mesocosm bags were filled to 10 L, each containing a base of 80% (8 L) seawater collected from the intake hose at the MLML Shore Lab and 20% (2 L) freshwater. While the seawater was the same for all nine bags, the freshwater source differed according to the treatment. For the three control (CONT) bags, the freshwater was collected in July 2022 from the Carmel River (Garland Park, CA). For the first treatment, the source of agricultural water was collected from the inlet (i.e. pre-treatment) to the Sea Mist bioreactor (PRE). For the second treatment, the source was agricultural water obtained from the outlet of the bioreactor (POST), i.e. that had passed through the bioreactor. All four of the water sources, collected in July 2022, were 0.22 micron filtered on the collection date and stored in the dark at room temperature until experimental set-up. Aliquots of the water sources were submitted to the MLML Nutrient Lab and analyzed for nutrient concentrations (NH_4, NO_3, NO_2, urea, PO_4, and dissolved silicate (Si)). The principal nitrogen source in the PRE and POST agricultural effluent was NO_3 and effluent additions were targeted to achieve an initial medium NO_3 concentration of approximately 400 µmol L^{-1}, obtained by diluting full-strength agricultural effluent with 80-85% seawater, at the start of the growth experiment. Initial NO_3 concentrations were adjusted so that they were similar across the two treatments and in the control (Table 8). For the *P. multiseries*

experiment, NO_3 concentration in the POST effluent was slightly less than the PRE effluent and therefore adjusted by addition of NO_3 stock from the NCMA F/2 media kit. Starting NO_3 concentration in the CON was adjusted from an initial concentration of 1 µmol L^{-1} by addition of NO_3 from the NCMA F/2 media kit. Similarly, starting PO_4 concentrations in CON, PRE, and POST bags were adjusted to approximately 15 µmol L^{-1} by addition of PO_4 from the NCMA F/2 media kit. Initial nutrient concentrations in the mesocosm at the start of the experiment were slightly above the target concentration in the CONT and elevated in the treatments after addition of the stock cultures (Table 8), suggesting that more than anticipated nitrogen were transferred in with the cultures or was present in the agricultural effluents.

For the *A. catenella* experiment (performed September 2022), nine mesocosm bags were filled to 13 L, each containing 85% (11 L) seawater and 15% freshwater (2 L). As with the *P. multiseries* experiment, treatments and controls were run in triplicate and amended with agricultural effluent obtained from the inlet to the Sea Mist bioreactor, the PRE treatment, and agricultural effluent that had passed through the bioreactor treatment, thePOSTtreatment, collected in July, 2022. The freshwater control water, the CONT, was obtained from the Carmel River. All three water types (seawater, freshwater, agricultural effluents were 0.22 micron filtered on the collection date and stored in the dark at room temperature until experimental set-up. For the *A. catenella* experiment, starting PO_4 concentrations in CON, PRE, and POST bags were adjusted to a target concentration of approximately 15 µmol L^{-1} by addition of PO_4 from the NCMA F/2 media kit. The starting CONT, PRE, and POST mesocosm NO_3 concentrations were more similar among treatments and slightly below the target concentration of approximately 400 µmol L^{-1} after addition of the stock cultures on the first day of the experiment (Table 8).

Table 8. Initial nutrient concentrations (µmol L^{-1}) in the control (CONT) and treatments (PRE, POST) at the start of the P. multiseries and A. catenella mesocosm experiments.

Analyte	CONT	PRE	POST
P. multiseries			
NH_4	1.4 ± 0.4	2.8 ± 0.2	7.3 ± 0.7
NO_2	1.4 ± 0.4	4.3 ± 0.4	2.0 ± 0.4
NO_3	430 ± 50	659 ± 78	603 ± 124
Urea	0.9 ± 0.1	0.9 ± 0.1	0.8 ± 0.1
PO_4	14.1 ± 4	15.9 ± 4	17.8 ± 4
Silica	46.8 ± 7	75.0 ± 9	69.1 ± 2
A. catenella			
NH_4	1.2 ± 0.3	0.8 ± 0.1	1.0 ± 0.1
NO_2	5.0 ± 3	6.9 ± 3	3.5 ± 3
NO_3	385 ± 5	343 ± 23	364.4 ± 5
Urea	2.7 ± 0.1	3.1 ± 0.6	2.8 ± 0.3
PO_4	11.4 ± 3	13.8 ± 1	13.1 ± 1

Cell Inoculations

In order to add equal cell concentrations of stock cultures to all the mesocosm bags on the first day of the experiment the acclimated *P. multiseries* and *A. catenella* cultures were enumerated on the day that the experiment was started, prior to additions of aliquots. Briefly, cultures grown to exponential phase were preserved with 1% acidic Lugol's solution and counted on a Sedgewick Rafter to determine cell concentration (McAlice 1971). *P. multiseries* and *A. catenella* were added into all mesocosm bags (CON, PRE, POST) at a final concentration of either 940 cells mL^{-1} or 480 cells mL^{-1}, respectively.

Sampling

Subsamples over the incubation periods were collected near-daily at day=0 (initial), 2, 3, 4, 5, 6, and 7 for the *P. multiseries* experiment and at day=0, 2, 4, 5, 6, 7, 8, 9, 10 and 12 for the *A. catenella* experiment. The difference in growth rates between these two species was reflected in the experiment time period. Subsampling involved siphoning (from mid-volume in each bag) an 800 mL aliquot into a clean autoclaved glass beaker kept on a stir plate to maintain sample homogeneity. The following subsamples were taken from each glass beaker (representing the mesocosm):

a. Active Fluorescence Measurements: Phytoplankton photophysiology, determined by the photochemical efficiency of photosystem (PS) II, was measured as the variable over maximum fluorescence (F_v/F_m). A 3 mL aliquot was transferred to a glass cuvette, dark adapted for 5 min, and read on a Phytoflash (Turner Designs).

b. Cell counts: 100 mL of sample was transferred to a sterile glass bottle, preserved with 1% acidic Lugol's solution, stored at room temperature in the dark, and counted on a Sedgewick rafter counting chamber to determine cell concentration (cells mL^{-1}).

c. Chlorophyll-a (Chl-a): Samples for the analysis of Chl-a from the *P. multiseries* (60 to 100 mL) and *A. catenella* (10 to 100 mL) treatment bags were filtered onto 25-mm Whatman glass fiber filters (GF/F; 0.7 µm nominal pore size), placed into a cryovial, covered with aluminum foil, and stored at -80°C until analysis on a Trilogy Laboratory Fluorometer (Turner Designs) using the non-acidification method of Welschmeyer (1994). Briefly, filters were extracted overnight in 90% acetone at 4˚C. After 24 hours they were gently centrifuged for 30 s and diluted with 90% acetone before being analyzed on the Trilogy Fluorometer.

d. Nutrient panel: 60 mL samples were filtered through pre-combusted (450 °C, 4 h) Whatman GF/F filters using a Swinnex filter holder and syringe directly into Falcon tubes. Two Falcon tubes containing the filtrate were collected using two separate filters for each analysis and the tubes stored frozen at -20°C until analysis. Concentrations of NO_3, NO_2, PO_4, NH_4, urea, and Si (the latter only for the *P. multiseries* samples) were analyzed on a Lachat Quickchem 8000 Flow Injection Analyzer with the ability to measure up to five analytes on the same sample aliquot.

e. Particulate Carbon (POC) and Nitrogen (PON) analysis: The two GF/F filters (particulate matter from 60 mL on each) collected as described in section (d) above were archived in separate 8.8 cm^2 petri dishes, dried overnight at 50°C in a Precision™ Compact Oven (Thermo Electron Corporation) and then stored in a dessicator. One of the duplicate filters was packaged into 9 x 10 mm tin cups and shipped with a dessicator packet to the SOEST Laboratory for Analytical

Biogeochemistry (University of Hawaii at Manoa). Analysis was performed on the Exeter Analytical model CE 440 elemental CHN analyzer following the general methodology of Gordon (1969) and Sharp (1974).

f. Total Dissolved Nitrogen (TDN) and Phosphate (TDP): Filtrates for analysis were prepared by passing 60 mL of sample through a combusted GF/F filter (450 °C, 4 h) and storing frozen in an HDPE bottle at -20°C. The persulfate oxidation method by Valderrama (1981) was originally going to be used to analyze TDN and TDP but issues with contamination of the reagent prevented analysis of the samples in time for the writing of this report. Currently sample analysis is on hold and a different method of analysis of the samples is being considered.

g. Toxin analysis: Samples for particulate toxin were filtered onto two GF/F filters (50 mL each), placed into separate cryovials, and stored at -80°C until analysis. For the *P. multiseries* experiment, 1.5 mL of filtrate was archived in -20°C for later analysis of dissolved domoic acid (dDA). At the time of this report, the dDA samples have not yet been analyzed. For particulate domoic acid (pDA) analysis, 3 mLs of 10% methanol was added to the filter, followed by sonication at 10 W for a total of 30 sec (10 sec on, 10 sec off for 1 min) using a Fisher Brand D100 sonic dismembrator (Fisher Scientific Inc., Massachusetts, USA). Material was clarified through a Millex® Sterile PVDF 33 mm filter (MilliporeSigma) attached to a syringe. Samples for pDA analysis were further clarified through a Bond Elut C18 SPE column (Agilent Technologies) following Wang et al. (2007) and analyzed by liquid chromatography-mass spectrometry (LC-MS) at the Department of Ocean Sciences Institute of Marine Science at UC Santa Cruz. Remaining toxin analyses to be completed prior to submission of manuscript for publication in the peer-reviewed literature include dDA from the *P. multiseries* experiment, saxitoxin from the *A. catenella* experiment, as well as pDA, dDA and saxitoxin from a subset of transect cruise samples.

h. Quantitative PCR (qPCR) - 50 mL (*P. multiseries*) or 10-100 mL depending on visual cell density (*A. catenella*) were filtered onto a 0.65 micron PVDF Durapore filter (Sigma-Aldrich) and stored at -80°C until extraction with the GeneJet Plant Extraction kit (ThermoFisher Scientific). As of the time of the writing of this report, these samples have not been run yet but are scheduled to be completed in the coming month.

Results

The two HAB species tested here differed greatly with respect to their photophysiology and patterns of growth. The diatom *P. multiseries* had a relatively high starting F_v/F_m which increased rapidly with no lag over the first 3 days to reach above 0.6 (Figure 24) suggesting that it acclimated very well to growing in the mesocosms. Over the first 4 days Chl-a concentrations increased by 90 to 110-fold across all the treatments. After day 4 there was a rapid decline in F_v/F_m and also Chl-a (Figure 24).

In contrast, the dinoflagellate *A. catenella* had a lower starting F_v/F_m and experienced a 2-day period of adjustment and decrease in F_v/F_m before F_v/F_m increased and reached close to 0.4 in all the treatments by day 4. After day 4, F_v/F_m remained at approximately 0.4 before slowly decreasing the last 2 days of the experiment. Although increases in Chl-a were slower in the *A. catenella* mesocosms, increases persisted throughout the 12-day time course in all the treatments (Figure 24). Despite the difference in the time it took to attain maximum Chl-a concentrations, the Chl-a maxima were similar between the two HAB

species across all the treatments by end of their respective time courses. For both species, higher Chl-a maxima were attained in the CONT and PRE compared with the POST treatments (Figure 24), suggesting a different response in both HAB species to the POST treatment that contained agricultural run-off that had been treated in the woodchip bioreactor. For *P. multiseries*, in addition to lower maximum Chl-a concentration, there was not a sharp decrease after day 4 in the POST treatment compared with the CONT and PRE treatment.

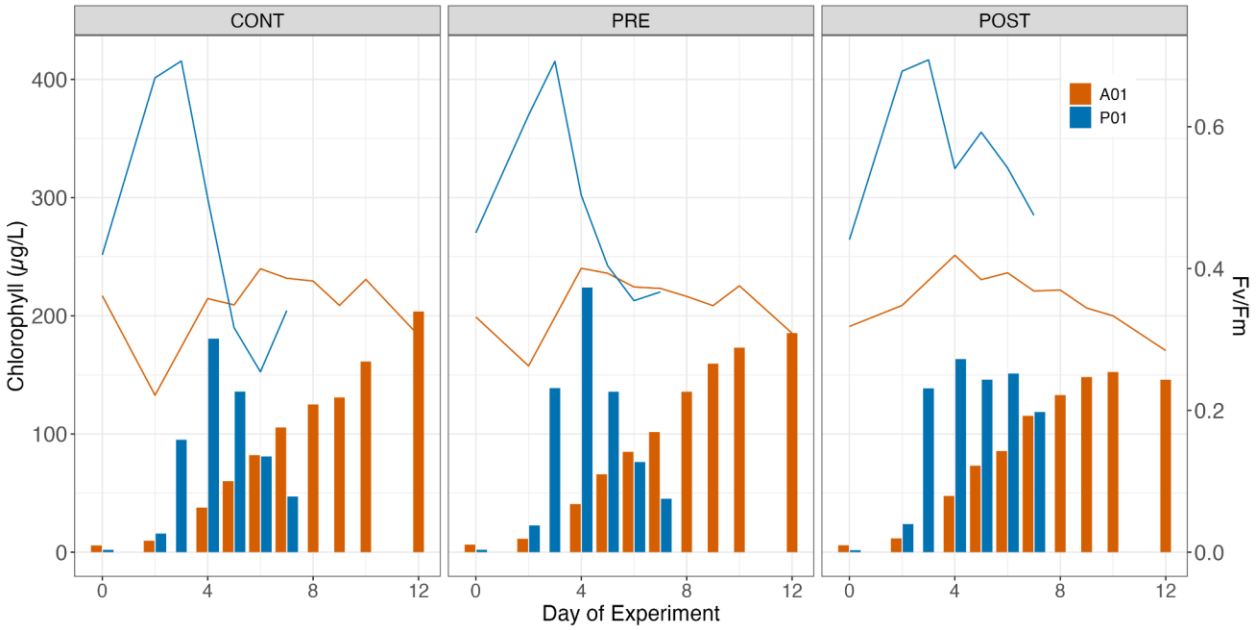

Figure 24. Concentrations of Chl-a (ug L^{-1}) represented by bars and Fv/Fm represented by lines as a function of day in the CONT, PRE, and POST treatments of the P. multiseries (P01) and A. catenella (A01) mesocosm experiments.

Higher rates of growth by *P. multiseries* compared with *A. catenella* was underscored by the much faster increase in cell abundance in the *P. multiseries* mesocosms (Figure 25). Rates of growth calculated based on change in cell abundance during the exponential phase demonstrated that *P. multiseries* grew at a rate of 1.3-1.4 d^{-1} which was 3 to 3.4-fold faster than *A. catenella* depending on the treatment (Table 9). This rate of growth is not only fast for diatoms overall (e.g. Berg et al. 2017), but also more than 60% faster growth than a previously published study of several strains of *P. multiseries* cultured at 20°C (Thessen et al. 2009). Concomitant with increased cell abundance, there was an increase in Chl-a per cell in *P. multiseries* from approximately 2 to 11 pg $Cell^{-1}$ in the control, from 2 to 7 pg $Cell^{-1}$ in the PRE and from 2 to 5 in the POST treatments over the exponential growth phase (Figure 25). In contrast, there was a slow decrease in Chl-a $Cell^{-1}$ across all the treatments from a high of 16-19 pg $Cell^{-1}$ over the exponential growth phase between days 2-8 in *A. catenella*. The higher concentration of Chl-a $Cell^{-1}$ in *A. catenella* compared with *P. multiseries*, i.e. 4-fold greater on day 4 of the experiments, explains why Chl-a concentrations attained by the end of the experiments were similar between the two species despite greater cell abundances for *P. multiseries* compared with *A. catenella*.

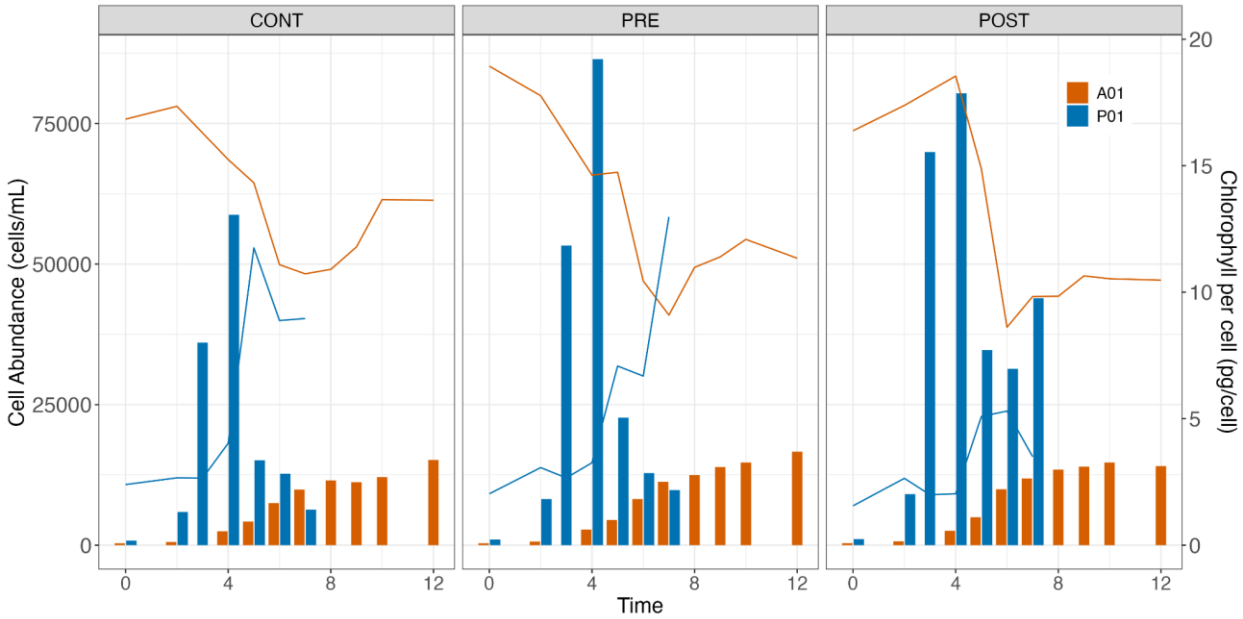

Figure 25. Cell abundance (cells mL^{-1}) represented by bars and Chl-a per cell (pg $cell^{-1}$) represented by lines as a function of day in the CONT, PRE, and POST treatments of the P. multiseries (P01) and A. catenella (A01) mesocosm experiments.

Table 9. Means and standard deviations (STD) of growth rates (d^{-1}) based on changes in cell abundance in individual mesocosms. Rates of NO_3 and PO_4 uptake (µmol L^{-1} d^{-1}) based regressions of nutrient concentrations (µmol L^{-1}) as a function of time (d) using data from triplicate mesocosms.

Parameters	P. multiseries			A. catenella		
	CONT	PRE	POST	CONT	PRE	POST
	Growth rates (d^{-1})					
Mean	1.29	1.38	1.37	0.39	0.45	0.45
STD	0.06	0.04	0.07	0.03	0.08	0.05
	Nitrate uptake (µmol L^{-1} d^{-1})					
Slope/uptake	45.6	55.8	90.1	41.3	38.8	43.3
R2	0.96	0.75	0.78	0.989	0.87	0.969
p value	7.76E-10	2.90E-05	2.90E-05	< 2.2e-16	3.16E-11	< 2.2e-16
	Phosphate uptake (µmol L^{-1} d^{-1}1)					
Slope/uptake	3.3	4.7	5.6	2.4	2.5	2.5
R2	0.53	0.74	0.78	0.97	0.93	0.83
p value	2.67E-02	2.90E-03	1.74E-03	7.31E-11	5.22E-09	2.82E-06

The sharp decrease in cell abundance for the *P. multiseries* experiment after day 4 (Figure 25) suggested that a limitation developed in the culturing media. Examining changes in nutrient concentrations, both PO_4 and Si decreased by day 4 (Figure 26). However, PO_4 was not drawn down completely, and increased in tandem with cessation of uptake by the cultures when they became limited. In contrast, Si was depleted from the media in the CONT and PRE treatment and remained depleted for the remainder of the time course (Figure 26). In the POST treatment, initial Si concentration was greater than in the other treatments and Si was not completely depleted by day 4. This was also the treatment where *P. multiseries* cell abundance remained relatively consistent and decreased less severely after day 4 of the experiment (Figure 25, Figure 26). Based on the changes in nutrient concentrations, it appeared the *P. multiseries* CONT and the PRE treatment became limited by Si on day 4. Limitation by Si was less pronounced in the POST treatment (Figure 26).

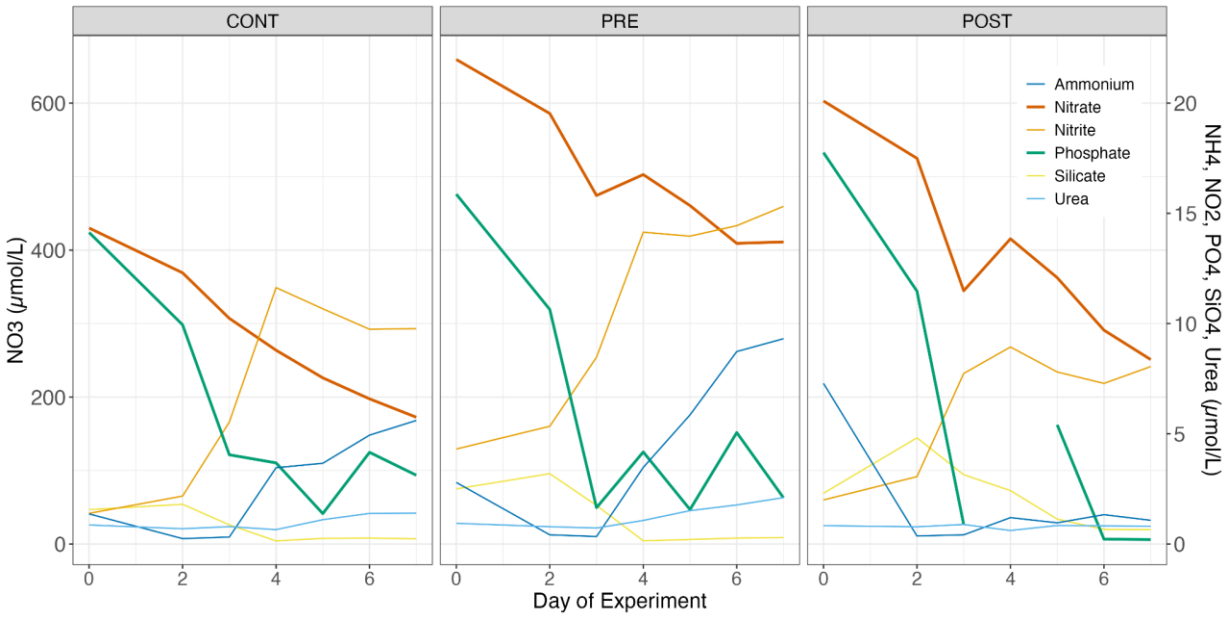

Figure 26. Changes in mean concentrations of NO_3 and Si (µmol L-1; primary y-axis), and PO_4, NO_2, NH_4, and urea (µmol L^{-1}; secondary axis) as a function of day of the experiment in the CONT, PRE, and POST P. multiseries mesocosms.

While multiple sources of nitrogen were present in the *P. multiseries* experiment, starting concentrations of NH_4 and urea in the PRE and POST treatments were very low, underscoring that the principal source of nitrogen in the agricultural effluent was NO_3 (Figure 26). During the first day or two, NH_4 was depleted across all treatments but then started to accumulate as cells went into Si-limited growth on day 3, as confirmed by the sharp decrease in F_v/F_m on day 3 (Figure 24). After day 4, NH_4 appeared to be regenerated and taken up simultaneously in the CON and POST treatment, with uptake lagging regeneration in the PRE treatment. Concentrations of NO_2 increased across the CONT, PRE, and POST treatments, possibly produced from reduction of NO_3, until day 4 after which concentrations reached a plateau or decreased suggesting NO_2 was being depleted at a faster rate than it was being produced. After day 4, several sources of nitrogen appeared to be consumed simultaneously including NO_3, NO_2,

and NH_4. Concentrations of urea in the mesocosms were too low to discern meaningful changes over time but did not appear to decrease (Figure 26).

Concentrations of NH_4 and urea in the PRE and POST treatments were also low relative to concentrations of NO_3 in the *A. catenella* experiment (Figure 27). Growth was slower for *A. catenella* and so was both NO_3 and PO_4 draw-down compared with that for *P. multiseries* (Table 9). As a result, the *A. catenella* mesocosms became nutrient-limited 4 days later than the *P. multiseries* mesocosms. Because PO_4 concentrations were depleted first at day 8 (Figure 27), it was inferred that growth became phosphorus-limited on day 8. Nutrient-limited growth was corroborated by concentrations of POC and PON per cell which increased after day 8 in the *A. catenella* treatments suggesting that cell division had slowed down. With respect to *P. multiseries*, increases in POC and PON per cell were observed after day 4 (Figure 28). In addition to P-limitation, the *A. catenella* cultures appeared to also become N-limited on day 9 when Chl-a concentrations had reached approximately 150 ug L^{-1} and no further biomass doublings could occur using NO_3 as the source of N for growth. Urea was only utilized after day 9, and, when urea concentrations were depleted on day 10, NO_2 concentrations were drawn down. This order of draw-down suggested NO_2 was the least preferred N substrate for *A. catenella*. This HAB species appeared to prefer NH_4, followed by NO_3, as sources of N for growth, with urea and NO_2 taken up only in the absence of the former sources and during N-limitation.

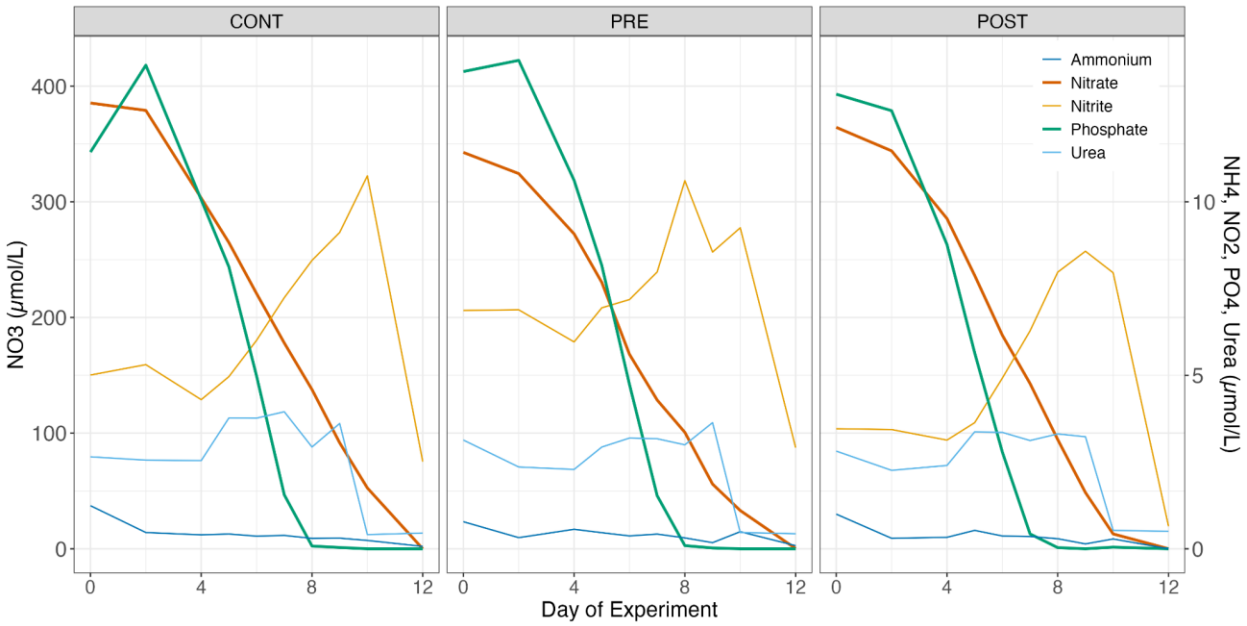

Figure 27. Changes in mean concentrations of NO_3 (µmol L-1; primary y-axis), and PO_4, NO_2, NH_4, and urea (µmol L^{-1}; secondary axis) as a function of day of the experiment in the CONT, PRE, and POST A. catenella mesocosms.

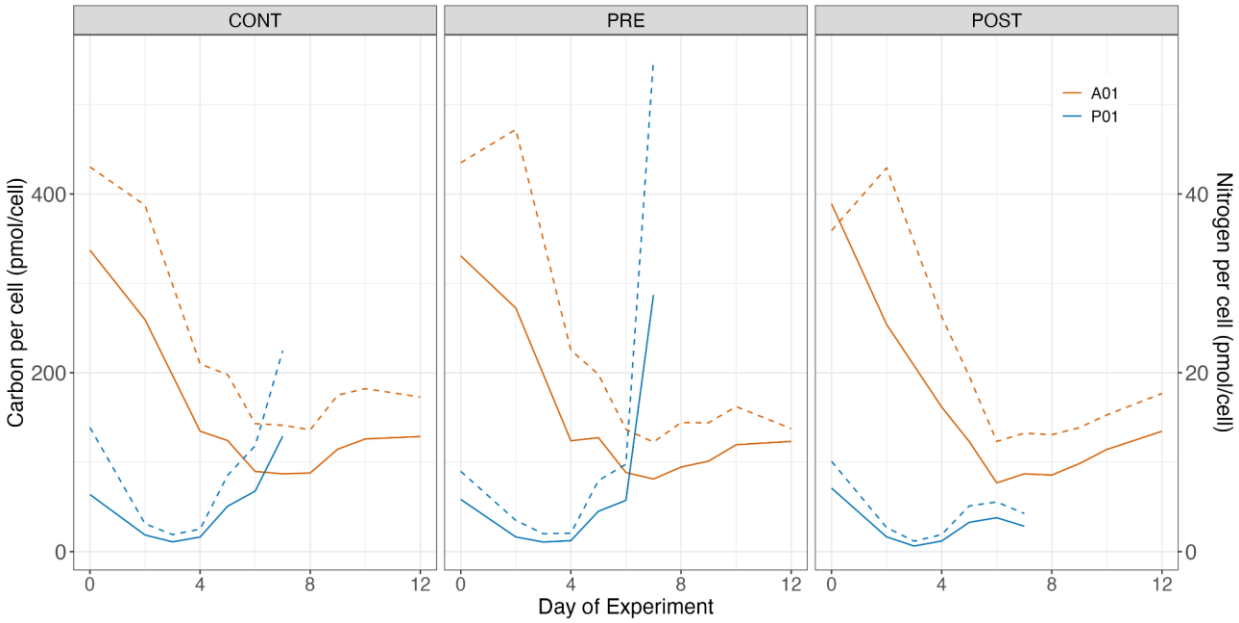

Figure 28. Change in particulate organic carbon (solid line) and particulate organic nitrogen (dashed line) per cell (pmol Cell^{-1}) as a function of day of the experiment during the P. multiseries (P01) and A. catenella (A01) mesocosm experiments.

In addition to a change in carbon and nitrogen content of the cells of both *P. multiseries* and *A. catenella* with onset of nutrient-limited growth, the *P. multiseries* cultures also started to produce domoic acid (pDA). Production of pDA only began after day 4 (CON and POST) or day 3 (PRE) of the time course indicating that DA production coincided with onset of nutrient limitation (Figure 24, Figure 29). While concentration of DA accumulated to the greatest extent in the POST treatment, pDA production normalized per cell was greatest in the CONT (Figure 29). Previous studies on production of pDA toxin in batch cultures by *Pseudo-nitzschia* species and strains demonstrate that it mainly occurs during lag phase, triggered by P- or Si limitation, when N is still available and at non-limiting concentrations (e.g. Subba Rao et al. 1980, Bates 1998, Kotaki et al. 1999, Lundholm et al. 2004). This was very similar to our cultures where nitrogen was plentiful at the time that the cultures went into Si-limited growth. The pattern of pDA concentration in the POST treatment also suggested that pDA production increases with degree of nutrient limitation as long as the cells were not so limited that they started going into cell death. The pDA concentrations measured here, with maximum concentrations varying from 0.5 to 1.5 pg Cell^{-1}, were similar to previous studies where maximum concentrations have been found to vary from 1.6 to 4.2 pg Cell^{-1} (Bates et al. 1993, Thessen et al. 2009).

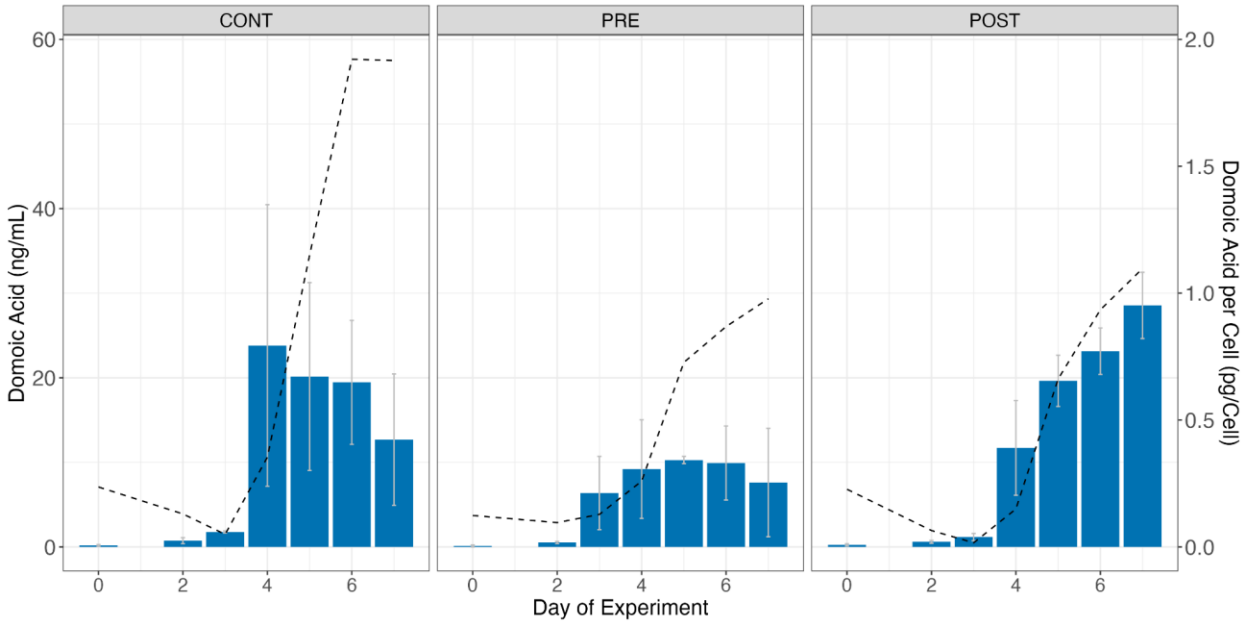

Figure 29. Domoic acid (ng/mL; primary y-axis), and domoic acid per cell (pg/cell; secondary axis) over the course of the P. multiseries mesocosm.

Summary

A comparison of growth of two HAB species in mesocosm batch cultures demonstrated that the diatom *P. multiseries* had on average a 3 times faster growth rate than the dinoflagellate *A. catenella*. Both HAB species grew well on two different kinds of agricultural effluent as the sole source of nitrogen, one source that was raw untreated effluent and another source that was treated by passing it through a woodchip bioreactor. In both types of agricultural effluent, NO_3 was the primary source of nitrogen. While final cell abundances were greater for *P. multiseries* compared with *A. catanella*, the maximum cell abundances attained within each species by the end of the incubations were similar across the two sources of effluent suggesting they supported growth equally well. However, the onset of nutrient limitation and ensuing decrease in cell abundance was less when supplied with treated compared with untreated agricultural effluent for *P. multiseries*.

Both of the HAB species tested here evidenced nutrient limited growth. For *P. multiseries* Si was the primary limiting nutrient while for *A. catenella*, it was phosphorus followed by nitrogen a day later. *A catenella* utilized NH_4 and NO_3 as sources of N for growth during exponential phase growth and only utilized urea, and secondarily NO_2, during nitrogen-limited growth. *P. multiseries*, which did not experience nitrogen-limited growth, utilized NH_4 and NO_3 during exponential phase growth.

Offshore Transects

In order to examine and compare HAB species and non-HAB species responses to watershed nutrient loadings, phytoplankton biomass, community composition, and nutrient concentrations were monitored monthly along a nearshore transect in the vicinity of the point at which the Pajaro River discharges into Monterey Bay. While we had proposed to monitor fewer events in the vicinity of the mouths of both the Salinas River and Pajaro River, participating in monthly cruises in an already existing monitoring program established by the City of Watsonville afforded us a rare opportunity to examine the progression of HAB and non-HAB species across a larger temporal scale, i.e. the entire year. The advantages of participating in the Watsonville monitoring program were two-fold. First, we were not limited to a couple of months of sampling, and second, the Salinas River mouth is closed by a sand bank most of the year making it challenging to find a time when the river mouth is open. While the Pajaro River also experiences mouth closures through sand accretion, it remains open throughout most of the year due to natural riverine flushing (Kim et al. 2025). Closure events typically last only a few days in late winter and spring coincident with strong ocean wave events, and the longest closure events occur in summer or fall when strong wave events coincide with low streamflow (Kim et al. 2025).

The City of Watsonville transect sampling was part of a program to monitor fecal indicator bacteria and associated water quality parameters (water temperature, salinity, Chl-a) from surface water at eight stations (Figure 30). Stations 1-7, were located close to shore with stations 1-3 south of the Pajaro River mouth and stations 4-7 north of the Pajaro River mouth. Station 8 was located offshore directly above the outfall pipe of the City of Watsonville's wastewater treatment outfall, across from the River mouth (Figure 30).

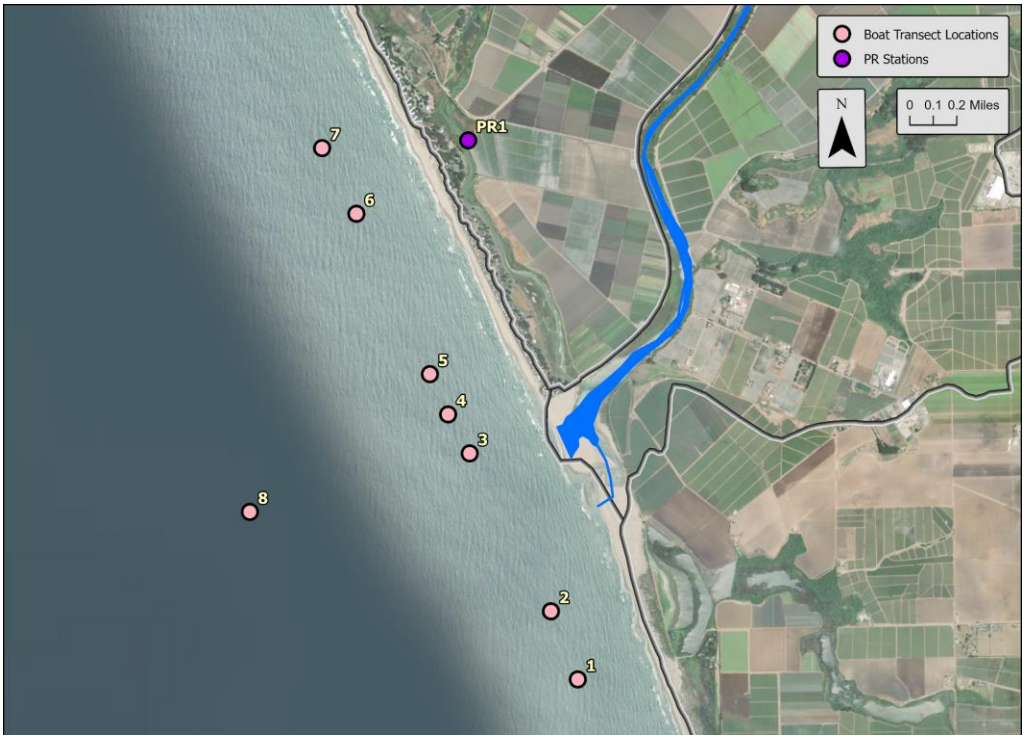

Figure 30. Offshore transect sample locations near the mouth of the Pajaro River.

Approach

We participated in twelve consecutive cruises from August 2022 through August 2023 (except the December 2022 cruise). During each cruise, samples were collected for phytoplankton enumeration, extracted Chl-a, nutrients (NH_4, NO_3, NO_2, urea, PO_4, and Si), particulate carbon and nitrogen, qPCR and toxin analyses. Whole water was collected from each station at the surface using a bucket and transferred to a cubitainer, which was kept in a cooler, for transport back to the lab. One cubitainer of water was collected from each station. Upon arrival at EBL, samples were immediately processed from each cubitainer as outlined briefly below (see above for the mesocosm experiments for more detailed protocols).

Briefly, 100 mL whole water sample was transferred to sterile glass bottle and preserved with 1% acidic Lugol's solution and stored in the dark for phytoplankton enumeration with a Sedgewick rafter counting chamber with an inverted microscope under 40x magnification (Alexis Scientific light microscope; Angstrom Sun Technologies Inc., Massachusetts, USA). During October's transect cruise, a paraformaldehyde preservative was used in a final concentration of 0.8% instead of Lugol's solution, for samples collected from stations 4, 5, and 6. Unfortunately, the paraformaldehyde disintegrated most of the samples and therefore we were not able to enumerate the phytoplankton community for those stations. For Chl-a, duplicate samples of 60-100 mL water was filtered onto Whatman GF/F filters, placed into cryovials, covered with aluminum foil, and stored at -80°C until analysis on a Trilogy Laboratory Fluorometer (Turner Designs). For nutrients, 60 mL samples were filtered through pre-combusted Whatman GF/F filters using a Swinnex filter holder and syringe directly into Falcon tubes. The filtrates in the Falcon tubes were frozen until analysis on a Lachat Quickchem 8000 Flow Injection Analyzer and the filters were dried overnight at 50°C and then stored in a dessicator until CHN analysis. Samples for qPCR were filtered onto 0.65 micron PVDF Durapore filter (Sigma-Aldrich) and stored at -80°C. Samples for particulate toxin were filtered onto two GF/F filters (50 mL each), placed into separate cryovials, and stored at -80°C until analysis.

Results

Seasonal Nearshore Phytoplankton Biomass

Nearshore phytoplankton biomass varied between "non-bloom" and "bloom" states (Figure 31). Chlorophyll concentrations during non-bloom months, which included January, February, March, May, September, and November, averaged 1.1 ± 0.7 µg L^{-1}. In April Chl-a concentrations increased at all stations and ranged from 4-8 µg L^{-1}. After a decrease to background concentrations in May, phytoplankton biomass and Chl-a increased again in June to reach 16 µg L^{-1} at stations 3 and 4 bracketing the Pajaro River mouth, while ranging from 9-13 µg L^{-1} at the remaining stations. Concentrations of Chl-a decreased somewhat in July and August relative to June but remained above non-bloom concentrations before decreasing down to non-bloom concentrations in September (Figure 31). During the month of October there was a phytoplankton bloom that was focused between stations 4 through 7. At these stations, Chl-a concentrations varied from 24-54 µg L^{-1}. These concentrations are typical for fall HAB blooms (e.g. Schulien et al. 2017). During this month, the lowest Chl-a concentrations were observed at station 8, in the offshore region, suggesting the bloom was limited to and concentrated in the very nearshore area. Moreover, relatively low Chl-a concentrations were also observed at station 1

suggesting that the prevailing currents were moving in a northerly direction and sustaining the bloom north of the River discharge point.

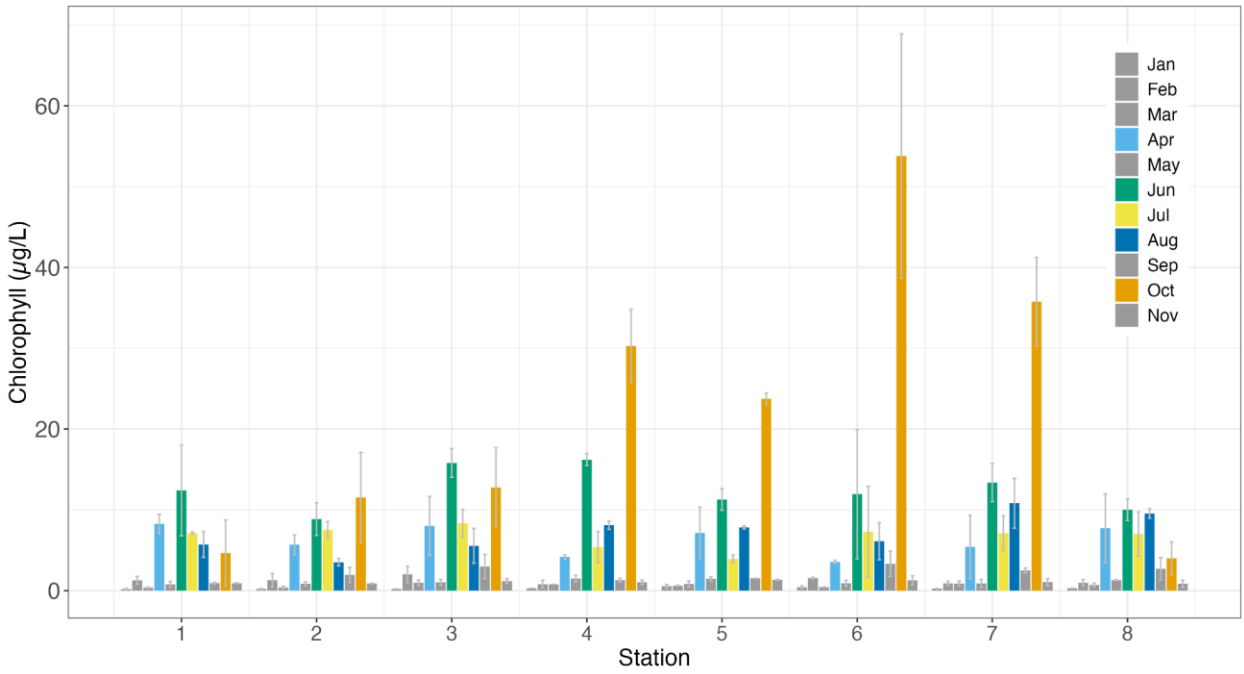

Figure 31. Mean (± standard deviation) Chl-a concentrations (µg L-1) as a function of station (1-8) and month along a nearshore transect (years 2022 and 2023) in the vicinity of the Pajaro River discharge into Monterey Bay. Grey bars represent months with no phytoplankton blooms and colored bars represent months with phytoplankton blooms.

Phytoplankton Community Composition

Composition of the phytoplankton communities varied substantially by month, both during the non-bloom and bloom states, across the year (Figure 32). The April spring bloom was dominated (i.e. 65-93% of community composition) by the diatom *Skeletonema* at 7 of the 8 stations (Figure 32). *Skeletonema*-dominated spring blooms are a usual occurrence and have been well-documented for Monterey Bay (Garrison 1979). The bloom in June was comprised of a mixed phytoplankton community consisting of three genera including *Prorocentrum* (19-30%), *Alexandrium* (23-29%), and *Pseudo-Nitzschia* (13-17%) across all 8 stations, with contributions of the diatom *Chaetoceros* (13-18%) at stations 1, 6 and 8. The community in the following two months was yet again different being mostly comprised (i.e. greater than 70% at all stations) by the diatom *Eucampia* (Figure 32). The bloom in October, which evidenced the greatest biomass accumulations, was composed almost entirely of the dinoflagellate HAB-former *Cochlodinium* (Figure 33). An increasing frequency of blooms of this species has occurred in Monterey Bay and in other locations along the California coast in the fall (Howard et al. 2012, Kudela and Gobler 2012).

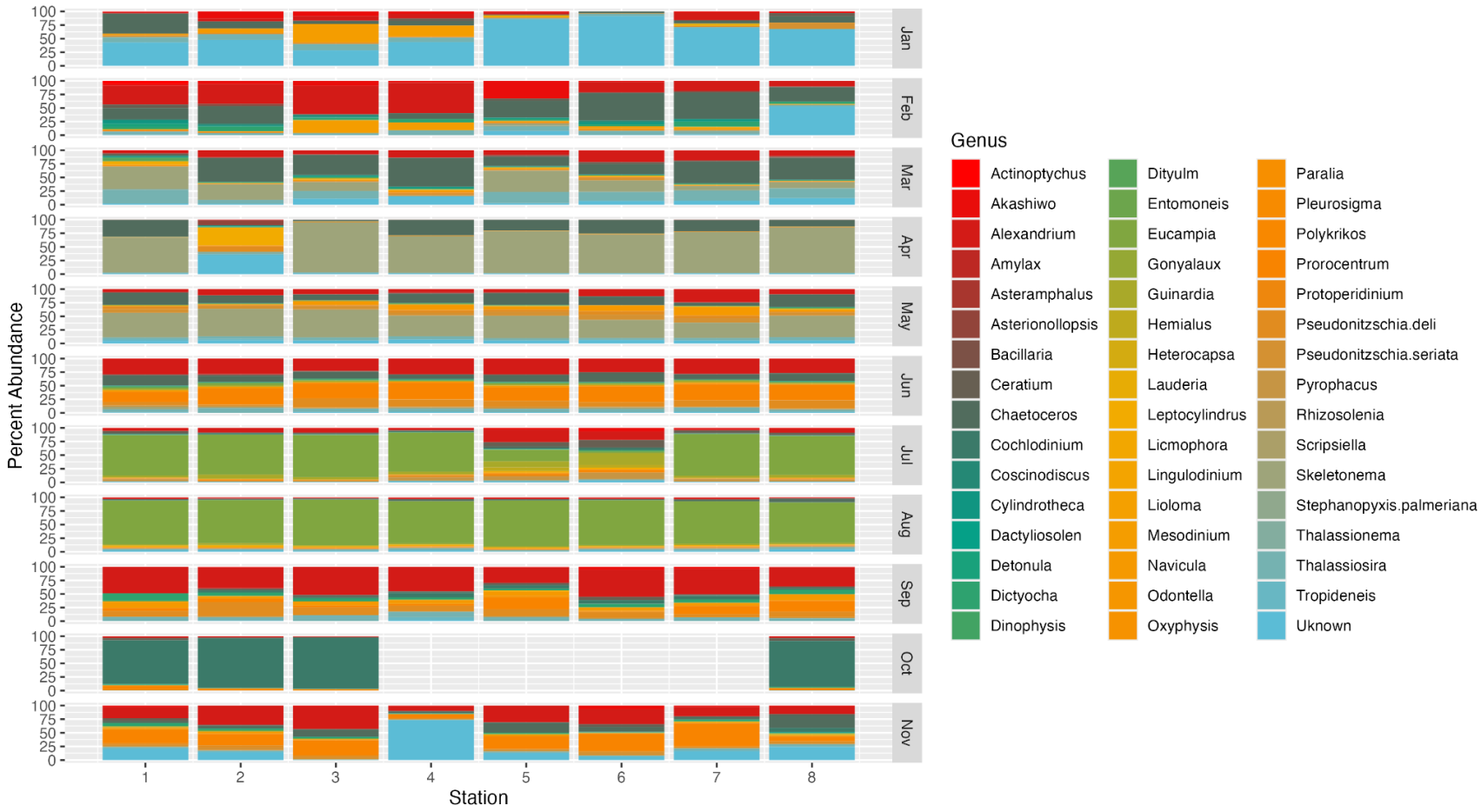

Figure 32. Phytoplankton community composition (percent of total station abundance) of phytoplankton visible at 40x magnification measured as a function of station (1-8) and month along a nearshore transect (years 2022 and 2023) in the vicinity of the Pajaro River discharge into Monterey Bay.

At the stations with lower overall phytoplankton biomass in October, including stations 1, 2 and 3, *Cochlodinium* comprised 80-94% of community composition (Figure 32). Unfortunately, a new preservative was tested for the enumeration samples collected from the stations with the greatest phytoplankton biomass (stations 4, 5, and 6) which disintegrated the sample before it could be counted. The stations north of the Pajaro River mouth discharge evidenced on average 4-fold higher biomass (as determined by Chl-a concentrations) than the stations south of the discharge (Figure 31). These stations were also dominated by *Cochlodinium* as corroborated by the phytoplankton enumerator (H. McGrath, *personal observation*).

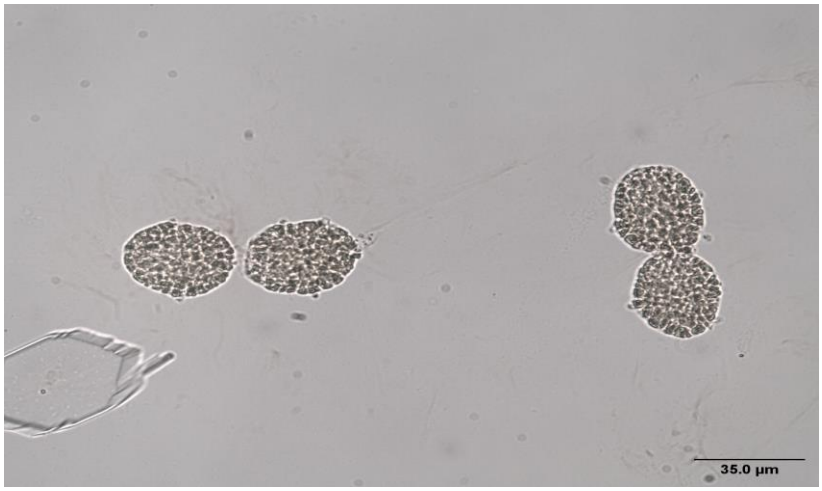

Figure 33. Cochlodinium cells imaged from the October, 2022 transect cruise. Photo credit: H. McGrath

Seasonal Nutrient Dynamics

Given the strong differences in phytoplankton communities composition according to month in the Monterey Bay nearshore, we wanted to examine the draw-down of nutrients to investigate whether there were any differences among bloom months. Our hypothesis was that since NO_3 is the primary N source to both offshore and nearshore waters, both during the upwelling period and in agricultural discharges, any draw-down in nutrients would mainly be proportional to phytoplankton biomass accumulation and that all measurable types of N would be depleted or reduced simultaneously.

Substantial depletions of NO_3, Si and PO_4 concentrations during the month of April, relative to concentrations in March (Figure 34, Figure 35), coincided with the April Spring bloom. Similar relative changes going from March to April were not observed in concentrations of urea (Figure 35). In June, concentrations of NO_3 remained low but concentrations of Si increased relative to the prior month (month of May). Concentrations of urea decreased substantially compared to concentrations in May suggesting the June bloom utilized all the available urea in the water column. In July nutrient concentrations were similar to June with the exception of Si which decreased substantially in July compared with June (Figure 34, Figure 35). During the month of October, NO_3, NO_2, and PO_4 completely disappeared from the water column. There was no decrease in urea concentration in October relative to September indicating that urea was not taken up and utilized during the month of October. Concentrations of NH_4 were at the limit of detection for the bloom months and low throughout the non-bloom months. Transient, high concentrations

(i.e. 10-20 µmol L^{-1}) were occasionally observed during non-bloom months at station 8 which was above the Watsonville outfall (Figure 34).

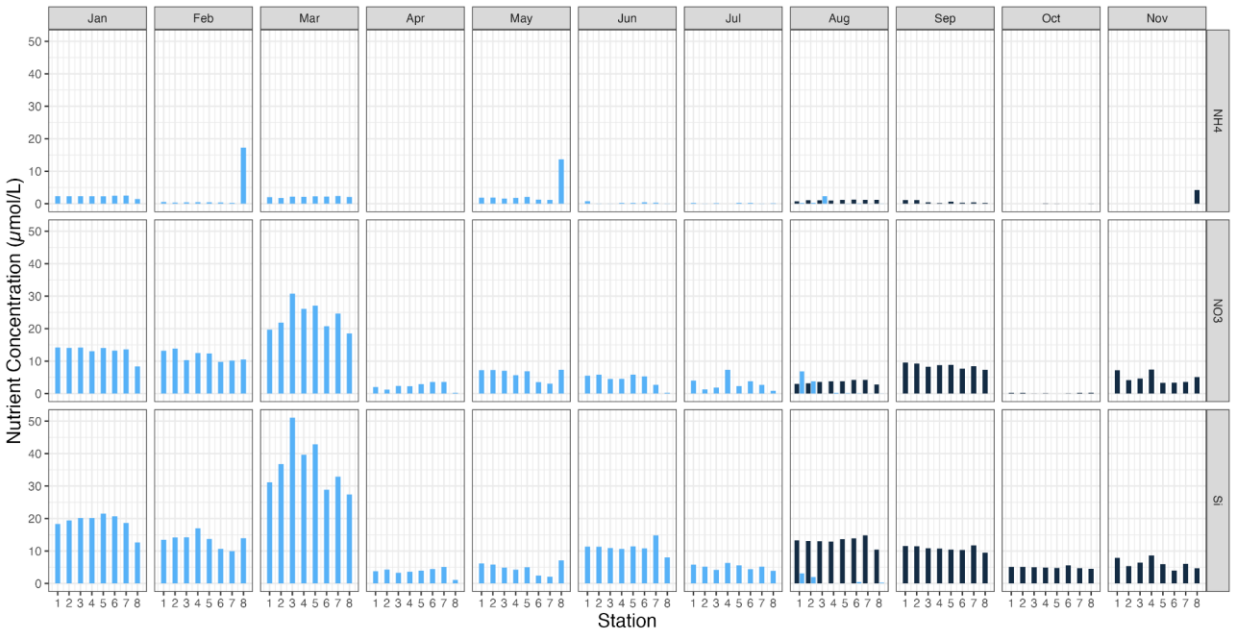

Figure 34. High-concentration nutrients including NH_4, NO_3 and Si (µmol L^{-1}) measured as a function of station (1-8) and month (Jan-Nov) along a nearshore transect (years 2022 and 2023) in the vicinity of the Pajaro River discharge into Monterey Bay. Blue bars are from 2022, and black bars are from 2023 (note the two August datasets are plotted together).

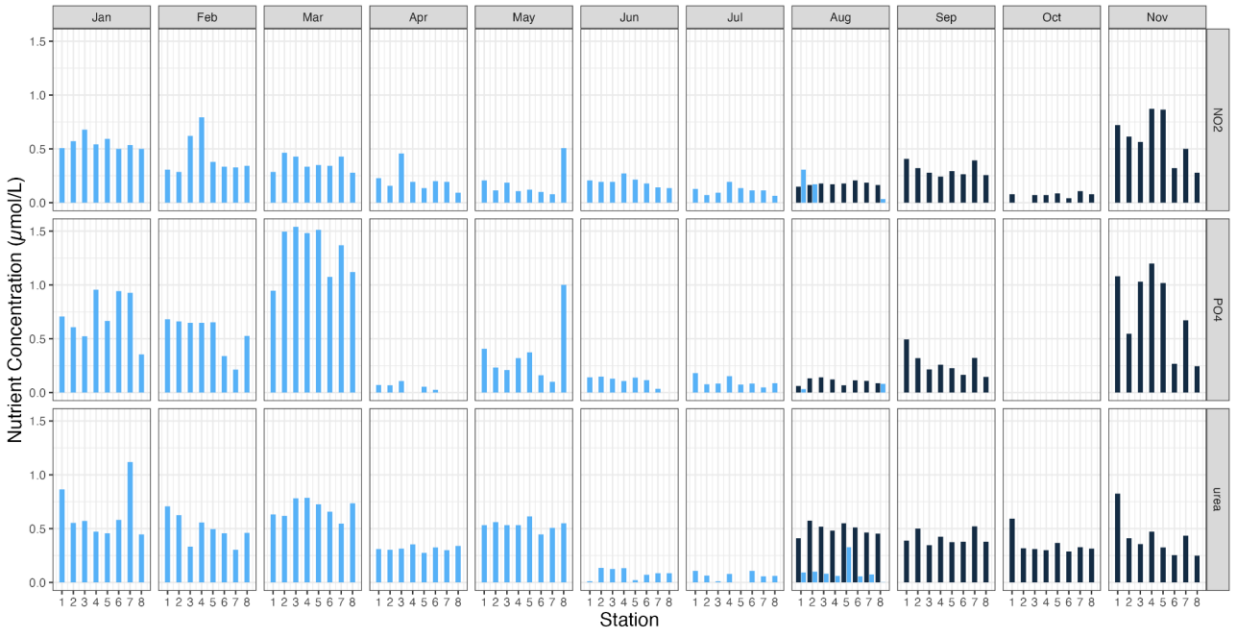

Figure 35. Low-concentration nutrients, including NO_2, PO_4 and urea (µmol L^{-1}) measured as a function of station (1-8) and month (Jan-Nov) along a nearshore transect (years 2022 and 2023) in the vicinity of the Pajaro River discharge into Monterey Bay. Blue bars are from 2022, and black bars are from 2023 (note the two August datasets are plotted together).

Summary

The spring bloom that occurred in April, as well as the July through August summer blooms, were dominated by non-HAB diatom species and depleted NO_3, Si, and PO_4 concentrations in the water column (Figure 34, Figure 35, Table 10). During these times, phytoplankton biomass was at similar levels at all stations, including the offshore station 8, suggesting no notable influence of riverine nutrient loading in bloom dynamics. During June, a mixed bloom of HAB species including both dinoflagellates and diatoms was also at similar levels at the nearshore stations (stations 1-7) and at station 8 offshore. However, the two nearshore stations bracketing the Pajaro River discharge (stations 3 and 4) had slightly greater phytoplankton biomass than the other nearshore stations suggesting potentially higher nutrient concentrations at those stations supported the higher biomass. This summer bloom also depleted urea from the water column which remained at a lower concentration compared with spring for the rest of the summer (Table 10).

The fall October *Cochlodinium* dinoflagellate bloom was focused in the area north of the Pajaro River discharge. Phytoplankton biomass in this nearshore region was 6-14 fold greater than in the offshore region at station 8. This phytoplankton biomass pattern suggested that the waters north in the transect better supported the bloom potentially due to greater nutrient concentrations in that area. This scenario is in accordance with the predominance of a northerly flow pattern during the fall period of upwelling relaxation when discharges from the Pajaro River, the Salinas River, and the Elkhorn Slough estuary are carried northward along the coast (Fischer et al. 2014, Kudela et al. 2014). The upwelling relaxation period and northerly current flow pattern coincides with high concentrations of nitrogen discharged by agricultural return flows and corresponding heavy nitrogen loads to the rivers (Fischer et al. 2014).

Table 10. Summary of bloom months, dominant phytoplankton genera, and nutrient depletions in the nearshore region.

Month	Dominant Phytoplankton	Nutrient Depletions				
April	*Skeletonema*	NO_3			Si	PO_4
June	*Prorocentrum, Alexandrium, Pseudo-nitzschia*	NO_3		Urea		PO_4
July - Aug	*Eucampia*	NO_3		Urea	Si	PO_4
October	*Cochlodinium*	NO_3	NO_2			PO_4

The fall *Cochlodinium* bloom was primarily supported by NO_3 as evidenced by the complete depletion of NO_3 in the water column (Figure 34, Table 10). Urea was not utilized during this bloom as evidenced by the lack of decrease in urea concentration compared with the previous month when there was no bloom and phytoplankton biomass was 30-fold lower. Whether the nutrient source to support phytoplankton blooms in the nearshore region originates primarily from upwelling or from riverine discharge, the main nitrogenous nutrient to support the growth of both HAB and non-HAB phytoplankton species appears to be NO_3. Concentrations of urea in the water column typically vary around 0.5 µmol L^{-1} and comprise 4% or less of the total dissolved nitrogen pool. Even when there is utilization of urea, as evidenced by a decrease in concentration, its starting concentration is so low that it can support a very minor fraction of the phytoplankton biomass during a bloom. Moreover, urea does not appear to play a role in blooms of non-HAB versus HAB species.

SYNTHESIS

Monterey Bay, home to one of the world's most diverse marine ecosystems, is part of the largest marine National Sanctuary on the West Coast of the US. Given high loadings of agriculturally derived nutrients, and the seasonal link with HAB event risks to marine life, our project had three overarching goals: 1) to gauge the efficacy of several different types of wetland treatment systems in removal of nitrogen-based nutrients from agricultural drainages, 2) to quantify loading of nitrogen from the agriculturally dominated watersheds and subwatersheds within Monterey Bay, and 3) to investigate the linkage between agriculturally derived nitrogen and HAB species responses.

In order to characterize the efficiency of different types of wetland treatment systems in removing nitrogen from nutrient-rich agricultural influent, we tested 8 treatment systems, including four wetlands and four bioreactors. Based on changes in concentrations of NO_3 in the inlet and outlet of the treatment systems, efficiencies of removal varied from 20-90% with an average removal efficiency of 68%. In experiments to test nitrogen removal efficiencies of specific treatment habitats (vegetated/unvegetated, shallow/deep, wetland/drainage channel) we found that the most efficient habitat with respect to nitrogen loss was a drainage channel followed by a shallow wetland. We also found that the addition of vegetation did not increase nitrogen loss from any of the tested habitats suggesting that sediment-associated microbial activity was primarily responsible for nitrogen loss from wetland habitats.

Nitrate was the primary substrate in the agricultural effluents tested here, comprising 81-99% of the total dissolved nitrogen pool. Only one source of effluent, collected from the Castroville Slough, contained measurable concentrations of NH_4 and urea, comprising close to 20% of the total nitrogen pool. For the other effluent sources, NO_3 comprised 94-99% of the total dissolved nitrogen pool suggesting that it is a safe assumption to base watershed loading calculations on NO_3 only. Using agricultural effluent collected from the Castroville Slough added to a variety of wetland habitats, lower efficiencies of removal were observed for NH_4 and urea compared with NO_3. While NO_3 was removed with 41-77% efficiency, NH_4 was removed with 6-62% efficiency, and urea was removed with 20-57% efficiency by the various wetland treatment habitats.

With respect to NO_3 loading from the two agriculturally influenced watersheds examined here, the Pajaro River watershed and the Gabilan/Salinas River watershed, we found that loads varied more than 30-fold based on season and on precipitation and water flows. Total NO_3 loads originating from the Pajaro River watershed, as estimated from station PR4 at Chittenden, varied from 770 kg d^{-1} in fall 2022, which was an average flow year, to 5700 kg d^{-1} in the fall of 2023 which was a high flow year. In comparison, loads of NO_3 from Tembladero Slough, a subset of the Salinas watershed, averaged 600-800 kg d^{-1} in the fall. Because interannual variability in water flows were greater in the Pajaro River compared with Tembladero Slough, our estimates show that when averaging spring and fall loads, NO_3 loads from the Pajaro River were 4-fold higher in a low flow year and over 30-fold higher in high flow year compared with loads from Tembladero Slough.

Despite higher overall loads coming from the Pajaro River watershed, we focused our investigation on potential nutrient treatment strategies in the Gabilan watershed, and on Tembladero Slough, for two main reasons. One, the flows in this region are primarily regulated by farm irrigation and pumping making the

flows predictable and easy to “catch” for treatment purposes. Also, loads are concentrated which is beneficial for treatment purposes. By examining incoming loads along Tembladero Slough we identified the bottom 5.4 km region (between station SR1 and SR6) as the section receiving the most nitrogen discharge and therefore contributing disproportionately to the NO_3 load from the Slough and from the region. We then calculated that the acreage of treatment wetland needed to reduce the loads in this region would be on the order of 50-230 acres. This scale of treatment wetland installation would make a large impact in terms of reducing nutrients from the Gabilan watershed, on a similar scale to reducing Pajaro River loads from the fall season in a low-flow year.

An interesting finding from our investigations into the nitrogenous composition of agricultural effluent in the Monterey Bay region was that it was principally composed of NO_3. Other sources such as NH_4 and urea were minor components, mainly below 6% of the total dissolved nitrogen pool. This means that when fertilizer is applied on fields as urea, for example as liquid fertilizer termed fertigation, it will most likely be transformed to NO_3 before it enters waterways and becomes discharged into Monterey Bay. As a result, the quantity and timing of NO_3 loads are likely the most important for determining the link between agricultural discharges and phytoplankton blooms in Monterey Bay.

We investigated the growth of HAB phytoplankton species on agricultural effluent at a physiological scale in laboratory experiments and at the landscape-scale in transect studies in Monterey Bay. Our laboratory mesocosm experiments demonstrated that both treated and untreated agricultural effluent promoted growth of two toxin-producing HAB species, one diatom (*Pseudo-nitzschia*) and one dinoflagellate (*Alexandrium*). Both types of agricultural effluent promoted growth equally well compared with growth in a control containing pristine river water amended with nutrients. Growth was not impacted by the availability of different types of nitrogen as both species primarily utilized NO_3 during the exponential growth phase. The diatom grew 3-fold faster than the dinoflagellate due to intrinsic factors including a higher photosystem II photochemical efficiency. Production of domoic acid toxin by the diatom was triggered by nutrient limitation and increased with increasing limitation.

Nitrate was the primary source of nitrogen for growth of both HAB species tested here. The diatom primarily utilized NO_3, and also NH_4 before it was depleted, during the exponential growth phase. The dinoflagellate used NO_3, and also NH_4 before it was depleted, during the exponential growth phase and did not utilize urea or NO_2 until after it became nitrogen-limited. Most experiments that demonstrate utilization of urea by HAB species supply urea as the sole source of nitrogen in culture. Here we demonstrated for two HAB species that when supplied several sources of nitrogen simultaneously, as found in agricultural effluent, urea was only utilized after cells go into nitrogen limitation and is not a preferred source of nitrogen.

Monthly transect sampling in the nearshore region south and north of the Pajaro River discharge compared with the offshore region demonstrated that riverine nutrient inputs likely did not influence phytoplankton biomass accumulation and blooms in spring or summer. The primary source of nitrogen fueling both non-HAB and HAB responses in the nearshore region during this time was NO_3. Urea was a minor source of nitrogen in the nearshore, comprising 4% or less of the available nitrogen pool. During the fall season, the pattern of phytoplankton biomass accumulation changed and a bloom of the dinoflagellate HAB former *Cochlodinium* developed north of the Pajaro River discharge. Biomass of the bloom was up to 14-fold greater in the nearshore compared with the offshore region, and decreased in

density south of the Pajaro River mouth. This phytoplankton distribution was consistent with a northerly current flow pattern carrying high-concentrations of nitrogen discharged from the Pajaro River sustaining the bloom. The primary source of nitrogen fueling the bloom was NO_3. Despite depletion of NO_3 by the end of the bloom, urea concentrations did not change (i.e. decrease) suggesting *Cochlodinium* did not utilize urea.

Here we have demonstrated a link between agricultural effluent, accumulation of NO_3 in the nearshore coastal zone, and ensuing blooms of dinoflagellate HAB species, in Monterey Bay. This link was only evident in the fall season, i.e. not for spring or summer, highlighting the need for run-off treatment systems that can target regions and areas that contribute high nitrogen loads during the fall season to promote improvements in water quality in discharges and in Monterey Bay.

REFERENCES

(Ag Order 4.0) Central Coast Regional Water Quality Control Board. (2021). *General Waste Discharge Requirements for Discharges from Irrigated Lands*. Order No. R3-2021-0040.

(ACPF) Agricultural Conservation Planning Framework. (n.d.) *The framework*. U.S. Department of Agriculture. Retrieved August 5, 2025, from https://acpf4watersheds.org/the-framework/

Ashby, J. A., Bowden, W. B., & Murdoch, P. S. (1998). Controls on denitrification in riparian soils in headwater catchments of a hardwood forest in the Catskill mountains, USA. *Soil Biology and Biochemistry (United Kingdom)*, *30*(7). https://agris.fao.org/search/en/providers/122469/records/64775d78bc45d9ecdbc28805

Bates, S. S., Worms, J., & Smith, J. C. (1993). Effects of Ammonium and Nitrate on Growth and Domoic Acid Production by *Nitzschia pungens* in Batch Culture. *Canadian Journal of Fisheries and Aquatic Sciences*, *50*(6), 1248–1254. https://doi.org/10.1139/f93-141

Berg, G. M., Driscoll, S., Hayashi, K., Ross, M., & Kudela, R. (2017). Variation in growth rate, carbon assimilation, and photosynthetic efficiency in response to nitrogen source and concentration in phytoplankton isolated from upper San Francisco Bay. *Journal of Phycology*, *53*(3), 664–679. https://doi.org/10.1111/jpy.12535

Blankenberg, A.-G. B., Haarstad, K., & Søvik, A.-K. (2008). Nitrogen retention in constructed wetland filters treating diffuse agriculture pollution. *Desalination*, *226*(1), 114–120. https://doi.org/10.1016/j.desal.2007.01.237

Bowers, H. A., Ryan, J. P., Hayashi, K., Woods, A. L., Marin, R., Smith, G. J., Hubbard, K. A., Doucette, G. J., Mikulski, C. M., Gellene, A. G., Zhang, Y., Kudela, R. M., Caron, D. A., Birch, J. M., & Scholin, C. A. (2018). Diversity and toxicity of Pseudo-nitzschia species in Monterey Bay: Perspectives from targeted and adaptive sampling. *Harmful Algae*, *78*, 129–141. https://doi.org/10.1016/j.hal.2018.08.006

Bruun, J., Pugliese, L., Hoffmann, C. C., & Kjaergaard, C. (2016). Solute transport and nitrate removal in full-scale subsurface flow constructed wetlands of various designs treating agricultural drainage water. *Ecological Engineering*, *97*, 88–97. https://doi.org/10.1016/j.ecoleng.2016.07.010

Collos, Y., & Harrison, P. J. (2014). Acclimation and toxicity of high ammonium concentrations to unicellular algae. *Marine Pollution Bulletin*, *80*(1–2), 8–23. https://doi.org/10.1016/j.marpolbul.2014.01.006

Curtiss, C. C., Langlois, G. W., Busse, L. B., Mazzillo, F., & Silver, M. W. (2008). The emergence of Cochlodinium along the California Coast (USA). *Harmful Algae*, *7*(3), 337–346. https://doi.org/10.1016/j.hal.2007.12.012

Deng, D., Pan, Y., Liu, G., Liu, W., & Ma, L. (2020). Seeking the hotspots of nitrogen removal: A comparison of sediment denitrification rate and denitrifier abundance among wetland types with different hydrological conditions. *Science of The Total Environment*, *737*, 140253. https://doi.org/10.1016/j.scitotenv.2020.140253

Fischer, A. M., Ryan, J. P., Levesque, C., & Welschmeyer, N. (2014). Characterizing estuarine plume discharge into the coastal ocean using fatty acid biomarkers and pigment analysis. *Marine Environmental Research*, *99*, 106–116. https://doi.org/10.1016/j.marenvres.2014.04.006

Garrison, D. L. (1979). Monterey Bay phytoplankton I. Seasonal cycles of phytoplankton assemblages. *Journal of Plankton Research*, *1*(3), 241–265. https://doi.org/10.1093/plankt/1.3.241

Gordon Jr. (1969). Examination of methods of particulate organic carbon analyses. *Deep Sea Research*, *16*, 661–665.

Guillard, R. R. L. (1975). Culture of Phytoplankton for Feeding Marine Invertebrates. In W. L. Smith & M. H. Chanley (Eds.), *Culture of Marine Invertebrate Animals: Proceedings—1st Conference on Culture of Marine Invertebrate Animals Greenport* (pp. 29–60). Springer US. https://doi.org/10.1007/978-1-4615-8714-9_3

Hawkins, P. (2010). *Flow cytometry of Alexandrium catenella from Elkhorn Slough, California*. Moss Landing Laboratories.

Herrman, K. S., Bouchard, V., & Moore, R. H. (2008). Factors affecting denitrification in agricultural headwater streams in Northeast Ohio, USA. *Hydrobiologia*, *598*(1), 305–314. https://doi.org/10.1007/s10750-007-9164-4

Howard, M. D. A., Jones, A. C., Schnetzer, A., Countway, P. D., Tomas, C. R., Kudela, R. M., Hayashi, K., Chia, P., & Caron, D. A. (2012). Quantitative real-time polymerase chain reaction for *Cochlodinium fulvescens* (dinophyceae), a harmful dinoflagellate from California coastal waters[1]. *Journal of Phycology*, *48*(2), 384–393. https://doi.org/10.1111/j.1529-8817.2012.01120.x

Hunt J. W., Robinson S. M., Clark R. P., Endris C. A., Gregory J. N., Hammerstrom K. K., Null K. A. & O'Connor K. C. (2019). Storm Water Resource Plan for the Greater Monterey County Integrated Regional Water Management Region. California State Water Resources Control Board. 288 pp.

Jester, R. J., Baugh, K. A., & Lefebvre, K. A. (2009). Presence of Alexandrium catenella and paralytic shellfish toxins in finfish, shellfish and rock crabs in Monterey Bay, California, USA. *Marine Biology*, *156*(3), 493–504. https://doi.org/10.1007/s00227-008-1103-z

Krone, P., Clark, R., Adelaars, J., Leandro, M., Henson, A., Williamson, J., Bischel, H., Wrightwood, O., & Watson, F. (2022). Sizing an open-channel woodchip bioreactor to treat nitrate from agricultural tile drainage and achieve water quality targets. *Water Supply*, *22*(3), 2465–2477. https://doi.org/10.2166/ws.2022.007

Kudela, K., Anderson, C., Lucas, D., Caron, D., Jones, B., Sukhatme, G., Scholin, C., Ryan, J., Birch, J., Rajan, K., Smith, G., Chao, Y., & Doucette, G. (2014). A regional comparison of upwelling, coastal land use patterns, and HAB hotspots along the California coast. *Harmful Algae 2012, Proceedings of the 15th International Conference on Harmful Algae.*, 67–70.

Kudela, R. M., & Gobler, C. J. (2012). Harmful dinoflagellate blooms caused by Cochlodinium sp.: Global expansion and ecological strategies facilitating bloom formation. *Harmful Algae*, *14*, 71–86. https://doi.org/10.1016/j.hal.2011.10.015

Lefebvre, K. A., Bargu, S., Kieckhefer, T., & Silver, M. W. (2002). From sanddabs to blue whales: The pervasiveness of domoic acid. *Toxicon*, *40*(7), 971–977. https://doi.org/10.1016/S0041-0101(02)00093-4

Los Huertos, M., Gentry, L. E., & Shennan, C. (2001). Land Use and Stream Nitrogen Concentrations in Agricultural Watersheds Along the Central Coast of California. *The Scientific World Journal*, *1*(2), 856429. https://doi.org/10.1100/tsw.2001.315

McAlice, B. J. (1971). Phytoplankton sampling with the sedgwick-rafter cell1. *Limnology and Oceanography*, *16*(1), 19–28. https://doi.org/10.4319/lo.1971.16.1.0019

O'Geen, A. T., Budd, R., Gan, J., Maynard, J. J., Parikh, S. J., & Dahlgren, R. A. (2010). Chapter One—Mitigating Nonpoint Source Pollution in Agriculture with Constructed and Restored Wetlands. In D. L. Sparks (Ed.), *Advances in Agronomy* (Vol. 108, pp. 1–76). Academic Press. https://doi.org/10.1016/S0065-2113(10)08001-6

Powlson, D. S., & Addiscott, T. M. (2005). NITROGEN IN SOILS | Nitrates. In D. Hillel (Ed.), *Encyclopedia of Soils in the Environment* (pp. 21–31). Elsevier. https://doi.org/10.1016/B0-12-348530-4/00905-XReguera, B., Velo-Suárez, L., Raine, R., & Park, M. G. (2012). Harmful Dinophysis species: A review. *Harmful Algae*, *14*, 87–106. https://doi.org/10.1016/j.hal.2011.10.016

Rines, J. E. B., McFarland, M. N., Donaghay, P. L., & Sullivan, J. M. (2010). Thin layers and species-specific characterization of the phytoplankton community in Monterey Bay, California, USA. *Continental Shelf Research*, *30*(1), 66–80. https://doi.org/10.1016/j.csr.2009.11.001

Rosenfeld, L. K., Schwing, F. B., Garfield, N., & Tracy, D. E. (1994). Bifurcated flow from an upwelling center: A cold water source for Monterey Bay. *Continental Shelf Research*, *14*, 931–964. https://doi.org/10.1016/0278-4343(94)90058-2

Ruehl, C. R., Fisher, A. T., Huertos, M. L., Wankel, S. D., Wheat, C. G., Kendall, C., Hatch, C. E., & Shennan, C. (2007). Nitrate dynamics within the Pajaro River, a nutrient-rich, losing stream. *Journal of the North American Benthological Society*, *26*(2), 191–206. https://doi.org/10.1899/0887-3593(2007)26[191:NDWTPR]2.0.CO;2

Ryan, J. P., H. M. Dierssen, R. M. Kudela, C. A. Scholin, K. S. Johnson, J. M. Sullivan, A. M. Fischer, E. V. Rienecker, P. R. McEnaney, & F. P. Chavez (2005), Coastal ocean physics and red tides: An example from Monterey Bay, California. *Oceanography*, 18, 246–255.

Ryan, J. P., Gower, J. F. R., King, S. A., Bissett, W. P., Fischer, A. M., Kudela, R. M., Kolber, Z., Mazzillo, F., Rienecker, E. V., & Chavez, F. P. (2008). A coastal ocean extreme bloom incubator. *Geophysical Research Letters*, *35*(12), 2008GL034081. https://doi.org/10.1029/2008GL034081

Schulien, J., Peacock, M., Hayashi, K., Raimondi, P., & Kudela, R. (2017). Phytoplankton and microbial abundance and bloom dynamics in the upwelling shadow of Monterey Bay, California, from 2006 to 2013. *Marine Ecology Progress Series*, *572*, 43–56. https://doi.org/10.3354/meps12142

Seitzinger, S., Harrison, J. A., Böhlke, J. K., Bouwman, A. F., Lowrance, R., Peterson, B., Tobias, C., & Drecht, G. V. (2006). Denitrification Across Landscapes and Waterscapes: A Synthesis. *Ecological Applications*, *16*(6), 2064–2090. https://doi.org/10.1890/1051-0761(2006)016[2064:DALAWA]2.0.CO;2

Sharp, J. H. (1974). Improved analysis for “particulate” organic carbon and nitrogen from seawater. *Limnology and Oceanography*, *19*, 984–989.

Shea, R. E., & Broenkow, W. W. (1982). The role of internal tides in the nutrient enrichment of Monterey Bay, California. *Estuarine, Coastal and Shelf Science*, *15*(1), 57–66. https://doi.org/10.1016/0272-7714(82)90036-1

Thessen, A. E., Bowers, H. A., & Stoecker, D. K. (2009). Intra- and interspecies differences in growth and toxicity of *Pseudo-nitzschia* while using different nitrogen sources. *Harmful Algae*, *8*(5), 792–810. https://doi.org/10.1016/j.hal.2009.01.003

(USGS) U.S. Geological Survey. (2024). *USGS Pajaro River at Chittenden, CA* (Station 11159000). National Water Information System. Retrieved 2024, from https://waterdata.usgs.gov/monitoring-location/11159000/

(USGS) U.S. Geological Survey. (n.d). *How Streamflow Is Measured*. U.S. Department of the Interior. Accessed August 2023. https://www.usgs.gov/water-science-school/science/how-streamflow-measured.

Valderrama, J. C. (1981). The simultaneous analysis of total nitrogen and total phosphorus in natural waters. *Marine Chemistry*, *10*(2), 109–122. https://doi.org/10.1016/0304-4203(81)90027-X

Vymazal, J., Sochacki, A., Fučík, P., Šereš, M., Kaplická, M., Hnátková, T., & Chen, Z. (2020). Constructed wetlands with subsurface flow for nitrogen removal from tile drainage. *Ecological Engineering*, *155*, 105943. https://doi.org/10.1016/j.ecoleng.2020.105943

Wang, Z., King, K. L., Ramsdell, J. S., & Doucette, G. J. (2007). Determination of domoic acid in seawater and phytoplankton by liquid chromatography–tandem mass spectrometry. *Journal of Chromatography A*, *1163*(1–2), 169–176. https://doi.org/10.1016/j.chroma.2007.06.054

Welschmeyer, N. A. (1994). Fluorometric analysis of chlorophyll a in the presence of chlorophyll b and pheopigments. *Limnology and Oceanography*, *39*(8), 1985–1992. https://doi.org/10.4319/lo.1994.39.8.1985

Yan, X., Han, H., Li, X., Wen, J., Rong, X., Xia, Y., & Yan, X. (2024). Dissolved organic carbon and dissolved oxygen determine the nitrogen removal rate constant in small water bodies of intensive agricultural region. *Agriculture, Ecosystems & Environment*, *361*, 108822. https://doi.org/10.1016/j.agee.2023.108822

Zhang, W., Li, H., & Li, B. (2023). Whole-system estimation of hourly denitrification in a flow-through riverine wetland. *Journal of Hydrology*, *618*, 129132. https://doi.org/10.1016/j.jhydrol.2023.129132

PRESENTATIONS AND PUBLICATIONS

MBMNS Research Activity Panel meeting. “Water Quality Enhancement Projects in the Watershed and Capacity to Reduce Harmful Algal Blooms” (R. Clark, H. Bowers) March 11, 2022 (virtual).

Water & Ecosystems and Land & Groundwater Summer Meeting. R. Clark and H. Bowers hosted a PG&E wetland site visit for participants. June 16, 2022.

Bowers HA, Berg M, Pawlyk O, Fulkerson B, Turner J, O’Connor K, and Clark R. HAB Response to Agriculturally Derived Nutrient Loading. The 20th International Conference on Harmful Algae. Hiroshima, Japan. November 5 - 10, 2023 (oral).

EPA’s National Nutrient Management Team (NNMT) Monthly Call presentation. “Agricultural Nitrogen Loading and Cooperative Treatment Wetlands Links to Offshore Harmful Algal Blooms” (R. Clark) May 16, 2024 (virtual).

Water Quality Protection Program (WQPP) Committee Meeting. “Evaluating agricultural management practices benefiting the Monterey Bay: reducing nutrient loads and Harmful Algal Bloom (HAB) events” (H. Bowers, B. Fulkerson) September 4, 2025.

Graduate student Olivia Pawlyk has developed a related masters thesis from this work: “Impacts of Agricultural Microplastics on the Growth of Marine Phytoplankton in Monterey Bay”, and has presented the following:

Pawlyk O, Connolly T, Grand M, Krone P, Tinney C and Bowers H. Impacts of Agricultural Microplastics on the Growth of Marine Phytoplankton in Monterey Bay, California (USA). The 20th International Conference on Harmful Algae. Hiroshima, Japan. November 5 - 10, 2023 (poster).

Also presented to: Water Quality Protection Program (WQPP) Committee Meeting. March 6, 2025.

Acknowledgments:

We would like to thank Olivia Pawlyk for assistance in running the mesocosm experiments, participating in the City of Watsonville Wastewater cruises, and sample analysis. We also thank Hannah McGrath for running qPCR and domoic acid samples. Thank you to R. Kudela and K. Negrey (UC Santa Cruz) for toxin extraction training and performing domoic acid analysis on LC-MS.

APPENDIX A: TREATMENT SYSTEM EFFICIENCY

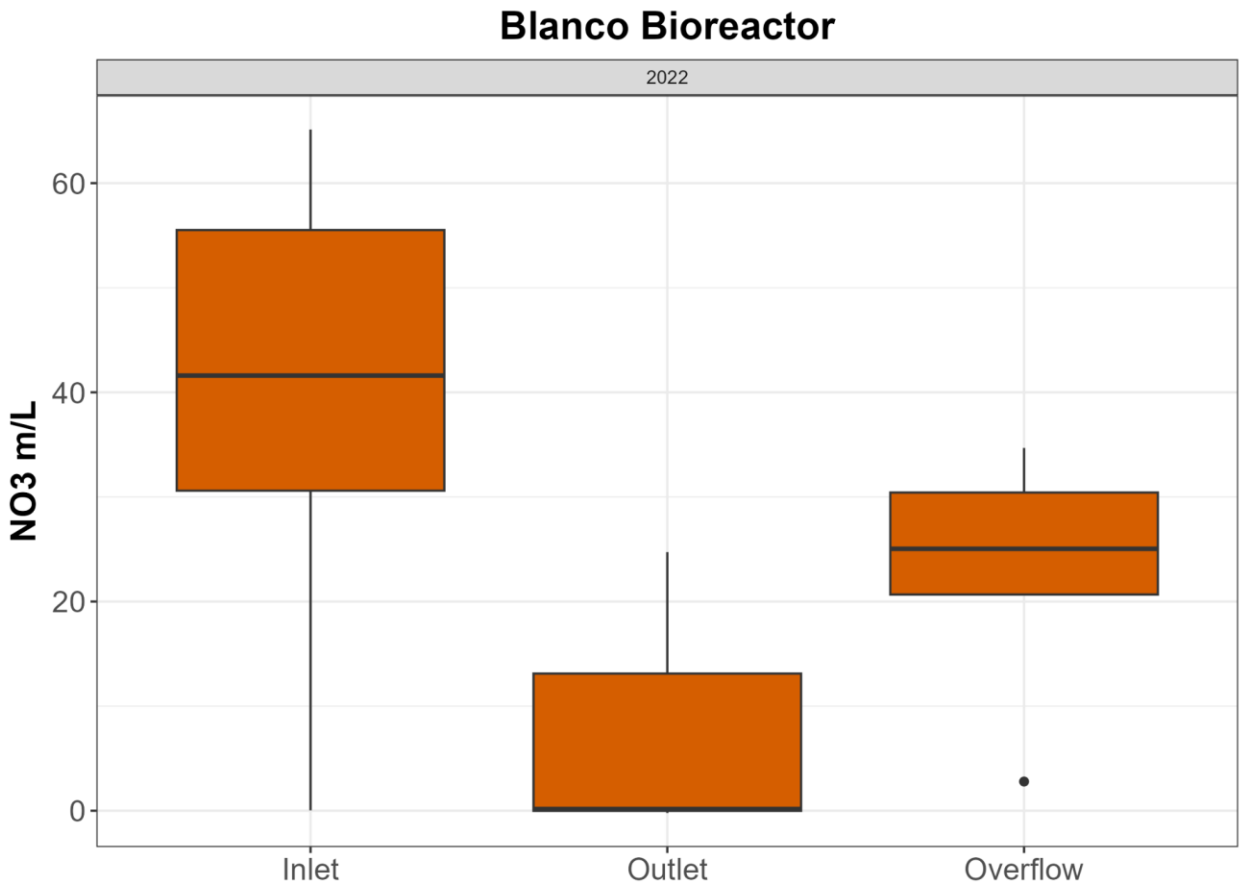

Figure A-1. Spread of concentrations sampled in the Blanco Bioreactor.

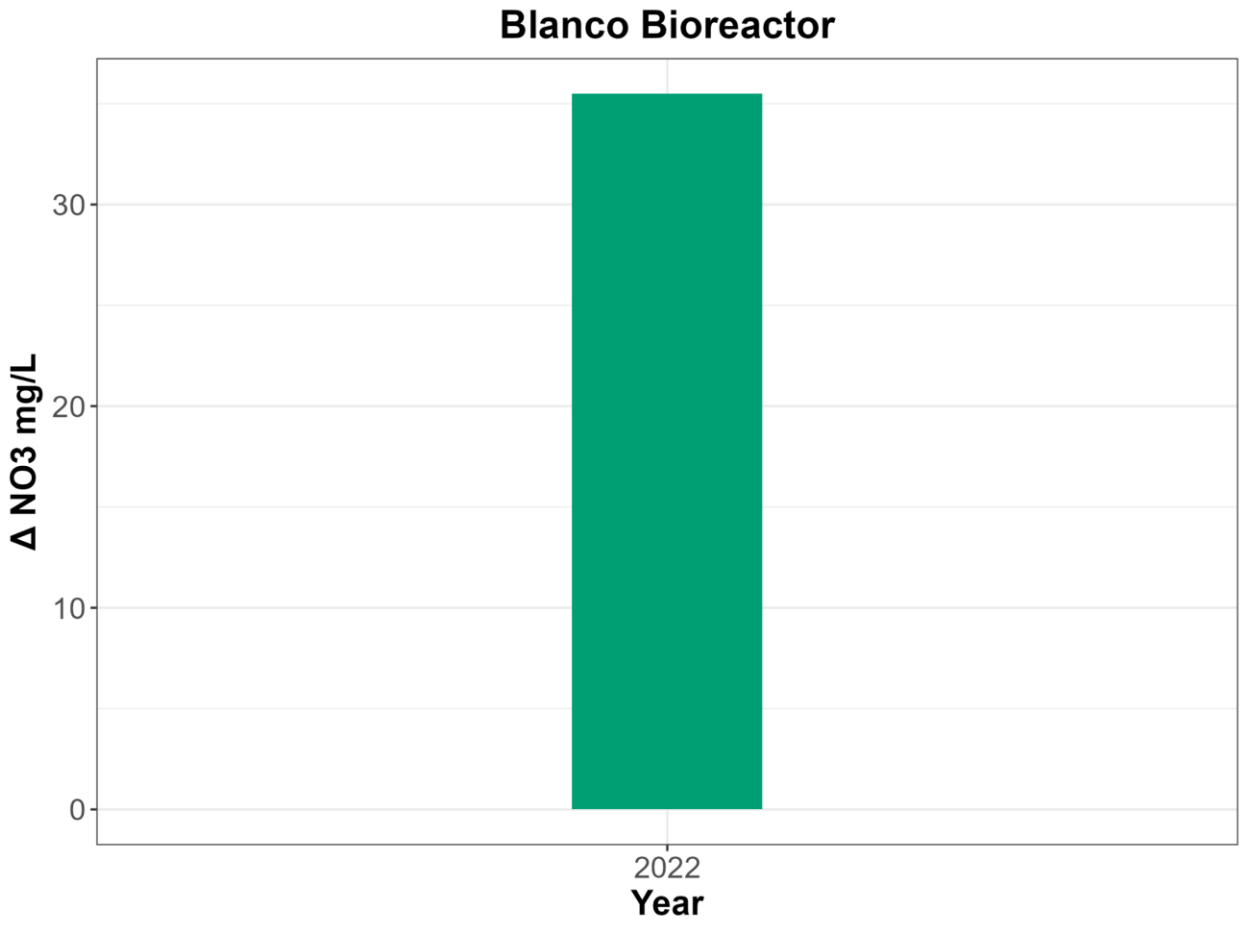

Figure A-2. Mean NO_3 reduction from inlet to outlet in the Blanco Bioreactor.

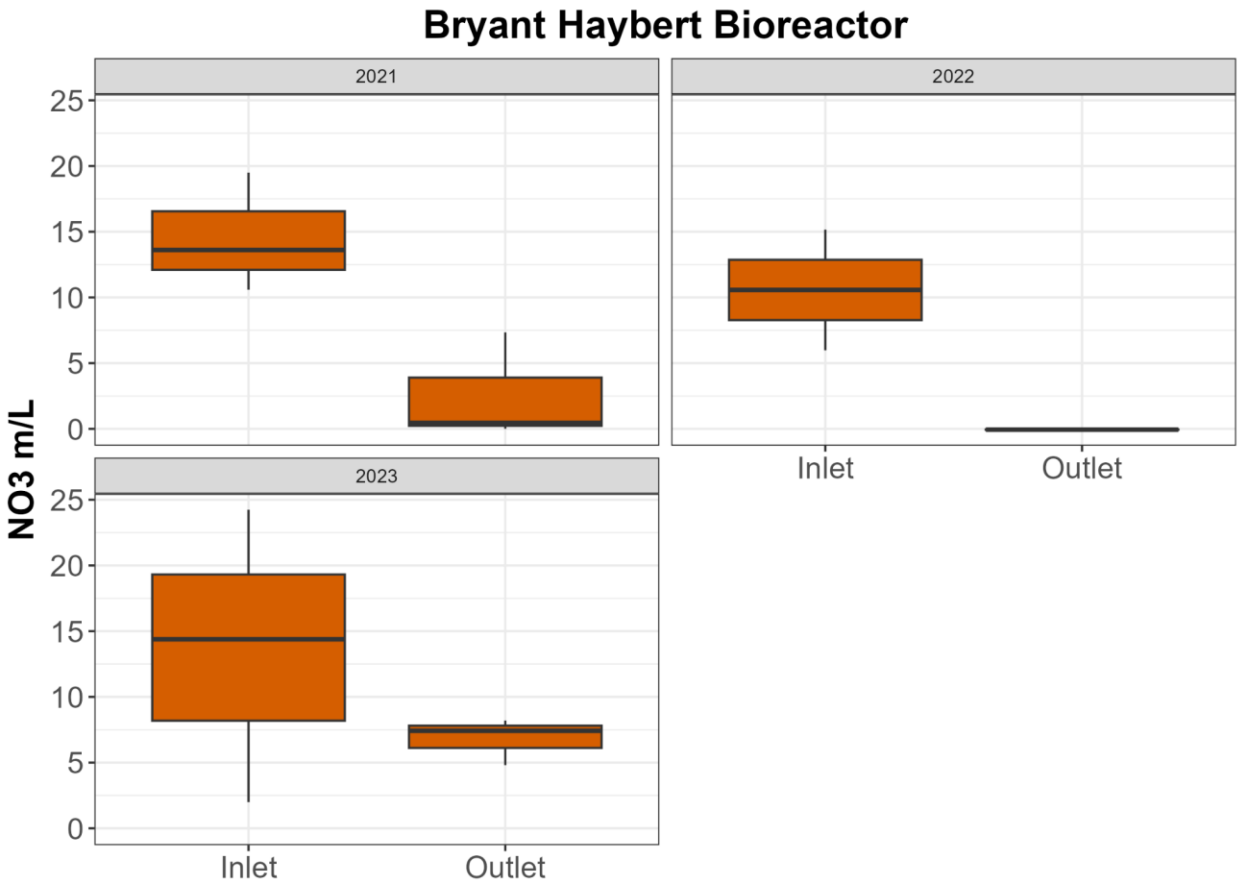

Figure A-3. Spread of concentrations sampled in the Bryant Haybert Bioreactor by year.

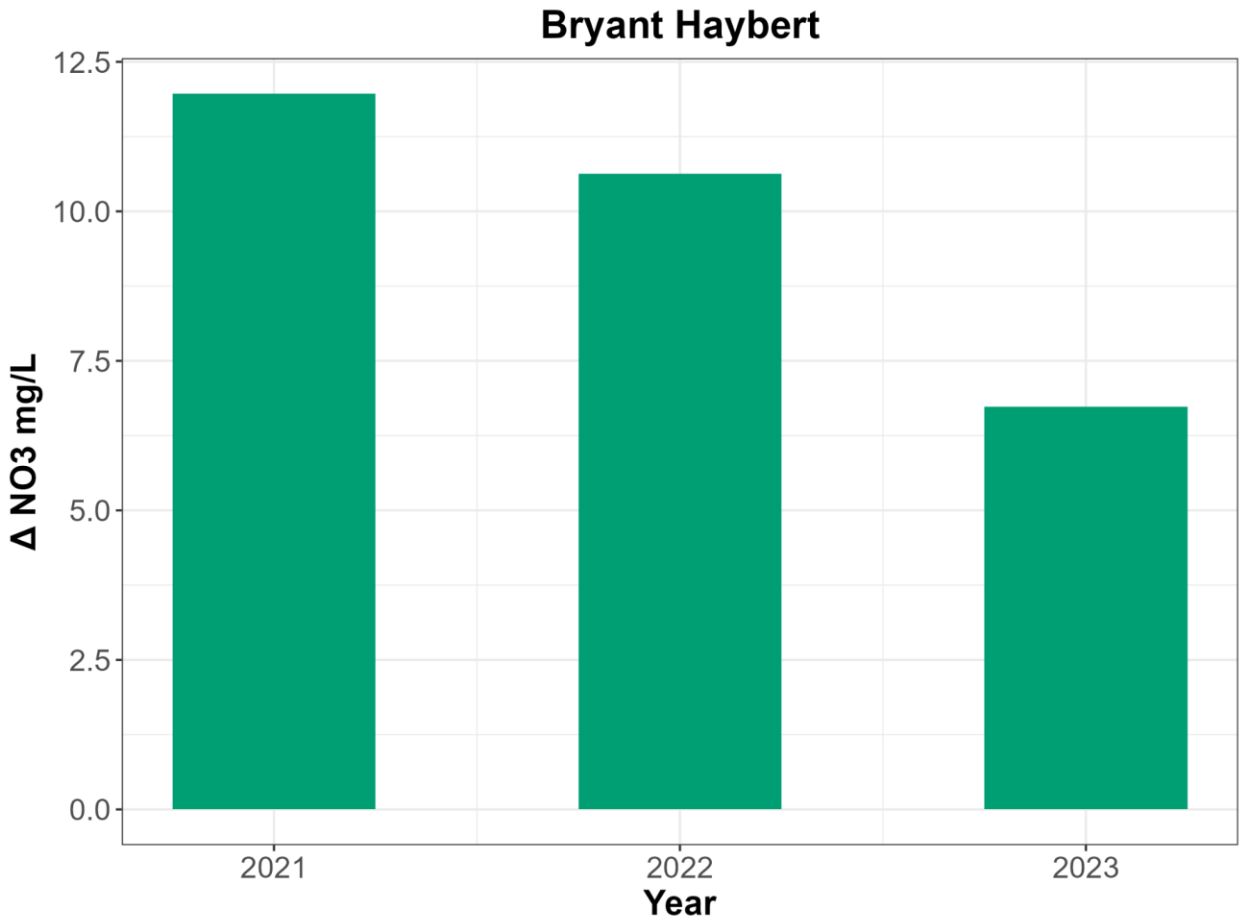

Figure A-4. Mean NO_3 reduction from inlet to outlet for each year in the Bryant Haybert Bioreactor.

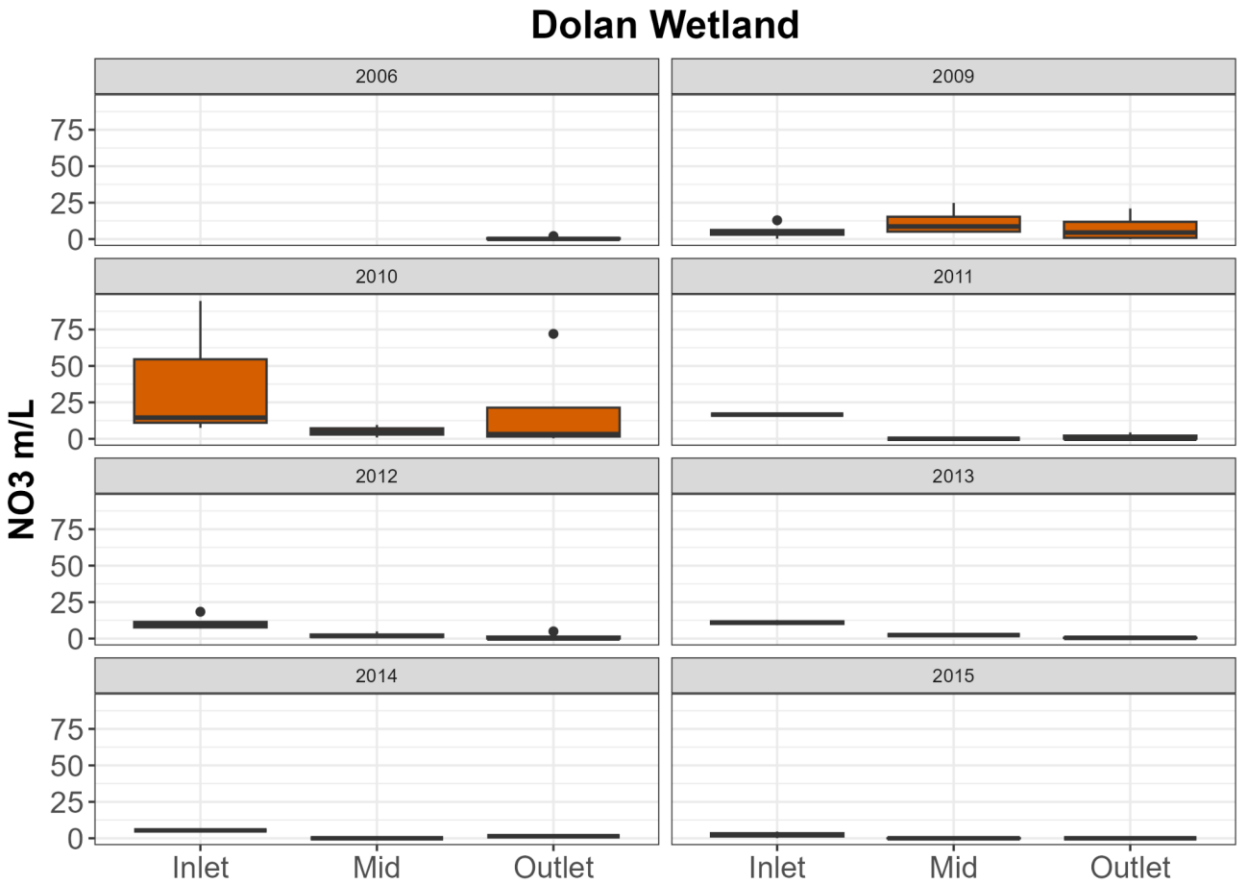

Figure A-5. Spread of concentrations sampled in the Dolan Wetland by year.

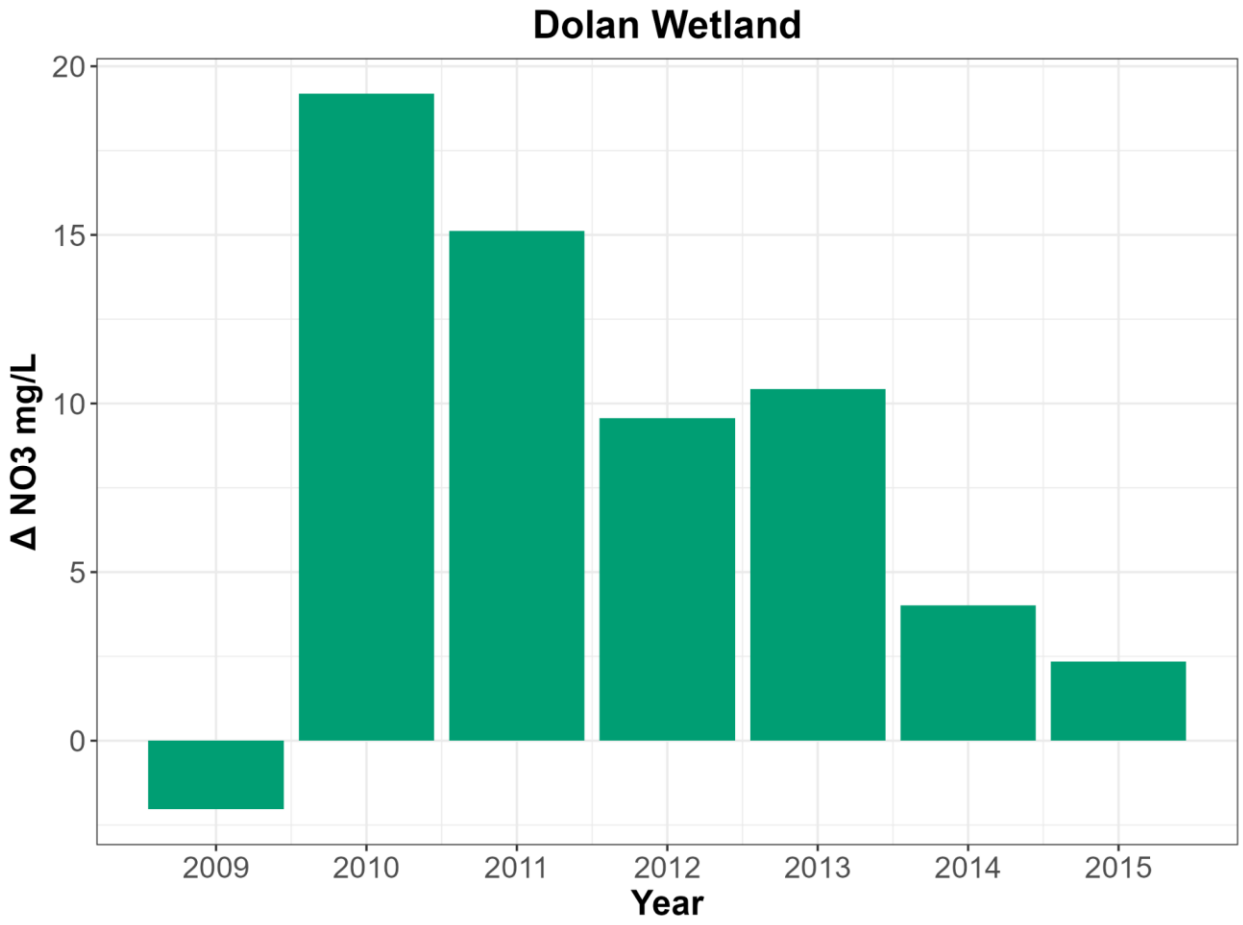

Figure A-6. Mean NO_3 reduction from inlet to outlet for each year in the Dolan Wetland.

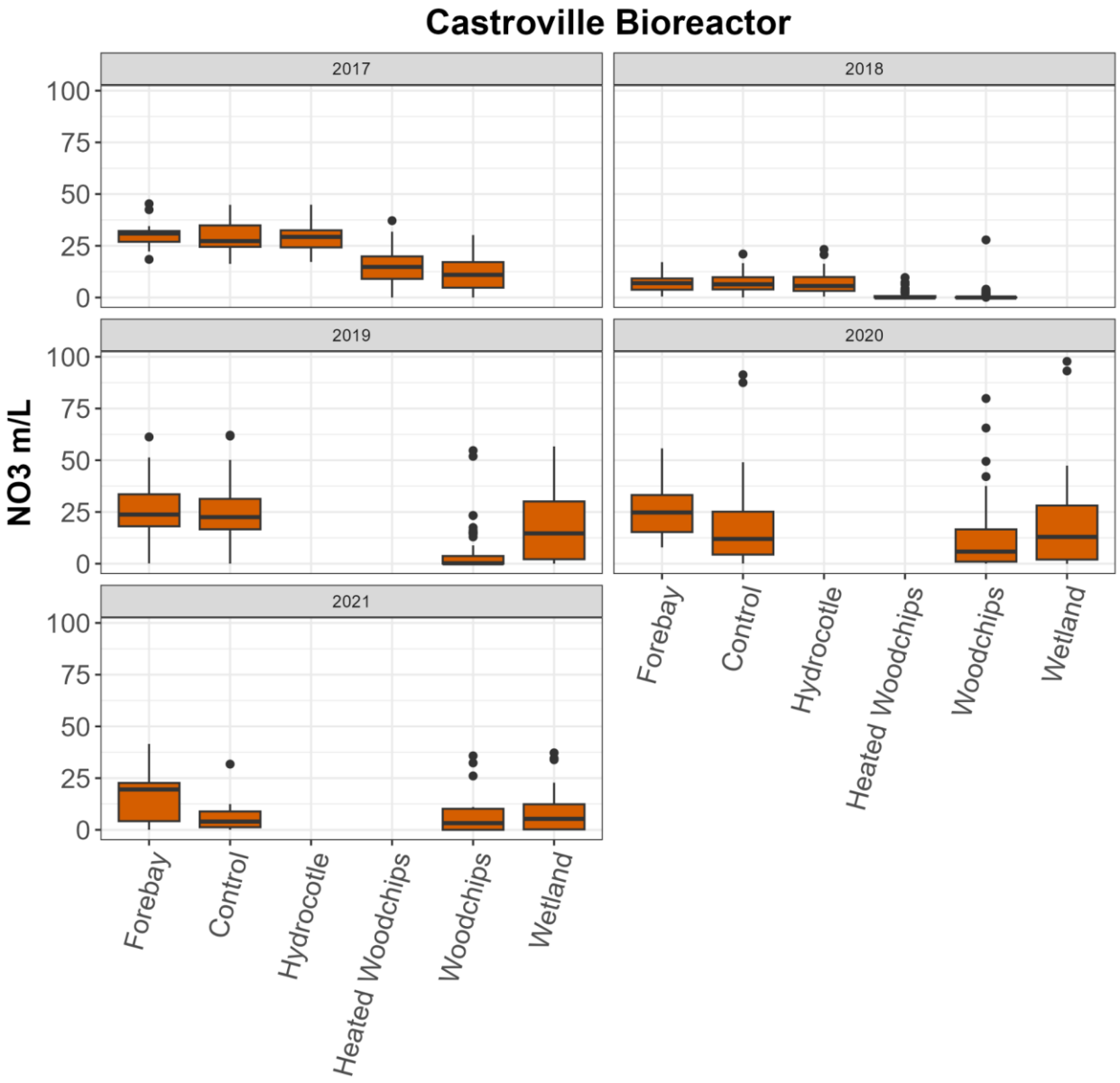

Figure A-7. Spread of concentrations sampled in the Castroville Multi Chamber Bioreactor by year.

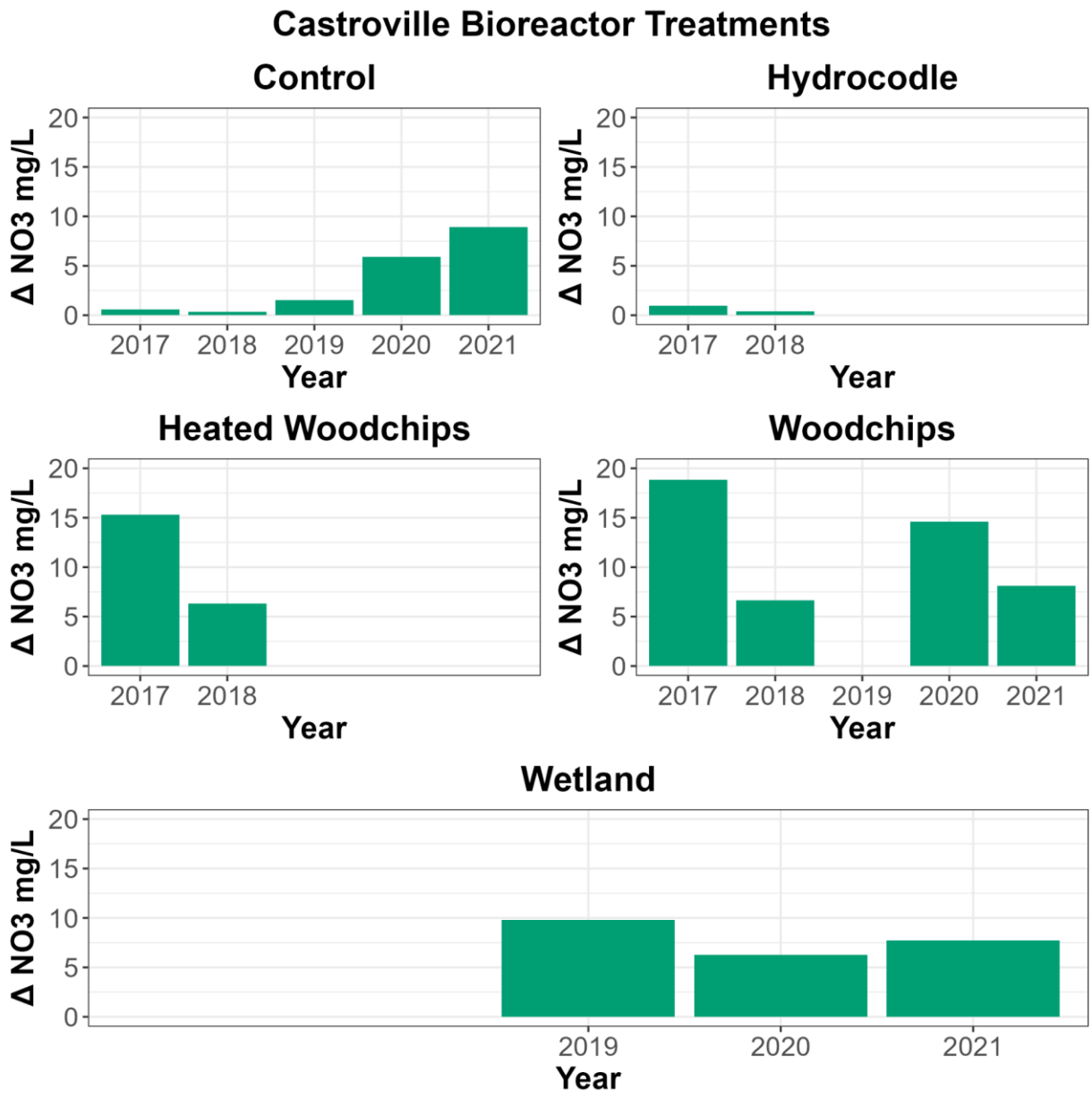

Figure A-8. Mean NO_3 reduction from inlet to outlet for each year in the Castroville Multi Chamber Bioreactor.

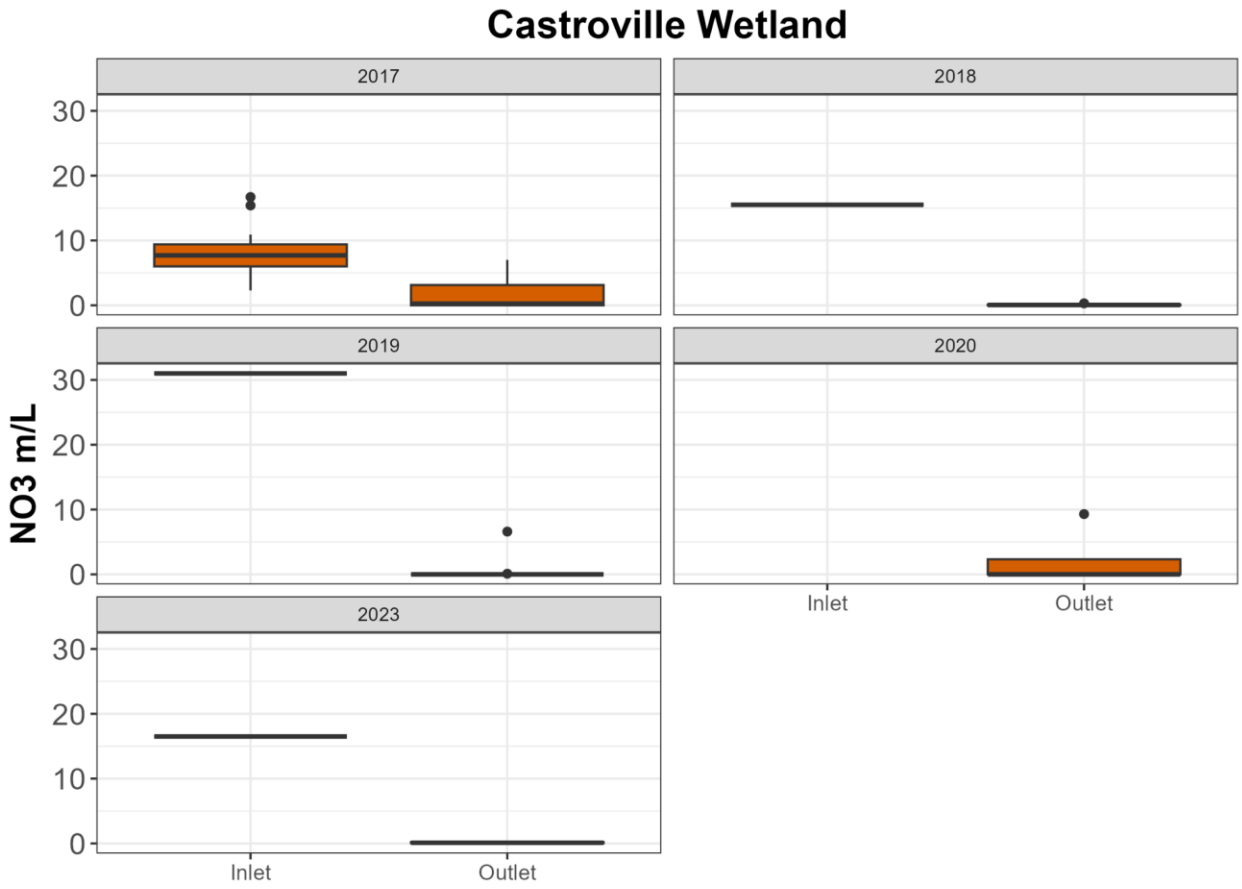

Figure A-9. Spread of concentrations sampled in the Castroville Wetland by year.

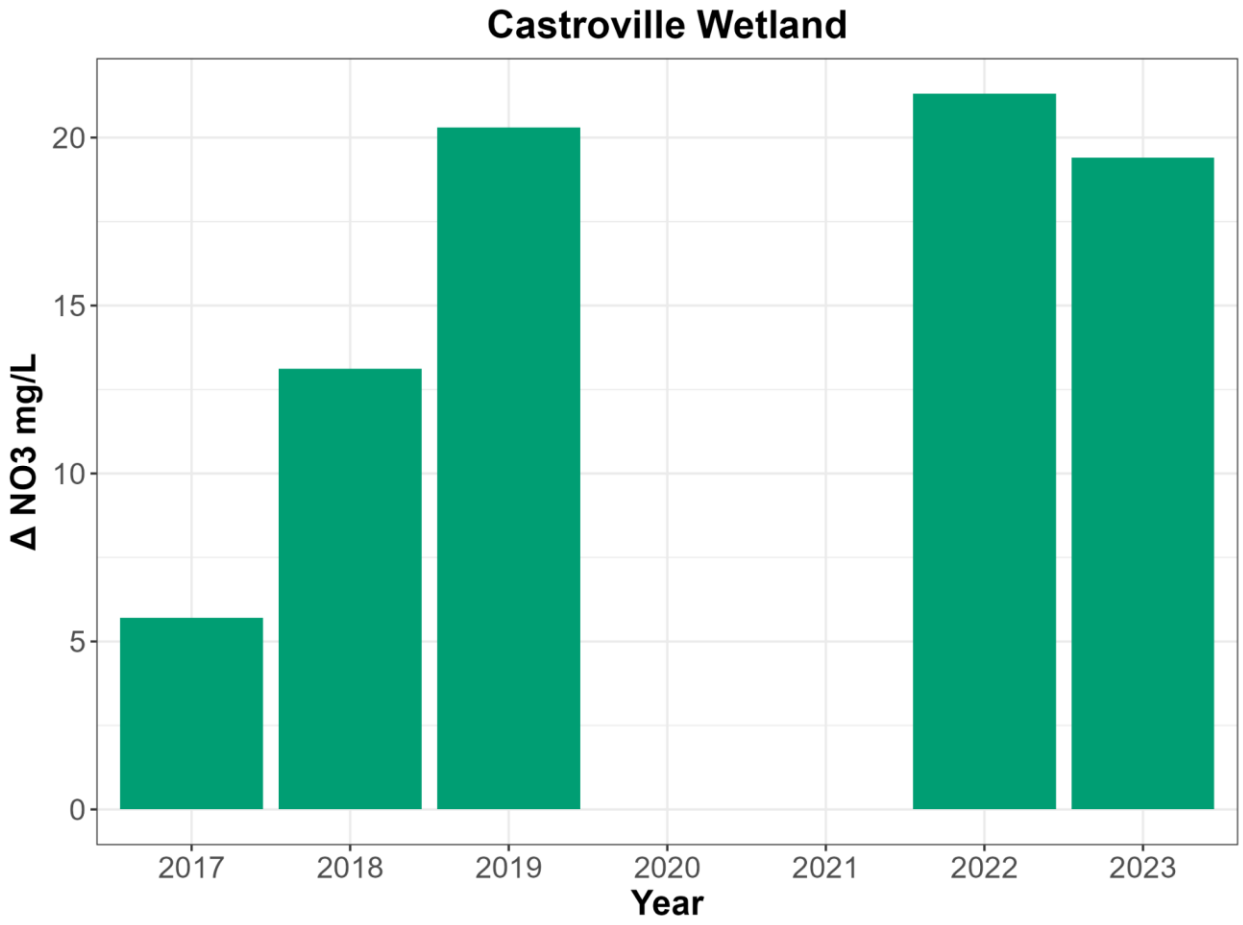

Figure A-10. Mean NO_3 reduction from inlet to outlet for each year in the Castroville Wetland.

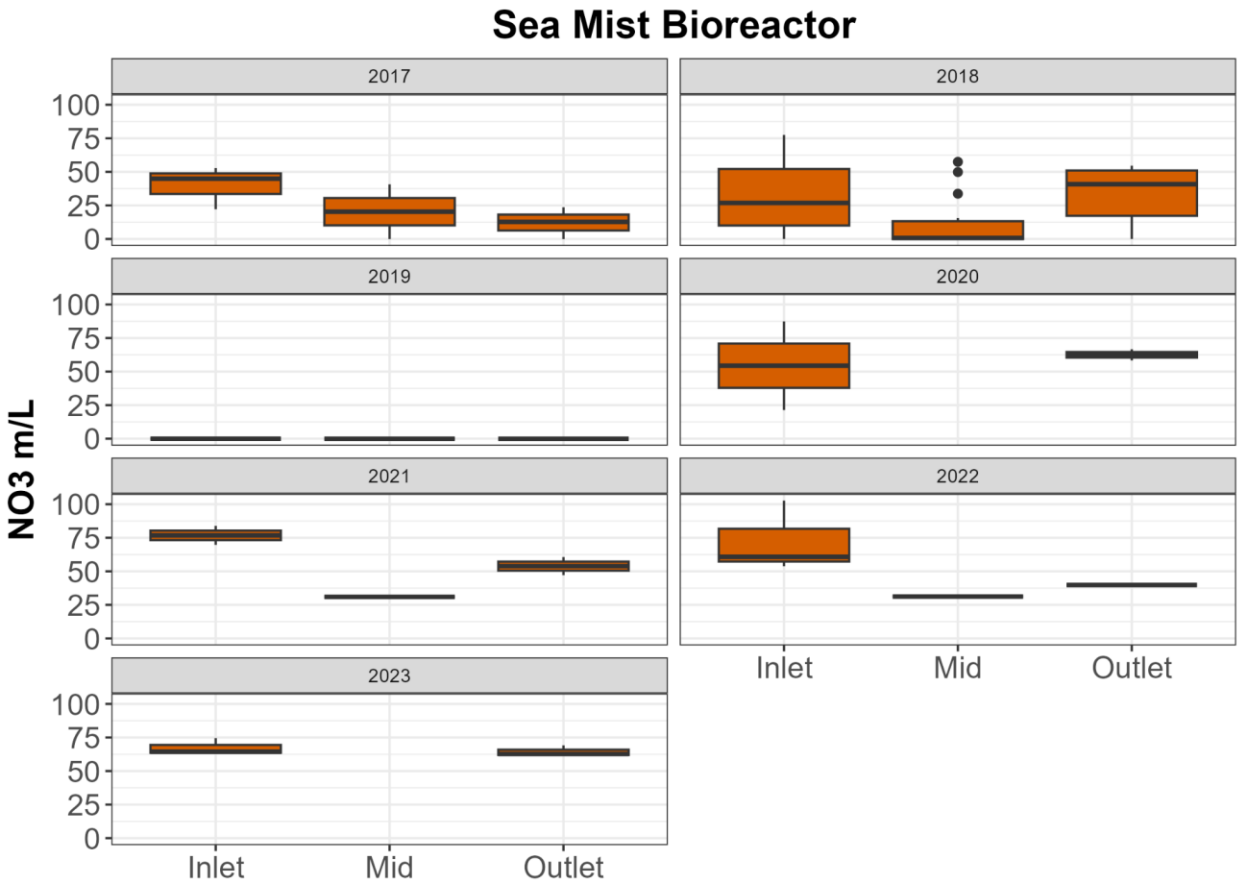

Figure A-11. Spread of concentrations sampled in the Sea Mist Bioreactor by year.

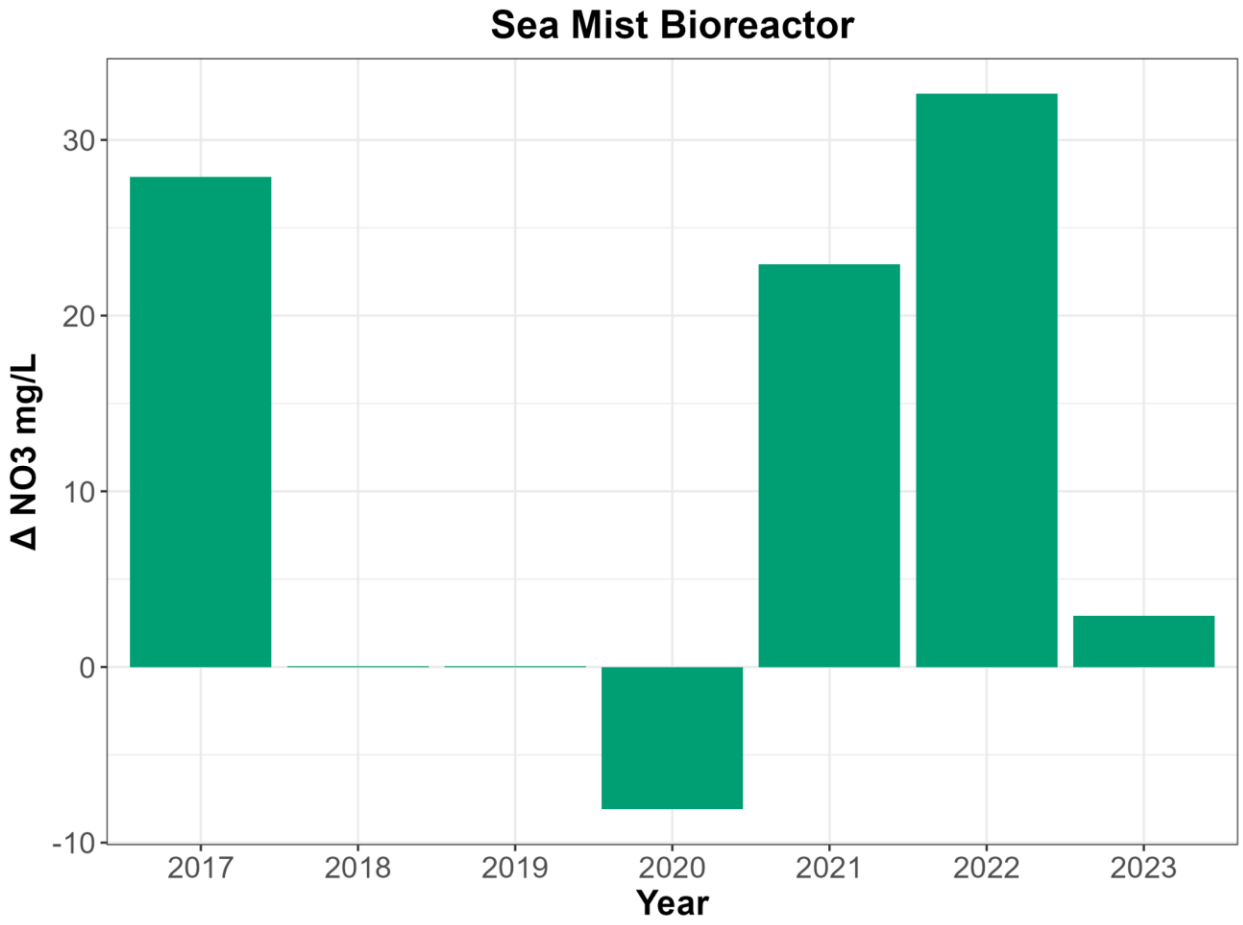

Figure A-12. Mean NO_3 reduction from inlet to outlet for each year in the Sea Mist Bioreactor.

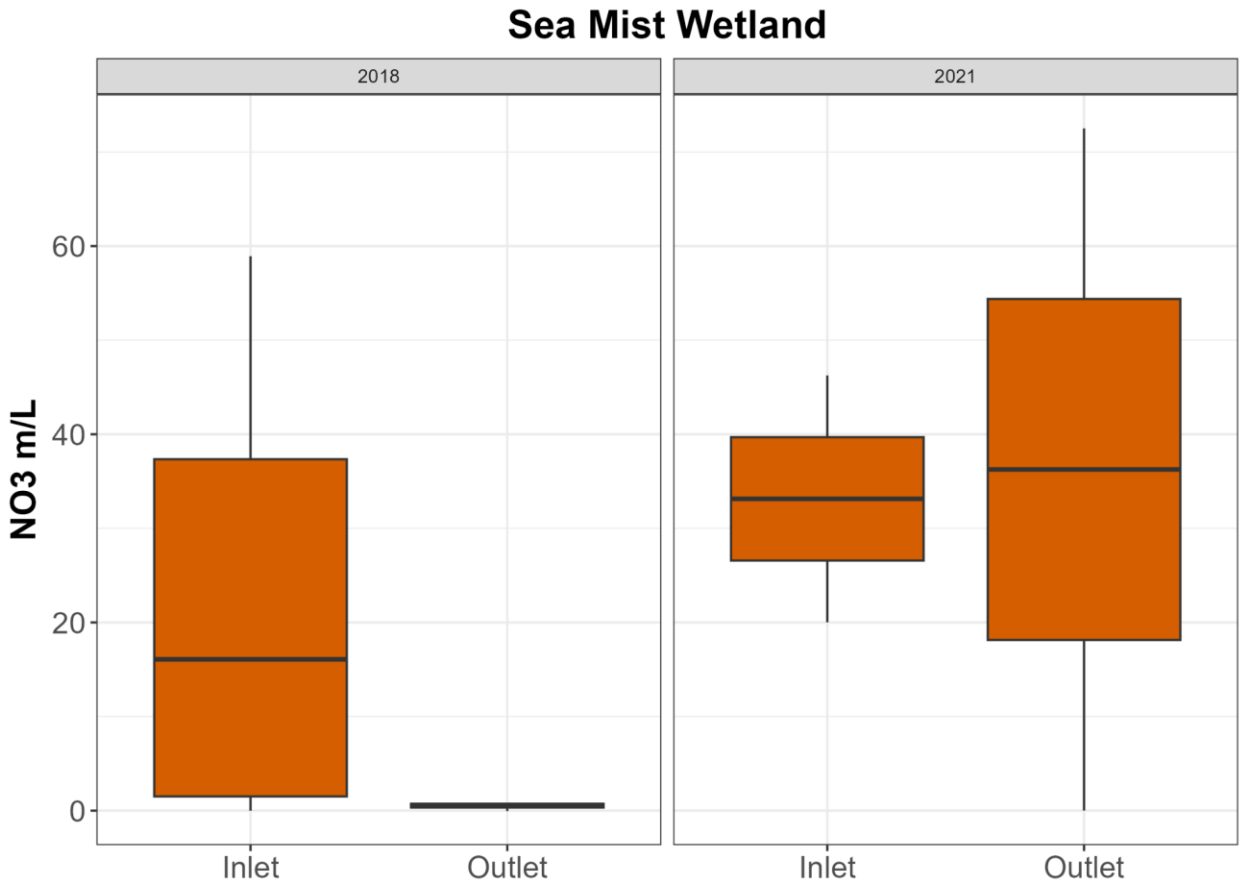

Figure A-13. Spread of concentrations sampled in the Sea Mist Wetland by year.

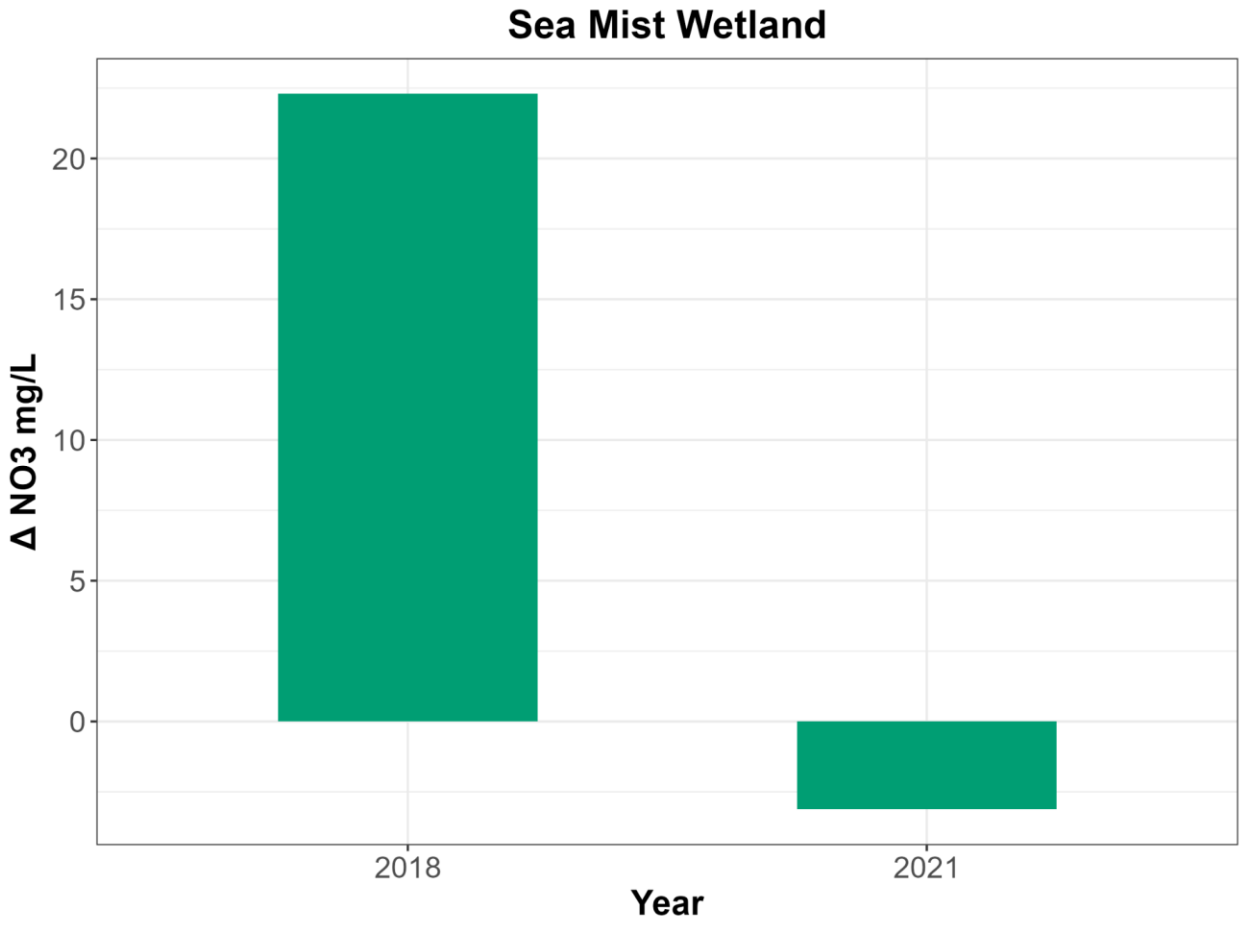

Figure A-14. Mean NO_3 reduction from inlet to outlet for each year in the Sea Mist Wetland.

APPENDIX B: NITROGEN LOSS EXPERIMENT

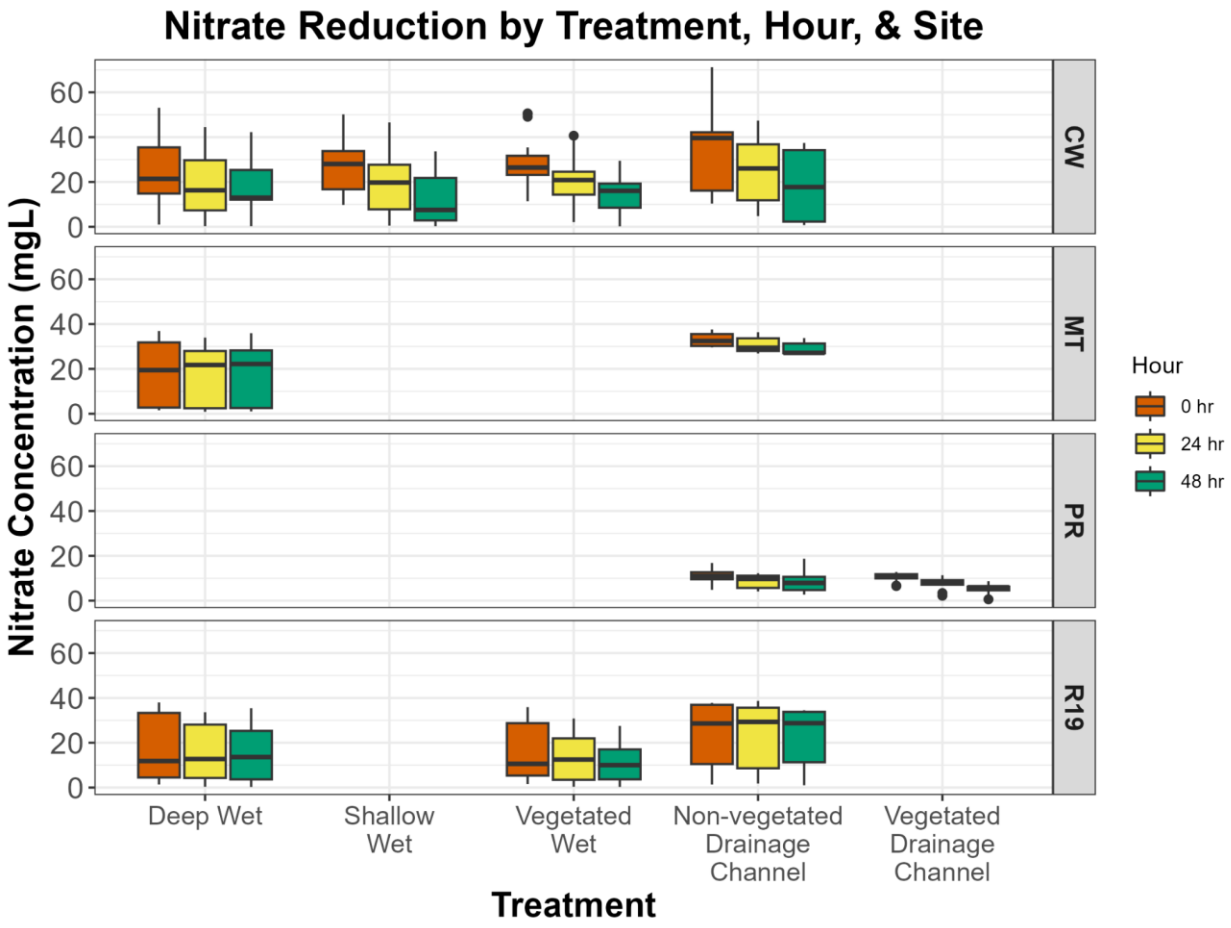

Figure B-1. Box plots of NO_3 concentrations at t=0 hours, 24 hours, and 48 hours in the five different treatment habitats within each of four sites. Data being shown represents all measurements taken from each habitat across all seasons. Line within box represents the median of measurements; box represents the interquartile range (IQR); whiskers represent the maximum over minimum values <1.5 IQR above/below box; and circles represent outliers. These data were processed with the SUNA.

Table B-1. Summary of NO_3 removal efficiency in SUNA samples.

Site	Treatment	Avg Temp (C°)	Avg Volume (L)	Nitrate		
				Concentration 0 Hrs	Concentration 48 Hrs	Removal Efficiency %
PG&E	Deep Wet	18.2	63.4	23.5	18.3	22.1
PG&E	Shallow Wet	18.5	22.1	27.1	12.9	52.5
PG&E	Vegetated Wet	17.0	32.0	28.1	14.3	49.1
PG&E	Non-vegetated Drainage Channel	18.4	59.0	31.5	18.5	41.2
MT	Deep Wet	17.1	94.5	19.1	17.7	7.1
MT	Non-vegetated Drainage Channel	19.8	66.7	32.9	29.0	11.8
R19	Deep Wet	18.1	45.0	16.5	14.3	13.3
R19	Vegetated Wet	17.2	42.3	15.1	11.2	25.4
R19	Non-vegetated Drainage Channel	17.9	94.9	23.4	22.3	4.7
PR	Non-vegetated Drainage Channel	16.1	60.4	10.7	8.1	24.3
PR	Vegetated Drainage Channel	18.0	56.4	10.4	5.3	49.3

APPENDIX C: OSMO EXPERIMENT RESULTS

At each site, we compared the OSMO composite NO_3 samples to grab samples taken by CCWG and CCWQP, as well as continuous flow to flow transects taken by CCWG and CCWQP. Figures C-1 through C-11 illustrate the similarities and differences between data collection methods. Each figure contains the following: for flow measurements (primary Y-axis), black lines represent instantaneous continuous flow, dashed blue lines represent average continuous flow, blue triangles represent flow transect measurements, and the green square represents the CMP flow measurement. For NO_3 concentrations (secondary Y-axis), orange lines represent OSMO NO_3 concentrations, orange circles represent grab NO_3 concentrations, the dashed orange line represents the average of the grab NO_3 concentrations, and the green circle represents the CMP grab NO_3 concentration. At the Chittenden station, USGS stream gage data were used in the Spring 2022 and Fall 2023 seasons due to equipment failure, as well as in Spring 2023 where high flows prevented CCWG equipment from being deployed (USGS 2024).

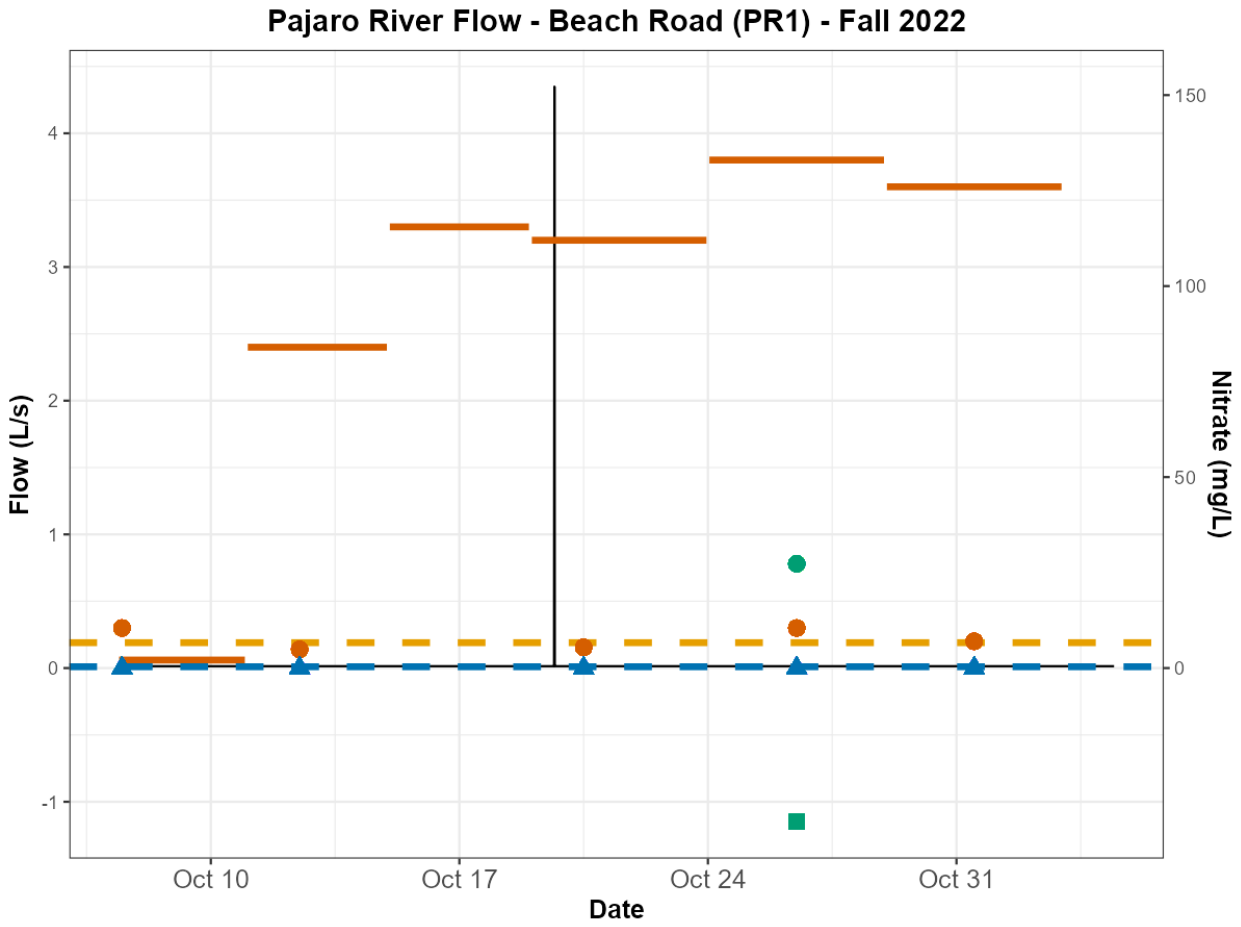

Figure C-1. Data collected from station PR1, Beach Road, in fall 2022.

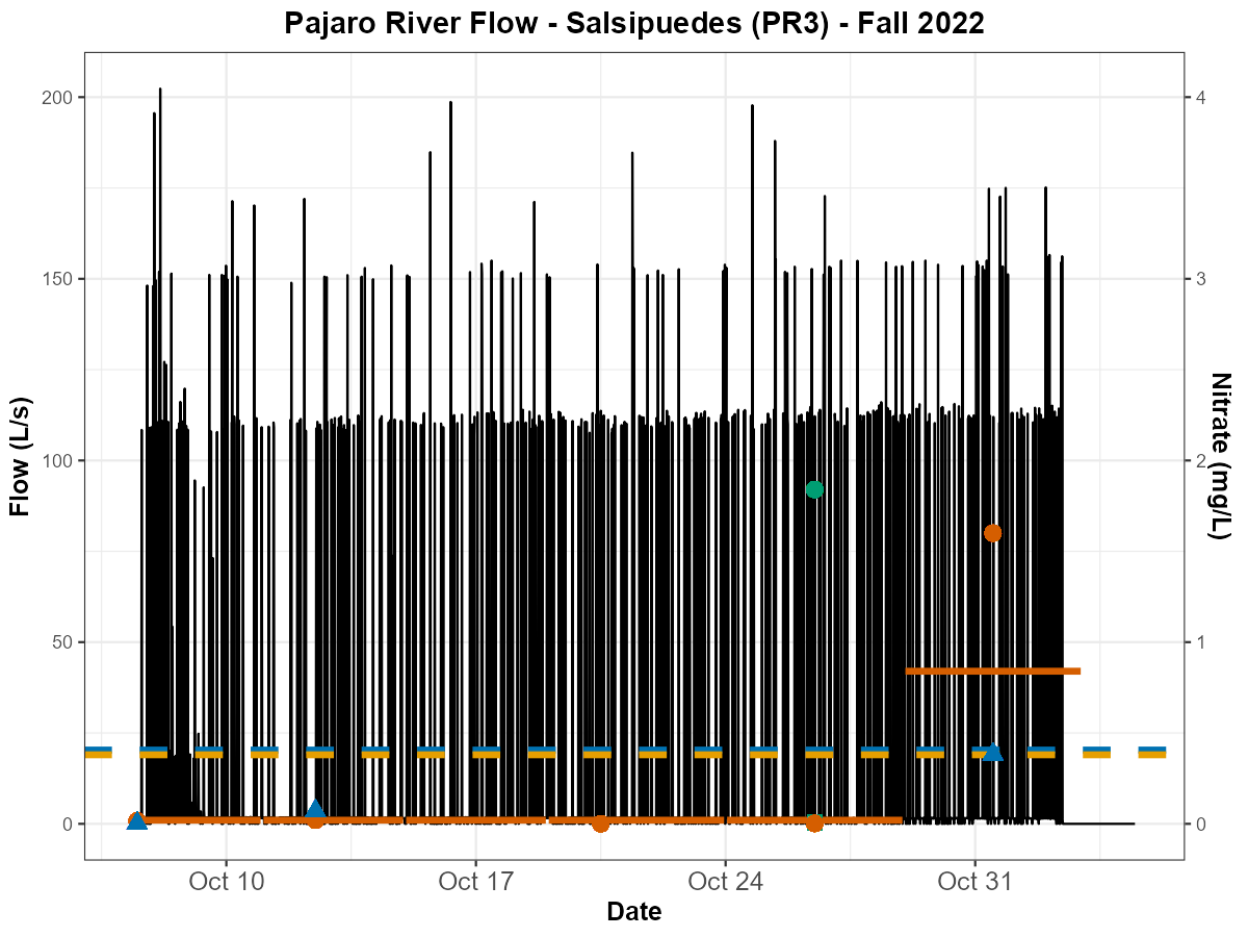

Figure C-2. Data collected from station PR3, Salsipuedes, in fall 2022.

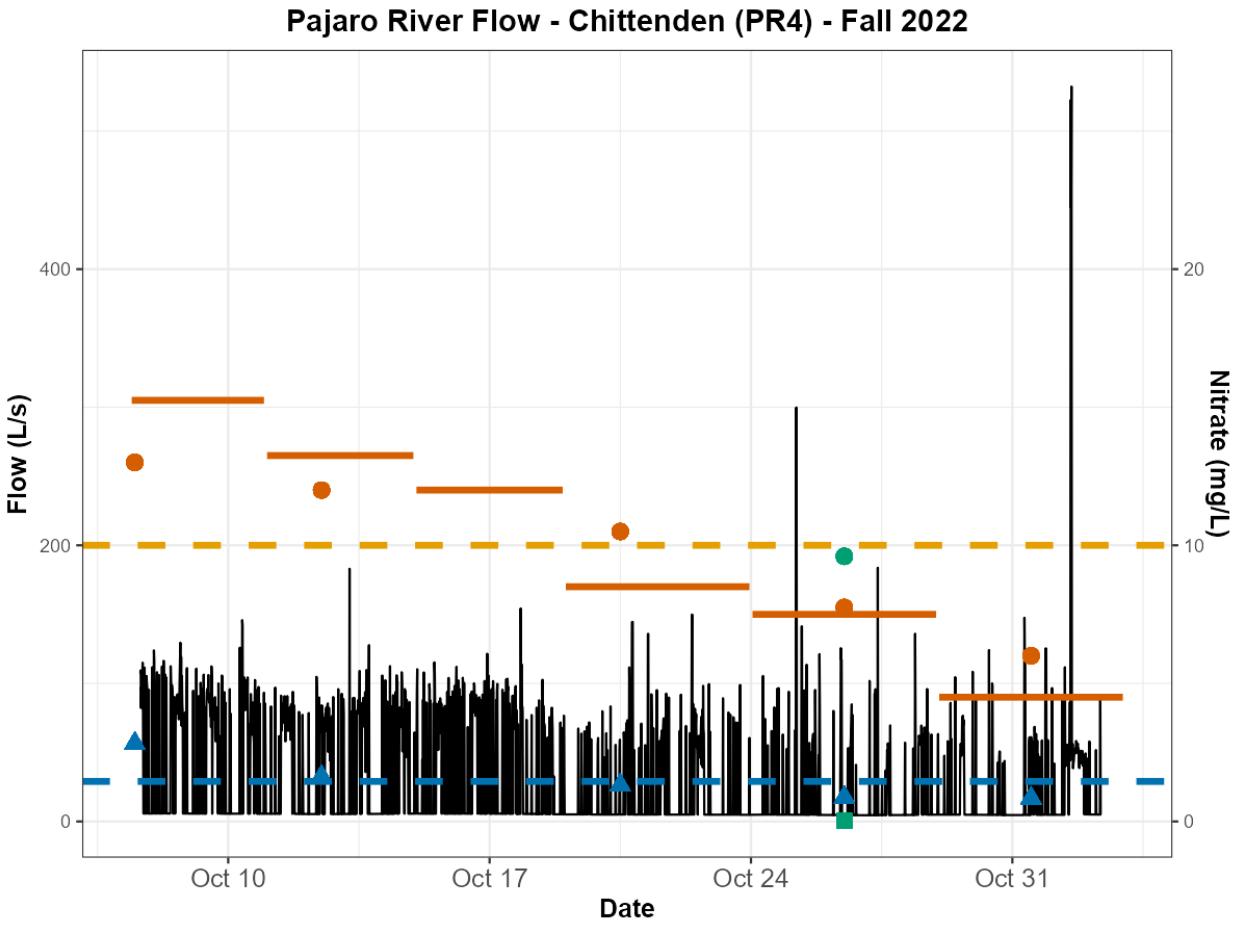

Figure C-3. Data collected from station PR4, Chittenden, in fall 2022.

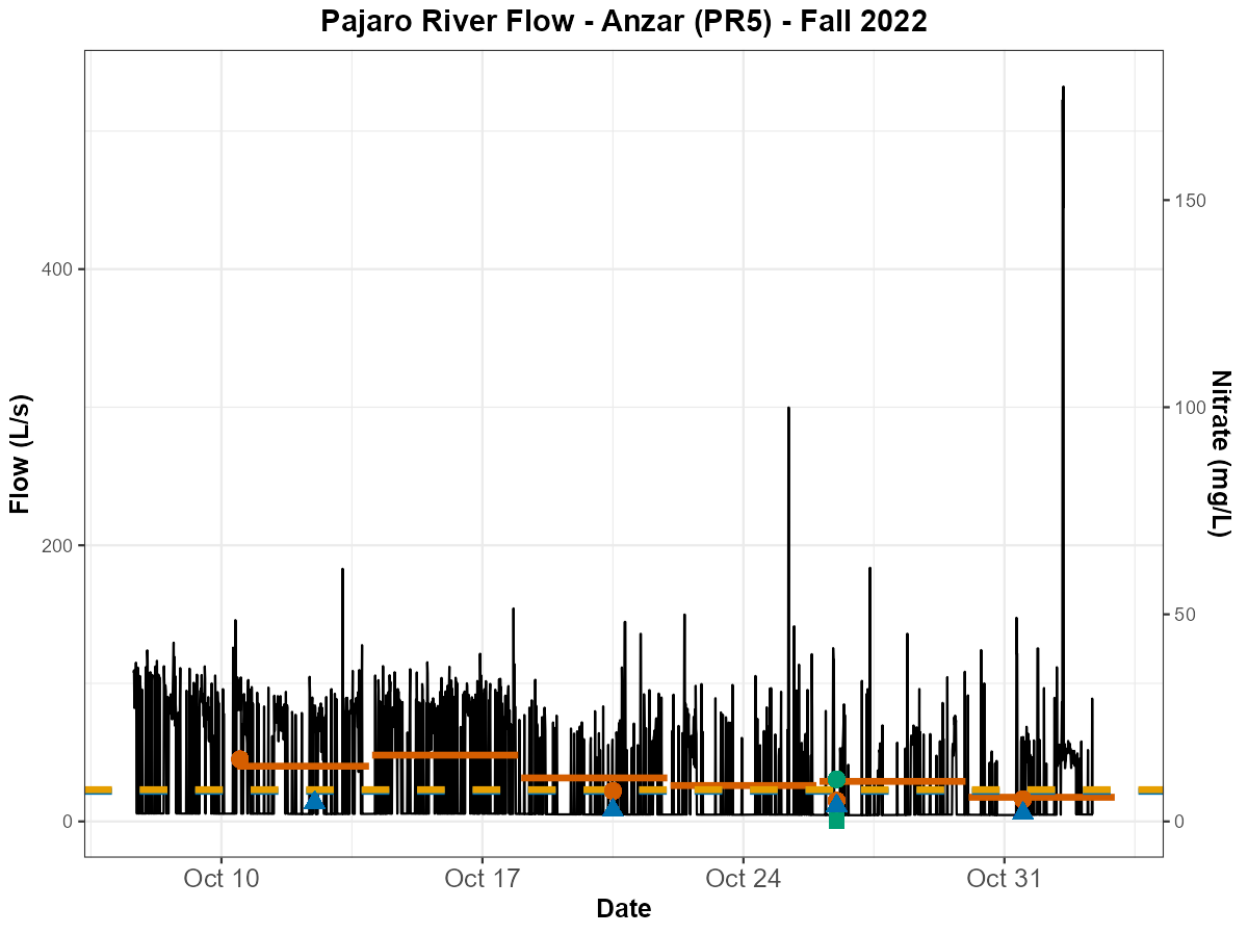

Figure C-4. Data collected from station PR5, Anzar, in fall 2022.

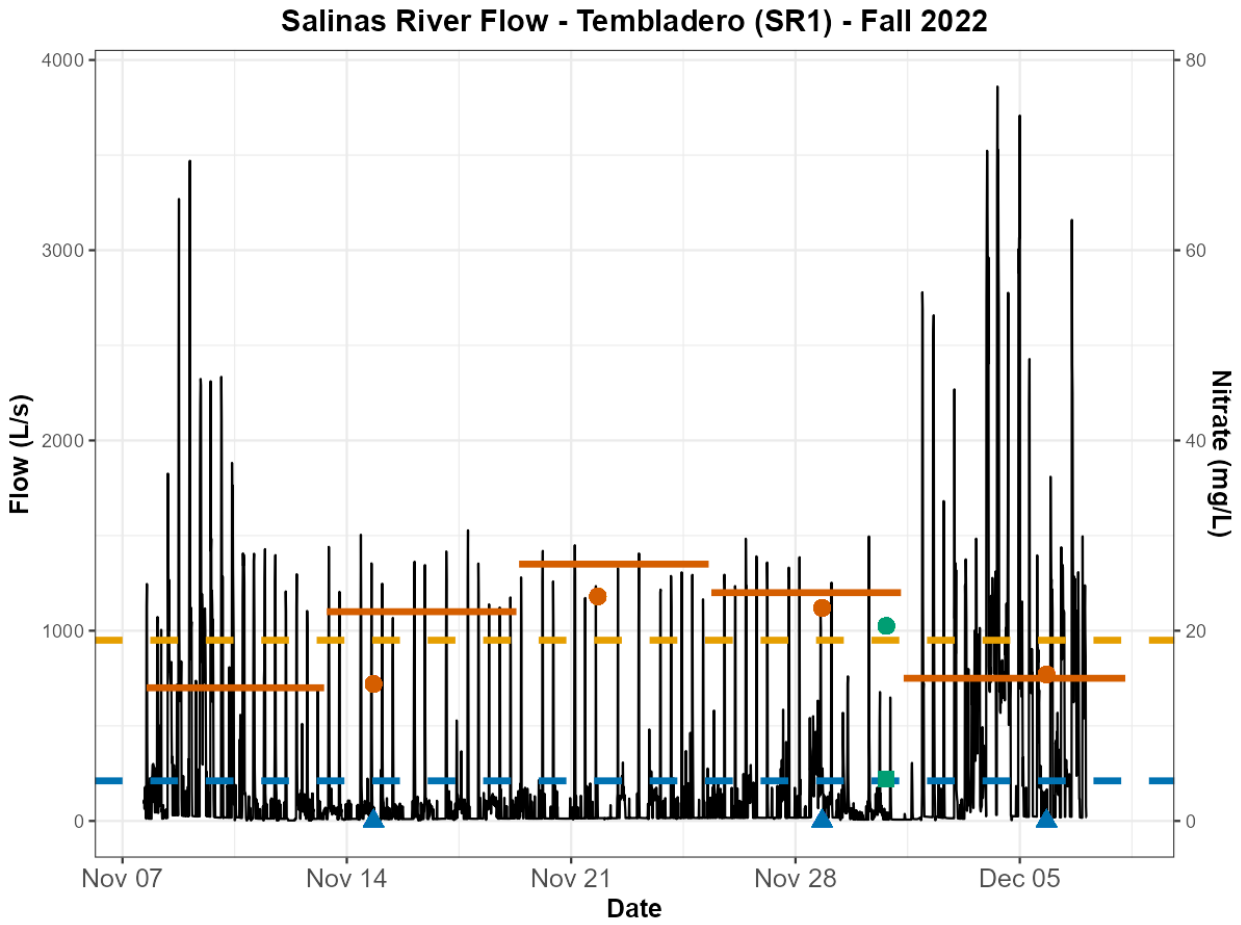

Figure C-5. Data collected from station SR1, Tembladero, in fall 2022.

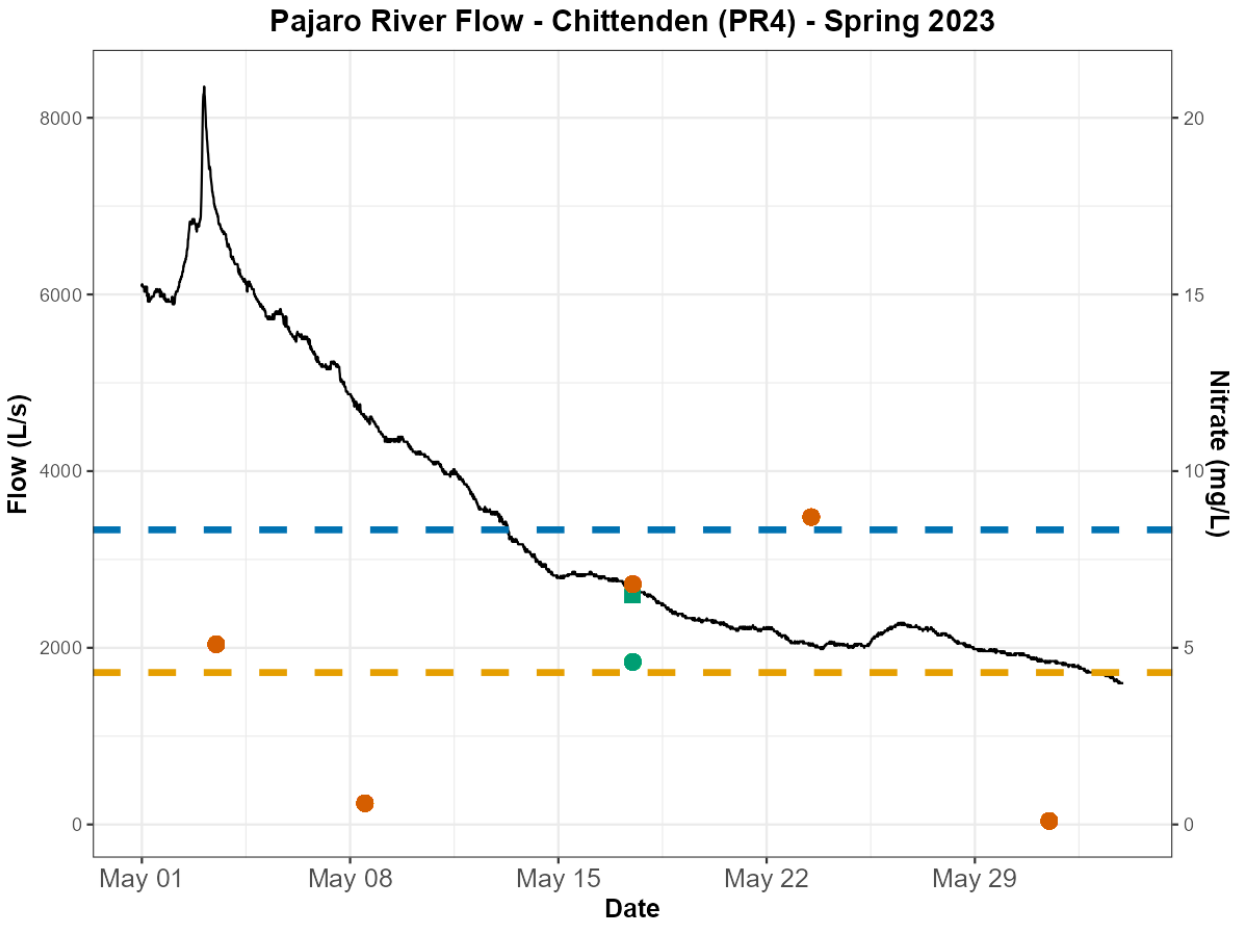

Figure C-6. Data collected from station PR4, Chittenden, in spring 2023.

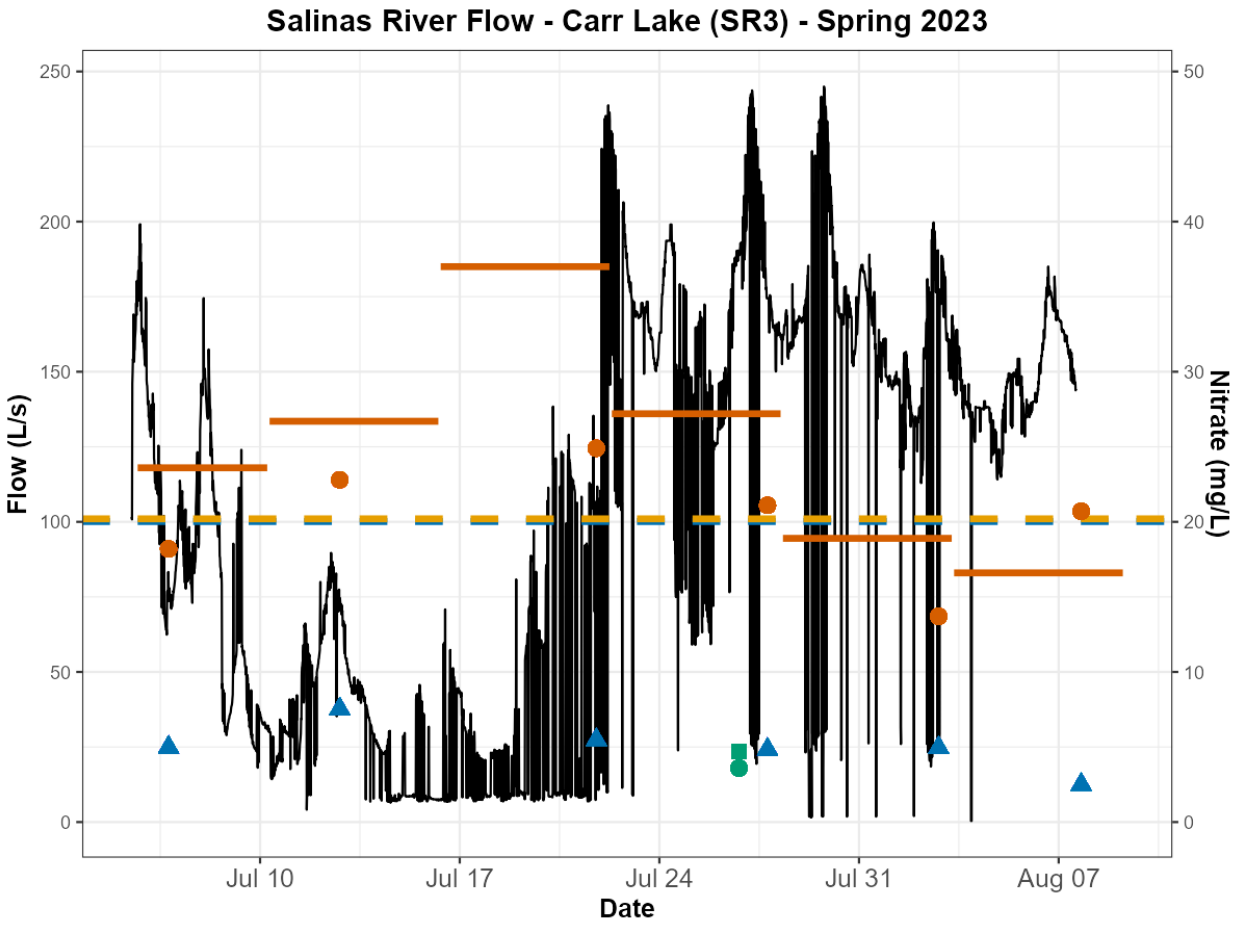

Figure C-7. Data collected from station SR3, Carr Lake, in spring 2023.

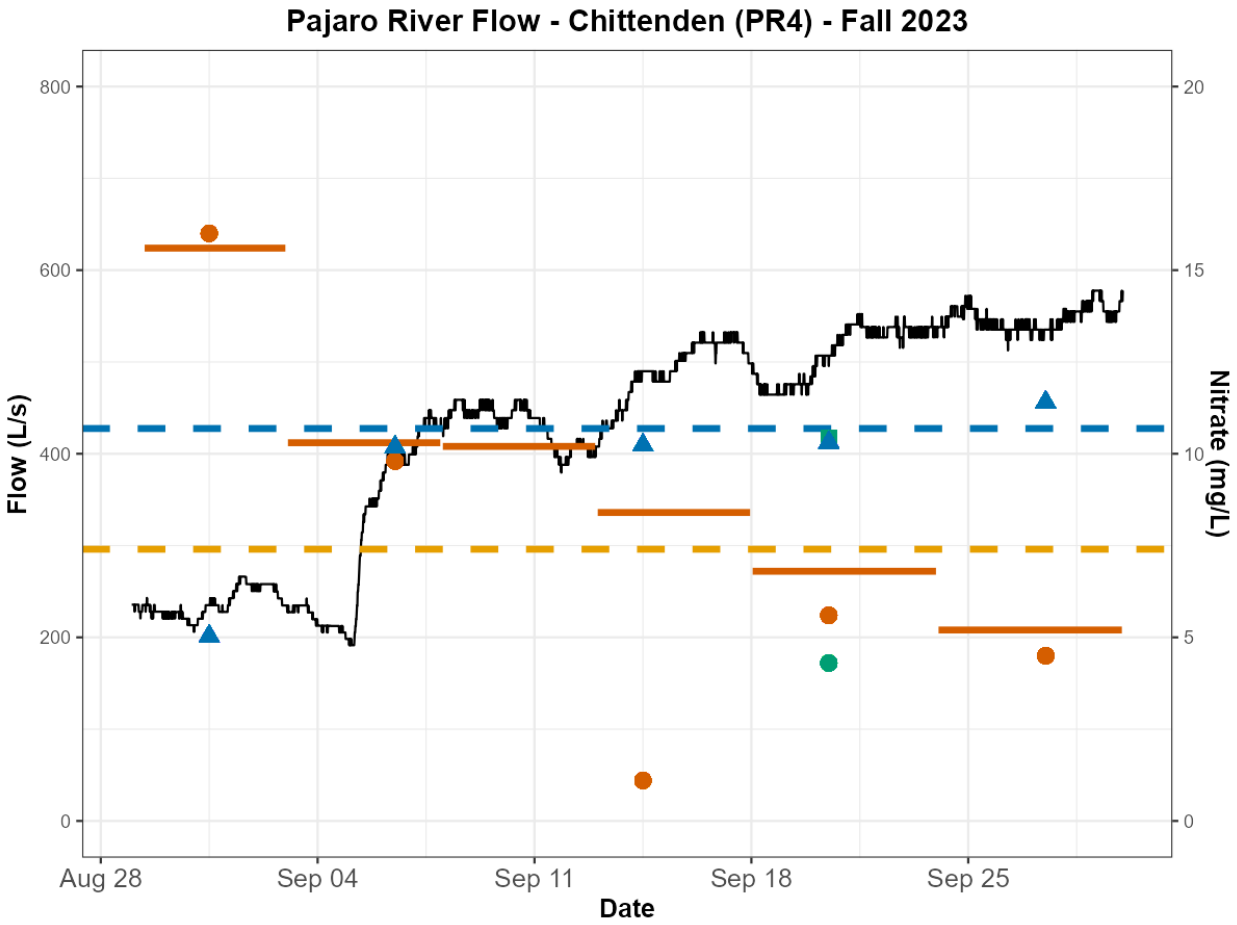

Figure C-8. Data collected from station PR4, Chittenden, in fall 2023.

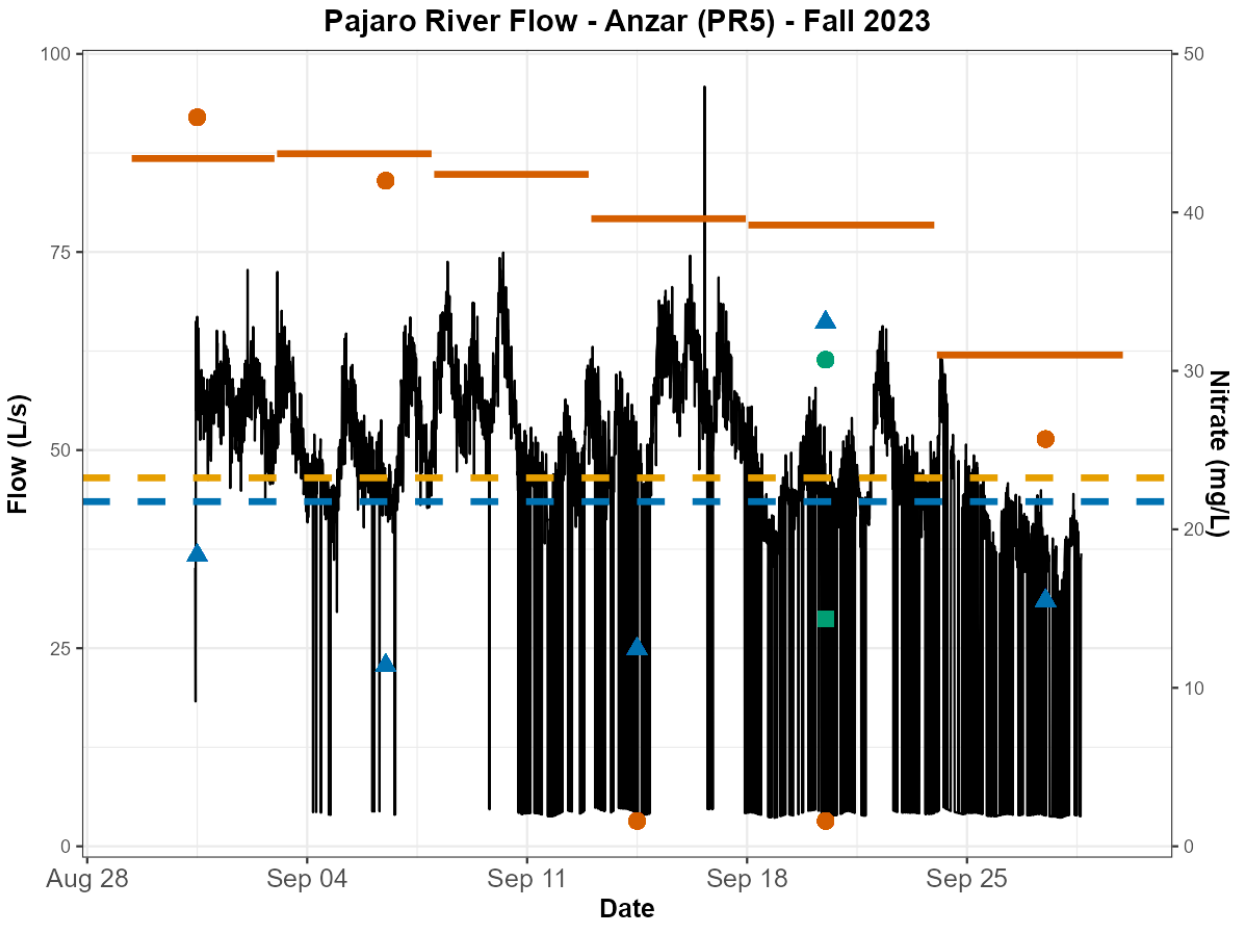

Figure C-9. Data collected from station PR5, Anzar, in fall 2023.

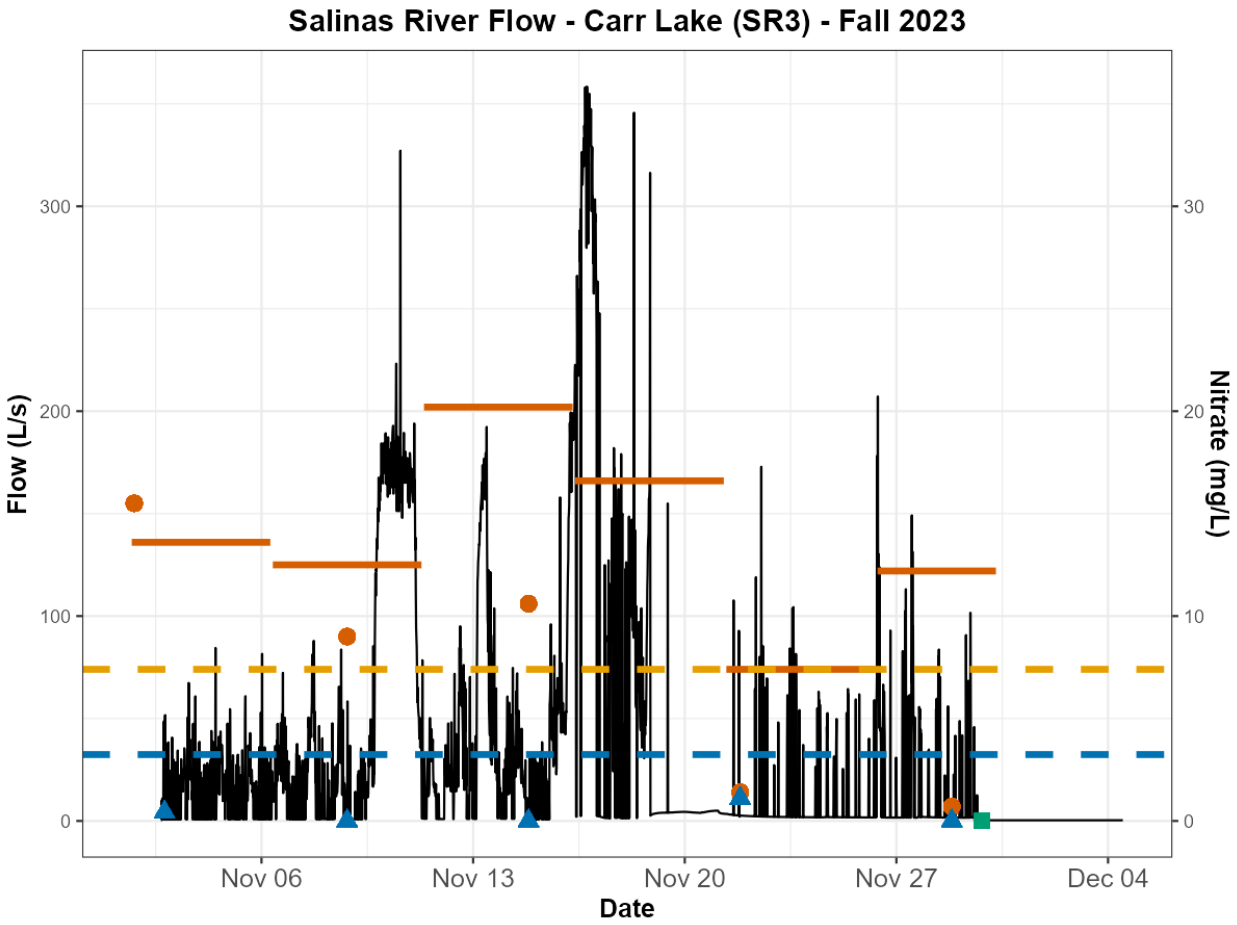

Figure C-10. Data collected from station SR3, Carr Lake, in fall 2023.

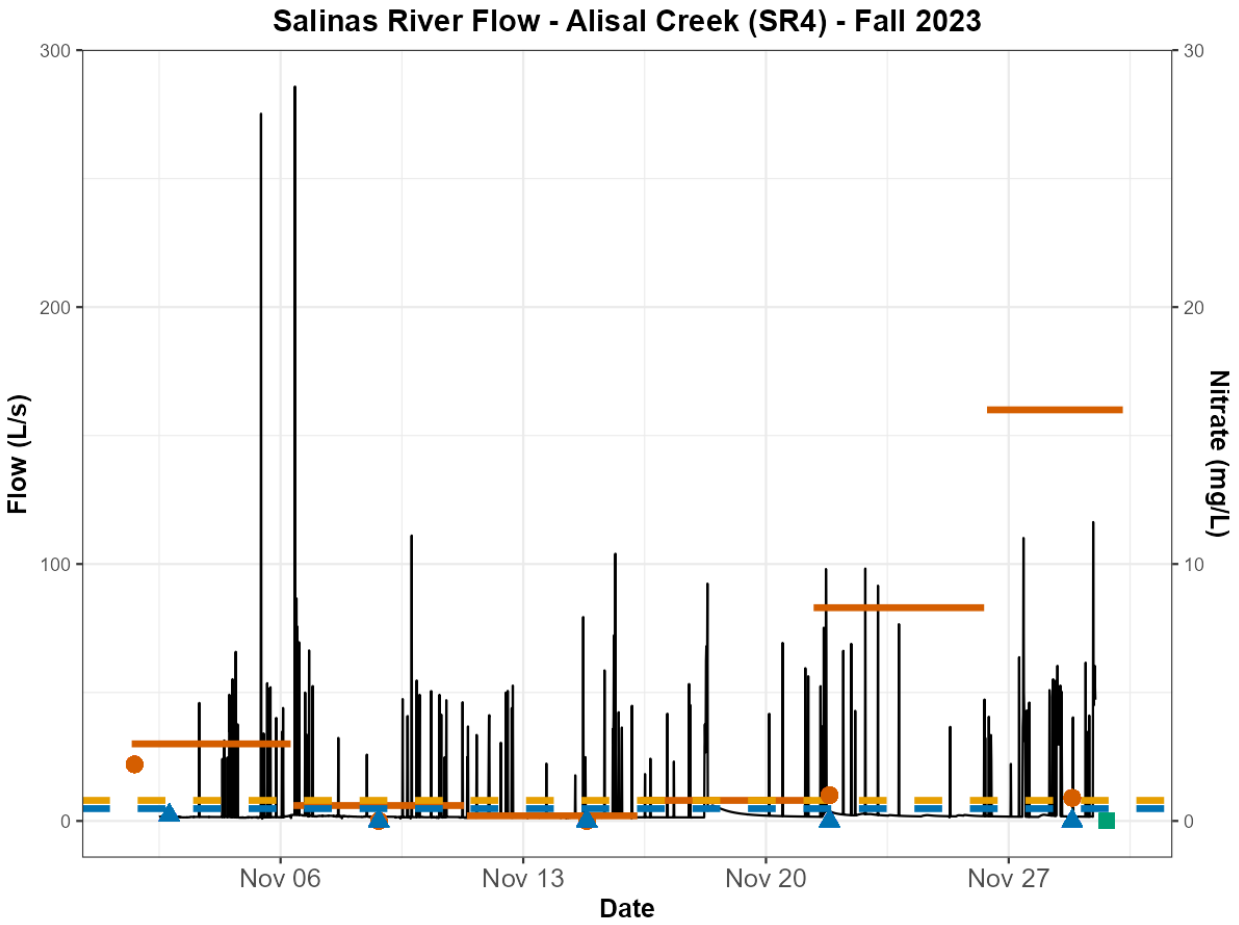

Figure C-11. Data collected from station SR4, Alisal Creek, in fall 2023.

These summary plots were only made for sites where we successfully collected continuous flow. All sites have nutrient samples and flow transects. Those data are summarized in the tables below.

Table C-1. Results from CCWG and CMP sampling efforts for station PR1, Beach Road.

Beach Road - PR1												
				Nitrate (mg/L)			Ammonia (mg/L)			Flow (L/s)		
Season	Year	Sample	Date	OSMO	Grab	Pres. Inc	OSMO	Grab	Pres. Inc	Avg Flow Meter	Transect	Pres. Inc
Spring	2022	1	3/21 - 3/26	0.0	2.8	22.8	0.0	0.1	0.1	NA	NA	5.0
Spring	2022	2	3/27 - 4/2	0.0	NA	NA	0.0	NA	NA	NA	NA	NA
Spring	2022	3	4/3 - 4/7	0.0	NA	NA	0.0	NA	NA	NA	0.0	NA
Spring	2022	4	4/8 - 4/12	0.0	24.1	NA	0.0	0.2	NA	NA	NA	NA
Spring	2022	5	4/13 - 4/17	0.1	21.9	NA	3.0	0.2	NA	NA	NA	NA
Spring	2022	6	4/18 - 4/22	0.0	11.5	NA	6.9	0.3	NA	NA	-14.5	NA
Spring	2022	**Average**	3/21-4/22	0.0	15.1	22.8	1.7	0.2	0.1	NA	-7.2	5.0
Fall	2022	1	10/7 - 10/10	0.0	11.2	NA	0.1	0.5	NA	0.0	-28.5	NA
Fall	2022	2	10/11 - 10/14	0.0	4.9	NA	84.9	1.5	NA	0.0	-12.0	NA
Fall	2022	3	10/15 - 10/18	0.0	NA	NA	112.5	NA	NA	0.0	NA	NA
Fall	2022	4	10/19 - 10/23	0.0	6.7	NA	110.0	0.2	NA	0.0	-12.0	NA
Fall	2022	5	10/24 - 10/28	0.0	11.4	21.5	127.1	0.1	0.3	0.0	-13.7	-32.8
Fall	2022	6	10/29 - 11/2	0.0	8.6	NA	120.2	0.2	NA	0.0	-18.6	NA
Fall	2022	**Average**	10/7-11/2	0.0	8.6	21.5	92.5	0.5	0.3	0.0	-17.0	-32.8
Spring	2023	1	4/24 - 5/1	20.3	28.4	32.4	3.3	0.1	0.1	NA	10.6	7.3
Spring	2023	2	5/2 - 5/8	28.3	18.5	NA	3.7	0.2	NA	NA	12.8	NA
Spring	2023	3	5/9 - 5/16	35.4	9.6	NA	9.4	0.2	NA	NA	12.2	NA
Spring	2023	4	5/17 - 5/24	37.2	18.2	24.7	4.0	0.2	0.1	NA	8.0	5.0
Spring	2023	5	5/23/2023	NA	10.2	NA	NA	0.2	NA	NA	6.6	NA
Spring	2023	**Average**	4/24 - 5/24	30.3	17.0	28.6	5.1	0.2	0.1	NA	10.0	6.2
Fall	2023	1	8/29 - 9/2	8.9	6.5	NA	0.1	0.4	NA	NA	54.6	NA
Fall	2023	2	9/3 - 9/7	12.0	5.1	NA	0.2	0.6	NA	NA	-64.4	NA
Fall	2023	3	9/8 - 9/12	13.8	NA	NA	0.1	NA	NA	NA	NA	NA
Fall	2023	4	9/13 - 9/17	13.7	0.1	NA	0.2	0.2	NA	NA	16.0	NA
Fall	2023	5	9/18 - 9/23	9.0	0.0	30.1	0.1	0.3	0.1	NA	-36.0	33.1
Fall	2023	6	9/24 - 9/29	4.4	24.6	NA	0.3	0.3	NA	NA	27.4	NA
Fall	2023	**Average**	8/29 - 9/29	10.3	7.3	30.1	0.2	0.4	0.1	NA	-0.5	33.1

Table C-2. Results from CCWG and CMP sampling efforts for station PR3, Salsipuedes Creek.

Salsipuedes Creek - PR3												
				Nitrate (mg/L)			Ammonia (mg/L)			Flow (L/s)		
Season	Year	Sample	Date	OSMO	Grab	Pres. Inc	OSMO	Grab	Pres. Inc	Avg Flow Meter	Transect	Pres. Inc
Spring	2022	1	3/21/2022	NA	0.2	0.4	NA	0.0	0.1	NA	759.3	782.9
Spring	2022	2	3/30/2022	NA	0.6	NA	NA	0.1	NA	NA	NA	NA
Spring	2022	3	4/8/2022	NA	0.1	NA	NA	0.0	NA	NA	NA	NA
Spring	2022	4	4/8/2022	NA	0.5	NA	NA	0.1	NA	NA	NA	NA
Spring	2022	5	4/22/2022	NA	0.4	NA	NA	0.1	NA	NA	907.1	NA
Spring	2022	**Average**	3/21 - 4/22	NA	0.4	0.4	NA	0.1	0.1	NA	833.2	782.9
Fall	2022	1	10/7 - 10/10	0.1	0.0	NA	0.0	0.1	NA	21.7	0.1	NA
Fall	2022	2	10/11 - 10/14	0.1	0.1	NA	0.2	0.0	NA	16.6	3.5	NA
Fall	2022	3	10/15 - 10/18	0.0	NA	NA	0.1	NA	NA	20.4	NA	NA
Fall	2022	4	10/19 - 10/23	0.0	0.0	NA	0.2	0.1	NA	20.2	NA	NA
Fall	2022	5	10/24 - 10/28	0.0	0.0	1.8	0.2	0.1	0.1	23.1	NA	8.5
Fall	2022	6	10/29 - 11/2	0.7	1.7	NA	0.2	0.0	NA	19.7	19.1	NA
Fall	2022	**Average**	10/7 - 11/2	0.2	0.3	1.8	0.1	0.1	0.1	20.3	7.6	8.5
Spring	2023	1	5/1 - 5/5	0.2	1.3	NA	0.0	0.1	NA	NA	778.1	NA
Spring	2023	2	5/6 - 5/10	0.1	1.0	NA	0.0	0.1	NA	NA	1166.4	NA
Spring	2023	3	5/11 - 5/15	0.1	NA	NA	0.0	NA	NA	NA	NA	NA
Spring	2023	4	5/16 - 5/21	0.1	1.1	0.9	0.0	0.0	0.2	NA	929.4	907.5
Spring	2023	5	5/22 - 5/27	0.2	0.6	NA	0.0	0.1	NA	NA	801.0	NA
Spring	2023	6	5/28 - 6/2	0.2	2.2	NA	0.0	0.1	NA	NA	707.4	NA
Spring	2023	**Average**	5/1 - 6/2	0.2	1.3	0.9	0.0	0.1	0.2	NA	876.5	907.5
Fall	2023	1	8/29 - 9/2	7.3	6.0	NA	0.1	0.0	NA	NA	75.3	NA
Fall	2023	2	9/3 - 9/7	8.0	6.1	NA	0.0	0.0	NA	NA	24.7	NA
Fall	2023	3	9/8 - 9/12	8.0	NA	NA	0.3	NA	NA	NA	NA	NA
Fall	2023	4	9/13 - 9/17	6.1	0.4	NA	0.3	0.1	NA	NA	97.1	NA
Fall	2023	5	9/18 - 9/23	6.3	0.5	4.2	0.3	0.0	0.0	NA	15.9	18.9
Fall	2023	6	9/24 - 9/29	6.7	5.5	NA	0.2	0.0	NA	NA	19.3	NA
Fall	2023	**Average**	8/29 - 9/29	7.1	3.7	4.2	0.2	0.0	0.0	NA	46.5	18.9

Table C-3. Results from CCWG and CMP sampling efforts for station PR4, Chittenden Creek.

Chittenden Creek - PR4												
				Nitrate (mg/L)			Ammonia (mg/L)			Flow (L/s)		
Season	Year	Sample	Date	OSMO	Grab	Pres. Inc	OSMO	Grab	Pres. Inc	Avg Flow Meter	Transect	Pres. Inc
Spring	2022	1	3/21 - 3/26	2.1	1.3	8.0	0.0	0.0	0.1	NA	605.4	528.0
Spring	2022	2	3/27 - 4/2	2.1	NA	NA	0.0	NA	NA	NA	NA	NA
Spring	2022	3	4/3 - 4/7	2.1	NA	NA	0.0	NA	NA	NA	476.5	NA
Spring	2022	4	4/8 - 4/12	1.7	4.9	NA	0.0	0.1	NA	NA	NA	NA
Spring	2022	5	4/13 - 4/17	1.6	4.7	NA	0.0	0.1	NA	NA	NA	NA
Spring	2022	6	4/18 - 4/22	1.3	5.7	NA	0.0	0.1	NA	NA	796.3	NA
Spring	2022	**Average**	3/21 - 4/22	1.8	4.1	8.0	0.0	0.1	0.1	NA	626.1	528.0
Fall	2022	1	10/7 - 10/10	14.9	13.6	NA	0.2	0.1	NA	45.4	56.5	NA
Fall	2022	2	10/11 - 10/14	13.1	12.3	NA	0.1	0.1	NA	34.9	32.5	NA
Fall	2022	3	10/15 - 10/18	12.1	NA	NA	0.1	NA	NA	41.1	NA	NA
Fall	2022	4	10/19 - 10/23	7.9	10.9	NA	0.1	0.1	NA	20.6	26.3	NA
Fall	2022	5	10/24 - 10/28	6.4	7.9	9.3	0.1	0.1	0.1	18.4	17.5	10.5
Fall	2022	6	10/29 - 11/2	4.8	6.1	NA	0.1	0.1	NA	23.6	17.0	NA
Fall	2022	**Average**	NA	9.9	10.2	9.3	0.1	0.1	0.1	30.7	30.0	10.5
Spring	2023	1	5/1 - 5/6	NA	4.9	NA	NA	0.1	NA	6142.7	1631.5	NA
Spring	2023	2	5/7 - 5/13	NA	0.5	NA	NA	0.1	NA	4157.4	1151.4	NA
Spring	2023	3	5/14 - 5/20	NA	6.7	4.2	NA	0.2	0.1	2617.5	647.9	2592.7
Spring	2023	4	5/21 - 5/27	NA	8.5	NA	NA	0.2	NA	2137.1	NA	NA
Spring	2023	5	5/28 - 6/2	NA	0.0	NA	NA	0.1	NA	1872.4	NA	NA
Spring	2023	**Average**	5/1 - 6/2	NA	4.1	4.2	NA	0.1	0.1	3385.4	1143.6	2592.7
Fall	2023	1	8/29 - 9/2	15.5	16.0	NA	0.1	0.1	NA	236.9	201.2	NA
Fall	2023	2	9/3 - 9/7	10.2	9.8	NA	0.2	0.0	NA	309.7	407.1	NA
Fall	2023	3	9/8 - 9/12	10.2	NA	NA	0.0	NA	NA	431.0	NA	NA
Fall	2023	4	9/13 - 9/17	8.4	1.0	NA	0.0	0.1	NA	489.6	409.3	NA
Fall	2023	5	9/18 - 9/23	6.8	5.5	4.4	0.1	0.1	0.2	510.0	412.3	417.4
Fall	2023	6	9/24 - 9/29	5.1	4.5	NA	0.1	0.0	NA	547.4	456.1	NA
Fall	2023	**Average**	8/29 - 9/29	9.4	7.3	4.4	0.1	0.1	0.2	420.8	377.2	417.4

Table C-4. Results from CCWG and CMP sampling efforts for station PR5, Anzar Ditch.

Anzar Ditch - PR5												
				Nitrate (mg/L)			Ammonia (mg/L)			Flow (L/s)		
Season	Year	Sample	Date	OSMO	Grab	Pres. Inc	OSMO	Grab	Pres. Inc	Avg Flow Meter	Transect	Pres. Inc
Spring	2022	1	3/21 - 3/26	14.5	4.8	50.9	0.0	0.5	0.1	2.1	21.8	12.9
Spring	2022	2	3/27 - 4/2	12.1	NA	NA	0.0	NA	NA	1.9	NA	NA
Spring	2022	3	4/3 - 4/7	14.6	NA	NA	0.0	NA	NA	1.8	10.5	NA
Spring	2022	4	4/8 - 4/12	12.1	37.0	NA	0.0	0.3	NA	4.6	NA	NA
Spring	2022	5	4/13 - 4/17	11.0	40.1	NA	0.0	0.4	NA	5.5	NA	NA
Spring	2022	6	4/18 - 4/22	6.8	NA	NA	0.0	NA	NA	7.9	86.3	NA
Spring	2022	**Average**	3/21 - 4/22	11.8	27.3	50.9	0.0	0.4	0.1	4.0	39.6	12.9
Fall	2022	1	10/10 - 10/13	12.2	15.1	NA	1.1	2.1	NA	25.5	13.7	NA
Fall	2022	2	10/14 - 10/17	16.0	NA	NA	0.5	NA	NA	24.6	NA	NA
Fall	2022	3	10/18 - 10/21	10.6	7.6	NA	0.4	0.8	NA	20.1	8.1	NA
Fall	2022	4	10/22 - 10/25	7.6	NA	NA	0.2	NA	NA	17.9	NA	NA
Fall	2022	5	10/26 - 10/29	8.8	5.1	10.5	0.7	3.4	1.3	23.5	11.4	9.9
Fall	2022	6	10/30 - 11/2	6.1	5.8	NA	0.3	0.3	NA	18.7	5.8	NA
Fall	2022	**Average**	10/10 - 11/2	10.2	8.4	10.5	0.5	1.7	1.3	21.7	9.8	9.9
Spring	2023	1	4/24 - 4/28	41.0	20.8	44.5	0.7	0.3	1.2	NA	69.9	89.9
Spring	2023	2	4/29 - 5/3	36.7	28.8	NA	0.7	2.0	NA	NA	75.6	NA
Spring	2023	3	5/4 - 5/8	32.7	29.8	NA	0.5	2.1	NA	NA	47.0	NA
Spring	2023	4	5/9 - 5/13	39.1	NA	NA	0.4	NA	NA	NA	NA	NA
Spring	2023	5	5/14 - 5/18	42.1	33.6	42.1	0.1	2.6	2.5	NA	53.2	62.2
Spring	2023	6	5/19 - 5/24	34.7	31.7	NA	0.2	2.8	NA	NA	55.4	NA
Spring	2023	**Average**	4/24 - 5/24	37.7	29.0	43.3	0.4	1.9	1.8	NA	60.2	76.1
Fall	2023	1	8/29 - 9/2	43.0	43.4	NA	0.4	2.6	NA	55.6	36.7	NA
Fall	2023	2	9/3 - 9/7	43.6	40.1	NA	0.2	1.9	NA	49.6	22.8	NA
Fall	2023	3	9/8 - 9/12	42.0	NA	NA	0.4	NA	NA	48.5	NA	NA
Fall	2023	4	9/13 - 9/17	39.5	0.3	NA	0.1	1.3	NA	49.6	24.9	NA
Fall	2023	5	9/18 - 9/23	39.1	0.7	30.0	0.1	0.9	0.7	37.3	66.1	28.7
Fall	2023	6	9/24 - 9/29	30.8	24.8	NA	0.2	0.9	NA	26.1	31.0	NA
Fall	2023	**Average**	8/29 - 9/29	39.7	21.9	30.0	0.2	1.5	0.7	44.5	36.3	28.7

Table C-5. Results from CCWG and CMP sampling efforts for station SR1, Tembladero.

Tembladero - SR1												
				Nitrate (mg/L)			Ammonia (mg/L)			Flow (L/s)		
Season	Year	Sample	Date	OSMO	Grab	Pres. Inc	OSMO	Grab	Pres. Inc	Avg Flow Meter	Transect	Pres. Inc
Spring	2022	1	5/13 - 5/17	14.6	23.7	NA	0.8	0.5	NA	NA	NA	NA
Spring	2022	2	5/18 - 5/22	15.3	33.3	NA	0.7	0.5	NA	NA	17.0	NA
Spring	2022	3	5/23 - 5/27	16.2	24.8	21.5	0.9	0.4	0.1	NA	NA	-226.5
Spring	2022	4	5/28 - 6/1	21.9	NA	NA	0.8	NA	NA	NA	NA	NA
Spring	2022	5	6/2 - 6/6	19.4	19.4	NA	0.7	0.6	NA	NA	-7.1	NA
Spring	2022	6	6/7 - 6/10	17.6	11.9	NA	0.4	0.3	NA	NA	NA	NA
Spring	2022	**Average**	5/13 - 6/10	17.5	22.6	21.5	0.7	0.5	0.1	NA	5.0	-226.5
Fall	2022	1	11/7 - 11/12	13.8	NA	NA	1.2	NA	NA	284.1	NA	NA
Fall	2022	2	11/13 - 11/18	22.3	13.9	NA	0.8	0.5	NA	103.6	-11.2	NA
Fall	2022	3	11/19 - 11/24	27.0	22.2	NA	0.4	1.5	NA	94.9	NA	NA
Fall	2022	4	11/25 - 11/30	23.5	22.1	21.7	0.2	0.2	0.1	125.0	-17.5	2.3
Fall	2022	5	12/1 - 12/7	15.5	14.9	NA	0.7	0.4	NA	450.6	-21.7	NA
Fall	2022	**Average**	11/7 - 12/7	20.4	18.3	21.7	0.6	0.7	0.1	211.6	-16.8	2.3
Spring	2023	1	7/5 - 7/9	19.3	21.8	NA	0.1	0.3	NA	NA	5.7	NA
Spring	2023	2	7/10 - 7/15	24.3	19.6	NA	0.2	0.3	NA	NA	2.6	NA
Spring	2023	3	7/16 - 7/21	19.1	21.7	NA	0.4	0.0	NA	NA	1.3	NA
Spring	2023	4	7/22 - 7/27	24.4	24.3	24.8	0.2	0.0	0.1	NA	13.8	-169.9
Spring	2023	5	7/28 - 8/2	15.5	1.2	NA	0.9	0.0	NA	NA	9.3	NA
Spring	2023	6	8/3 - 8/8	20.5	13.9	NA	0.2	0.2	NA	NA	0.5	NA
Spring	2023	**Average**	7/5 - 8/8	20.5	17.1	24.8	0.3	0.2	0.1	NA	5.5	-169.9
Fall	2023	1	11/1 - 11/5	18.5	14.5	NA	0.1	0.1	NA	NA	8.0	NA
Fall	2023	2	11/6 - 11/10	13.5	12.5	NA	0.1	0.3	NA	NA	-2.1	NA
Fall	2023	3	11/11 - 11/15	16.5	15.4	NA	0.2	0.4	NA	NA	-2.1	NA
Fall	2023	4	11/16 - 11/20	19.3	NA	NA	0.2	NA	NA	NA	NA	NA
Fall	2023	5	11/21 - 11/25	14.1	9.4	NA	0.1	0.6	NA	NA	3.1	NA
Fall	2023	6	11/26 - 11/29	16.5	0.8	16.4	0.0	0.1	0.1	NA	2.7	34.0
Fall	2023	**Average**	11/1 - 11/29	16.4	10.5	16.4	0.1	0.3	0.1	NA	1.9	34.0

Table C-6. Results from CCWG and CMP sampling efforts for station SR2, Espinosa.

Espinosa - SR2												
				Nitrate (mg/L)			Ammonia (mg/L)			Flow (L/s)		
Season	Year	Sample	Date	OSMO	Grab	Pres. Inc	OSMO	Grab	Pres. Inc	Avg Flow Meter	Transect	Pres. Inc
Spring	2022	1	5/13 - 5/17	26.5	43.0	NA	0.7	0.3	NA	0.0	NA	NA
Spring	2022	2	5/18 - 5/22	27.1	47.2	NA	0.5	0.5	NA	0.1	0.7	NA
Spring	2022	3	5/23 - 5/27	19.0	17.9	18.8	2.0	3.7	3.7	0.2	NA	55.2
Spring	2022	4	5/28 - 6/1	11.7	NA	NA	2.8	NA	NA	1.8	NA	NA
Spring	2022	5	6/2 - 6/6	28.1	33.3	NA	0.8	0.5	NA	0.0	9.4	NA
Spring	2022	6	6/7 - 6/10	29.9	18.6	NA	0.1	0.5	NA	0.1	NA	NA
Spring	2022	**Average**	5/13 - 6/10	23.7	32.0	18.8	1.2	1.1	3.7	0.4	5.1	55.2
Fall	2022	1	11/7 - 11/11	30.6	NA	NA	1.0	NA	NA	NA	NA	NA
Fall	2022	2	11/12 - 11/16	36.0	7.4	NA	0.7	1.1	NA	NA	-4.1	NA
Fall	2022	3	11/17 - 11/21	23.4	28.7	NA	0.5	0.1	NA	NA	NA	NA
Fall	2022	4	11/22 - 11/26	25.7	NA	NA	1.2	NA	NA	NA	NA	NA
Fall	2022	5	11/27 - 12/2	13.0	0.5	39.6	1.1	0.1	0.2	NA	-82.7	10.2
Fall	2022	6	12/3 - 12/8	10.6	NA	NA	2.7	NA	NA	NA	NA	NA
Fall	2022	7	12/9 - 12/14	9.7	NA	NA	1.2	NA	NA	NA	NA	NA
Fall	2022	8	12/15 - 12/20	10.6	8.9	NA	0.7	0.9	NA	NA	241.7	NA
Fall	2022	**Average**	11/7 - 12/20	19.9	11.4	39.6	1.1	0.5	0.2	NA	51.6	10.2
Spring	2023	1	7/5 - 7/9	16.3	23.6	NA	0.6	0.3	NA	NA	26.8	NA
Spring	2023	2	7/10 - 7/15	2.3	19.3	NA	1.9	0.2	NA	NA	0.6	NA
Spring	2023	3	7/16 - 7/21	NA	1.2	NA	NA	0.0	NA	NA	64.9	NA
Spring	2023	4	7/22 - 7/27	NA	1.4	16.5	NA	0.0	0.0	NA	-3.0	45.3
Spring	2023	5	7/28 - 8/2	NA	14.9	NA	NA	0.1	NA	NA	1.7	NA
Spring	2023	6	8/3 - 8/8	NA	13.5	NA	NA	0.4	NA	NA	-1.3	NA
Spring	2023	**Average**	7/5 - 8/8	9.3	12.3	16.5	1.2	0.2	0.0	NA	14.9	45.3
Fall	2023	1	11/1 - 11/4	31.3	15.7	NA	0.0	0.2	NA	NA	-1.3	NA
Fall	2023	2	11/5 - 11/8	20.1	0.8	NA	0.1	0.3	NA	NA	-1.2	NA
Fall	2023	3	11/9 - 11/12	3.3	NA	NA	0.6	NA	NA	NA	NA	NA
Fall	2023	4	11/13 - 11/16	15.7	0.4	NA	0.4	0.1	NA	NA	-3.0	NA
Fall	2023	5	11/17 - 11/20	1.2	NA	NA	0.8	NA	NA	NA	NA	NA
Fall	2023	6	11/21 - 11/24	0.0	0.7	NA	0.1	0.1	NA	NA	15.5	NA
Fall	2023	7	11/25 - 11/29	0.4	26.9	19.6	0.4	0.4	0.1	NA	1.7	-59.5
Fall	2023	**Average**	11/1 - 11/29	10.3	8.9	19.6	0.3	0.2	0.1	NA	2.4	-59.5

Table C-7. Results from CCWG and CMP sampling efforts for station SR3, Carr Lake.

Carr Lake - SR3												
				Nitrate (mg/L)			Ammonia (mg/L)			Flow (L/s)		
Season	Year	Sample	Date	OSMO	Grab	Pres. Inc	OSMO	Grab	Pres. Inc	Avg Flow Meter	Transect	Pres. Inc
Spring	2022	1	5/13 - 5/18	10.1	57.9	NA	0.0	0.2	NA	NA	NA	NA
Spring	2022	2	5/19 - 5/24	26.0	36.7	NA	0.5	0.7	NA	NA	-4.0	NA
Spring	2022	3	5/25 - 5/30	48.7	36.4	86.3	0.5	0.7	0.9	NA	NA	10.7
Spring	2022	4	5/31 - 6/5	52.1	20.4	NA	0.3	0.2	NA	NA	1.5	NA
Spring	2022	5	6/6 - 6/10	64.2	31.0	NA	0.1	0.4	NA	NA	NA	NA
Spring	2022	**Average**	5/13 - 6/10	40.2	36.5	86.3	0.3	0.4	0.9	NA	-1.3	10.7
Fall	2022	1	11/7 - 11/12	39.9	NA	NA	0.5	NA	NA	NA	NA	NA
Fall	2022	2	11/13 - 11/18	43.2	7.6	NA	0.7	0.5	NA	NA	-22.8	NA
Fall	2022	3	11/19 - 11/24	44.7	18.6	NA	0.3	0.2	NA	NA	NA	NA
Fall	2022	4	11/25 - 11/30	15.8	21.3	30.3	0.4	0.3	0.3	NA	4.5	59.2
Fall	2022	5	12/1 - 12/6	4.8	NA	NA	0.5	NA	NA	NA	NA	NA
Fall	2022	6	12/7 - 12/13	4.5	NA	NA	0.3	NA	NA	NA	NA	NA
Fall	2022	7	12/14 - 12/20	4.7	6.8	NA	0.9	0.7	NA	NA	70.4	NA
Fall	2022	**Average**	11/7 - 12/20	22.5	13.6	30.3	0.5	0.4	0.3	NA	17.4	59.2
Spring	2023	1	7/5 - 7/9	21.7	17.6	NA	1.9	0.5	NA	94.3	24.9	NA
Spring	2023	2	7/10 - 7/15	24.2	22.4	NA	2.6	0.4	NA	34.6	37.7	NA
Spring	2023	3	7/16 - 7/21	36.7	24.9	NA	0.3	0.1	NA	31.7	27.4	NA
Spring	2023	4	7/22 - 7/27	24.4	21.1	4.6	2.8	0.0	0.1	152.8	24.2	1812.3
Spring	2023	5	7/28 - 8/2	18.8	13.7	NA	0.1	0.0	NA	150.0	24.8	NA
Spring	2023	6	8/3 - 8/8	16.5	20.7	NA	0.1	0.0	NA	146.4	12.5	NA
Spring	2023	**Average**	7/5 - 8/8	23.7	20.1	4.6	1.3	0.2	0.1	101.7	25.3	1812.3
Fall	2023	1	11/1 - 11/5	13.6	15.4	NA	0.0	0.1	NA	15.9	4.3	NA
Fall	2023	2	11/6 - 11/10	12.5	8.8	NA	0.0	0.2	NA	56.0	-1.6	NA
Fall	2023	3	11/11 - 11/15	20.2	10.4	NA	0.0	0.2	NA	40.3	-1.9	NA
Fall	2023	4	11/16 - 11/20	16.2	NA	NA	0.5	NA	NA	78.7	NA	NA
Fall	2023	5	11/21 - 11/25	6.3	0.7	NA	1.1	0.6	NA	8.4	11.0	NA
Fall	2023	6	11/26 - 11/29	12.2	0.6	NA	0.0	0.0	NA	14.8	-0.9	0.0
Fall	2023	**Average**	11/1 - 11/29	13.5	7.2	NA	0.3	0.2	NA	35.7	2.2	0.0

Table C-8. Results from CCWG and CMP sampling efforts for station SR4, Alisal Creek.

Alisal Creek - SR4												
				Nitrate (mg/L)			Ammonia (mg/L)			Flow (L/s)		
Season	Year	Sample	Date	OSMO	Grab	Pres. Inc	OSMO	Grab	Pres. Inc	Avg Flow Meter	Transect	Pres. Inc
Spring	2022	1	5/13 - 5/17	72.6	50.1	NA	0.4	0.7	NA	6.0	NA	NA
Spring	2022	2	5/18 - 5/21	44.0	96.9	NA	1.2	4.1	NA	24.0	-14.6	NA
Spring	2022	3	5/22 - 5/25	45.3	NA	56.9	1.6	NA	0.682	32.6	NA	8.9
Spring	2022	4	5/26 - 5/29	53.0	43.8	NA	1.8	1.8	NA	29.2	NA	NA
Spring	2022	5	5/30 - 6/2	0.0	NA	NA	0.9	NA	NA	32.3	NA	NA
Spring	2022	6	6/3 - 6/6	54.3	65.5	NA	0.1	1.2	NA	28.3	-8.3	NA
Spring	2022	7	6/7 - 6/10	47.7	41.6	NA	0.2	2.0	NA	27.5	NA	NA
Spring	2022	**Average**	5/13 - 6/10	45.3	59.6	56.9	0.9	2.0	0.7	25.7	-11.4	8.9
Fall	2022	1	11/14/2022	NA	12.5	NA	NA	0.3	NA	NA	4.2	NA
Fall	2022	2	11/21/2022	NA	19.7	NA	NA	0.2	NA	NA	NA	NA
Fall	2022	3	11/28/2022	NA	40.4	30.3	NA	0.4	0.349	NA	-0.2	59.2
Fall	2022	4	12/5/2022	NA	4.5	NA	NA	0.3	NA	NA	82.0	NA
Fall	2022	**Average**	11/14 - 12/5	NA	19.3	30.3	NA	0.3	0.3	NA	28.6	59.2
Spring	2023	1	7/5 - 7/9	27.3	18.9	NA	0.3	0.4	NA	NA	-2.3	NA
Spring	2023	2	7/10 - 7/15	46.6	23.1	NA	0.0	0.4	NA	NA	4.2	NA
Spring	2023	3	7/16 - 7/21	30.7	39.3	NA	0.0	0.1	NA	NA	15.3	NA
Spring	2023	4	7/22 - 7/27	38.2	39.0	4.62	0.1	0.0	0.076	NA	1.7	1812.3
Spring	2023	5	7/28 - 8/2	34.3	2.9	NA	0.1	0.0	NA	NA	7.6	NA
Spring	2023	6	8/3 - 8/8	28.0	24.1	NA	2.0	0.1	NA	NA	-0.2	NA
Spring	2023	**Average**	7/5 - 8/8	34.2	24.5	4.6	0.4	0.2	0.1	NA	4.4	1812.3
Fall	2023	1	11/1 - 11/5	3.0	2.2	NA	0.0	0.1	NA	4.7	2.3	NA
Fall	2023	2	11/6 - 11/10	0.5	-0.2	NA	0.1	0.1	NA	4.6	-7.5	NA
Fall	2023	3	11/11 - 11/15	0.2	-0.3	NA	0.0	0.1	NA	3.6	-4.0	NA
Fall	2023	4	11/16 - 11/20	0.6	NA	NA	0.2	NA	NA	3.8	NA	NA
Fall	2023	5	11/21 - 11/25	8.2	0.6	NA	0.1	0.4	NA	4.5	-3.6	NA
Fall	2023	6	11/26 - 11/29	15.9	0.9	NA	0.1	0.0	NA	8.9	-8.5	0.0
Fall	2023	**Average**	11/1 - 11/29	4.7	0.6	NA	0.1	0.1	NA	5.0	-4.3	0.0

Table C-9. Results from CCWG and CMP sampling efforts for station SR5, Alisal Slough.

Alisal Slough - SR5												
				Nitrate (mg/L)			Ammonia (mg/L)			Flow (L/s)		
Season	Year	Sample	Date	OSMO	Grab	Pres. Inc	OSMO	Grab	Pres. Inc	Avg Flow Meter	Transect	Pres. Inc
Spring	2022	1	5/13 - 5/17	0.4	92.6	NA	0.0	4.6	NA	NA	NA	NA
Spring	2022	2	5/18 - 5/22	2.4	57.7	NA	0.0	0.2	NA	NA	73.0	NA
Spring	2022	3	5/23 - 5/27	0.9	1.1	43.3	0.1	0.3	0.3	NA	NA	39.6
Spring	2022	4	5/28 - 6/1	14.6	NA	NA	0.3	NA	NA	NA	NA	NA
Spring	2022	5	6/2 - 6/6	12.9	40.5	NA	0.0	0.5	NA	NA	-2.3	NA
Spring	2022	6	6/7 - 6/10	0.0	12.6	NA	0.0	0.5	NA	NA	NA	NA
Spring	2022	**Average**	5/13 - 6/10	5.2	40.9	43.3	0.1	1.2	0.3	NA	35.3	39.6
Fall	2022	1	11/7 - 11/11	22.9	NA	NA	0.5	NA	NA	NA	NA	NA
Fall	2022	2	11/12 -11/16	38.5	17.2	NA	0.2	0.1	NA	NA	16.9	NA
Fall	2022	3	11/17 - 11/21	32.2	20.3	NA	0.1	0.1	NA	NA	NA	NA
Fall	2022	4	11/22 - 11/26	9.7	NA	NA	0.1	NA	NA	NA	NA	NA
Fall	2022	5	11/27 - 12/1	0.2	31.5	53.3	0.2	0.1	0.1	NA	9.4	6.8
Fall	2022	6	12/2 - 12/7	6.3	24.8	NA	0.4	0.5	NA	NA	88.8	NA
Fall	2022	**Average**	11/7 - 12/7	18.3	23.5	53.3	0.3	0.2	0.1	NA	38.4	6.8
Spring	2023	1	7/5 - 7/9	45.9	21.6	NA	0.0	0.6	NA	NA	23.4	NA
Spring	2023	2	7/10 - 7/14	43.6	29.2	NA	0.1	0.5	NA	NA	56.2	NA
Spring	2023	3	7/15 - 7/19	36.2	NA	NA	0.0	NA	NA	NA	NA	NA
Spring	2023	4	7/20 - 7/24	37.6	29.4	NA	0.0	0.1	NA	NA	NA	NA
Spring	2023	5	7/25 - 7/29	21.4	48.5	53.9	0.1	0.0	0.1	NA	59.9	36.1
Spring	2023	6	7/30 - 8/3	20.3	30.6	NA	0.2	0.0	NA	NA	23.0	NA
Spring	2023	7	8/4 - 8/8	54.5	36.9	NA	0.1	0.0	NA	NA	42.8	NA
Spring	2023	**Average**	7/5 - 8/8	37.1	32.7	53.9	0.1	0.2	0.1	NA	41.1	36.1
Fall	2023	1	11/1 - 11/4	0.0	28.5	NA	0.0	0.8	NA	NA	16.2	NA
Fall	2023	2	11/5 - 11/8	22.2	19.5	NA	0.4	0.5	NA	NA	14.6	NA
Fall	2023	3	11/9 - 11/12	47.9	NA	NA	0.9	NA	NA	NA	NA	NA
Fall	2023	4	11/13 - 11/16	36.1	31.1	NA	0.5	0.2	NA	NA	33.4	NA
Fall	2023	5	11/17 - 11/20	42.0	NA	NA	0.3	NA	NA	NA	NA	NA
Fall	2023	6	11/21 - 11/24	30.3	27.2	NA	0.1	0.4	NA	NA	41.0	NA
Fall	2023	7	11/25 - 11/29	40.3	1.0	28.8	0.1	0.1	0.1	NA	12.6	6.2
Fall	2023	**Average**	11/1 - 11/29	31.2	21.4	28.8	0.3	0.4	0.1	NA	23.6	6.2

Table C-10. Results from CCWG and CMP sampling efforts for station SR6, OSR/Tembladero.

OSR/Tembladero - SR6												
				Nitrate (mg/L)			Ammonia (mg/L)			Flow (L/s)		
Season	Year	Sample	Date	OSMO	Grab	Pres. Inc	OSMO	Grab	Pres. Inc	Avg Flow Meter	Transect	Pres. Inc
Spring	2023	1	7/5 - 7/9	38.8	36.6	NA	0.5	0.3	NA	235.3	147.0	NA
Spring	2023	2	7/10 - 7/15	28.5	3.3	NA	0.5	0.2	NA	180.9	13.0	NA
Spring	2023	3	7/16 - 7/21	15.5	37.0	NA	0.6	0.0	NA	38.9	NA	NA
Spring	2023	4	7/22 - 7/27	39.0	36.9	37.4	0.1	0.0	0.1	316.2	NA	-85.6
Spring	2023	5	7/28 - 8/2	36.0	35.2	NA	0.0	0.0	NA	287.2	NA	NA
Spring	2023	6	8/3 - 8/8	26.7	23.7	NA	0.1	0.0	NA	207.7	NA	NA
Spring	2023	**Average**	7/5 - 8/8	30.7	28.8	37.4	0.3	0.1	0.1	211.0	80.0	-85.6
Fall	2023	1	11/1 - 11/4	8.1	1.0	NA	0.0	0.3	NA	-2.3	NA	NA
Fall	2023	2	11/5 - 11/8	8.2	4.5	NA	0.0	0.2	NA	0.0	NA	NA
Fall	2023	3	11/9 - 11/12	9.8	NA	NA	0.0	NA	NA	0.0	NA	NA
Fall	2023	4	11/13 - 11/16	11.5	6.0	NA	0.1	0.1	NA	293.4	NA	NA
Fall	2023	5	11/17 - 11/20	14.3	NA	NA	0.1	NA	NA	NA	NA	NA
Fall	2023	6	11/21 - 11/24	10.0	6.5	NA	0.1	0.6	NA	NA	NA	NA
Fall	2023	7	11/25 - 11/29	8.8	0.6	3.4	0.2	0.2	0.1	NA	NA	122.0
Fall	2023	**Average**	11/1 - 11/29	10.1	3.7	3.4	0.1	0.3	0.1	72.8	NA	122.0

APPENDIX D: MONITORING STATIONS

Monitoring Station Equipment List

Moro Cojo Station Equipment List - (36°47'46"N 121°47'00"W)

- Seabird Scientific SUNA V2
    - *Function:* Nitrate measurement using UV absorption spectrum
    - *Range:* 2 µM - 3000 µM
- Sontek Argonaut-SW Acoustic Doppler Profiler (ADP)
- YSI EXO1
    - *Parameters:* pH, optical dissolved oxygen, conductivity, temperature
- Raspberry Pi 3 (Data Logger) Time and Date
- Netgear Nighthawk M1 (Cell Modem)
- 12V 100 Ah Battery with 100W Solar Panel

OSR Equipment List

- **Seabird Scientific SUNA V2**
    - Nitrate: UV absorption spectrum
    - Range: 2 µM - 3000 µM
- **Sontek Argonaut-SW Acoustic Doppler Profiler (ADP)**
    - Flow volume (m^2)
- **YSI 600 OMS V2**
    - Parameters: Optical dissolved oxygen, conductivity, temperature

Tembladero Equipment List

- **Seabird Scientific SUNA V2**
    - Nitrate: UV absorption spectrum
    - Range: 2 µM - 3000 µM
- **Sontek IQ ADP**
    - Flow volume (m^2)
- **YSI 600 OMS V2**
    - Parameters: Optical dissolved oxygen, conductivity, temperature

Tembladero Results

Table D-1: Summary of nitrate load, flow data, model performance (RMSE and R^2), and relative importance of model inputs for the Tembladero station from 2021 to 2023. All values are reported annually. Nitrate data includes both measured and modeled data points.

Metric	2021	2022	2023
Total Nitrate (t)	358.9	395.8	672.5
Total Nitrate (t)	1589.7	1753.2	2979.1
Total Flow (10^3 m^3)	12,480,067	16,551,178	35,899,056
Total Flow (acre-ft)	10,117.8	13,418.3	29,103.9
Nitrate samples - Measured	3031 (11.5%)	13718 (52.2%)	12972 (49.3%)
Nitrate samples - Modeled	23249 (88.5%)	12586 (47.8%)	13332 (50.7%)
Flow samples - Measured	2997 (11.5%)	19337 (75.8%)	17868 (68.1%)
Flow samples - Modeled	23087 (88.5%)	6179 (24.2%)	8355 (31.9%)
Flow Model RMSE	0.0978	0.1477	0.2640
Flow Model R^2	0.9893	0.9903	0.9590
Relative Importance of Flow Model Inputs:	**2021**	**2022**	**2023**
USGS Lag	0.208	0.748	0.325
Tide height (m)	0.126	0.078	0.160
Tide Lag	0.041	0.057	0.111
USGS Height (m)	0.083	0.053	0.246
Rain_24h	0.518	0.050	0.125
Rain_3h	0.021	0.012	0.031
Rain (inches)	0.002	0.002	N/A

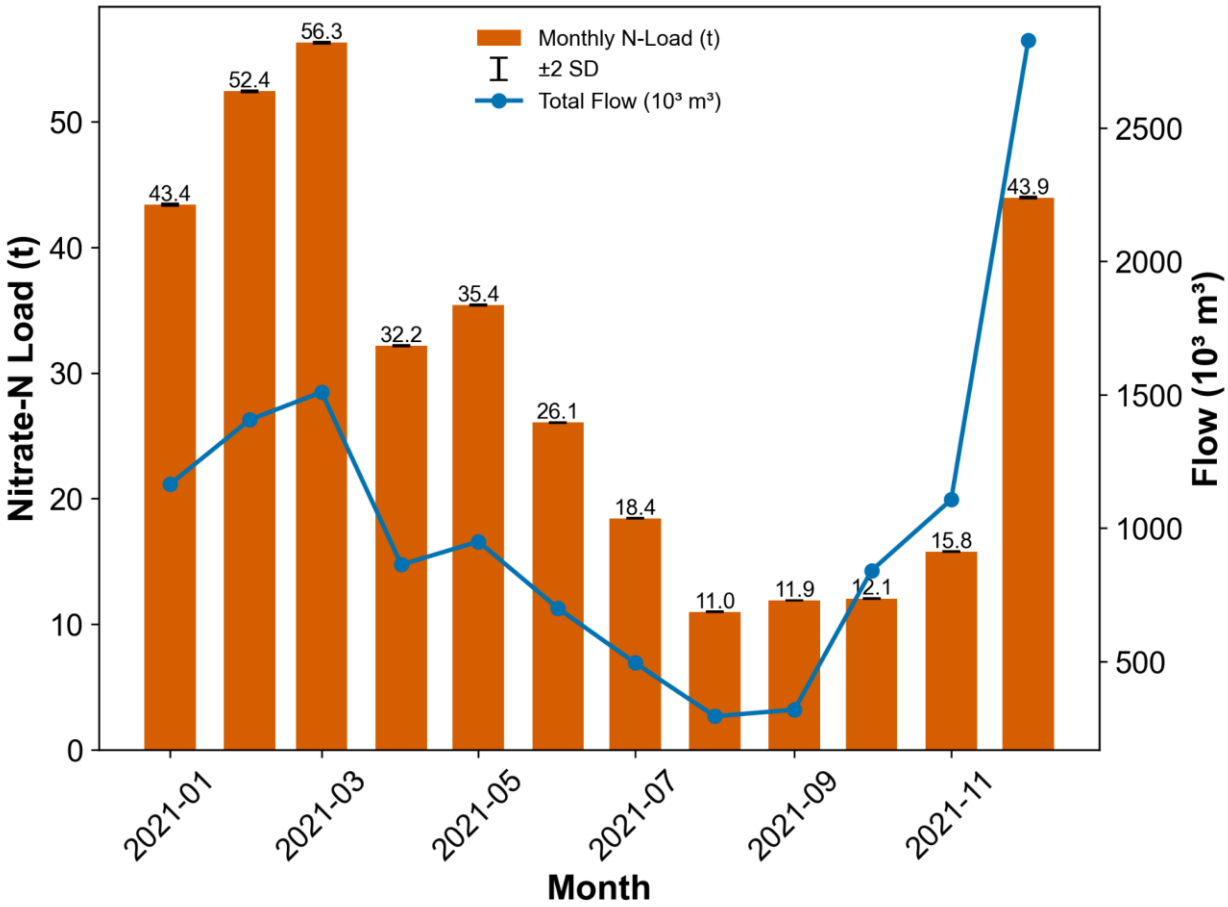

Figure D-1. Nitrate (t) load and flow (10^3 m^3) for each month in 2021 at the Tembladaro station. Values are total with error bars ∓ 2SD.

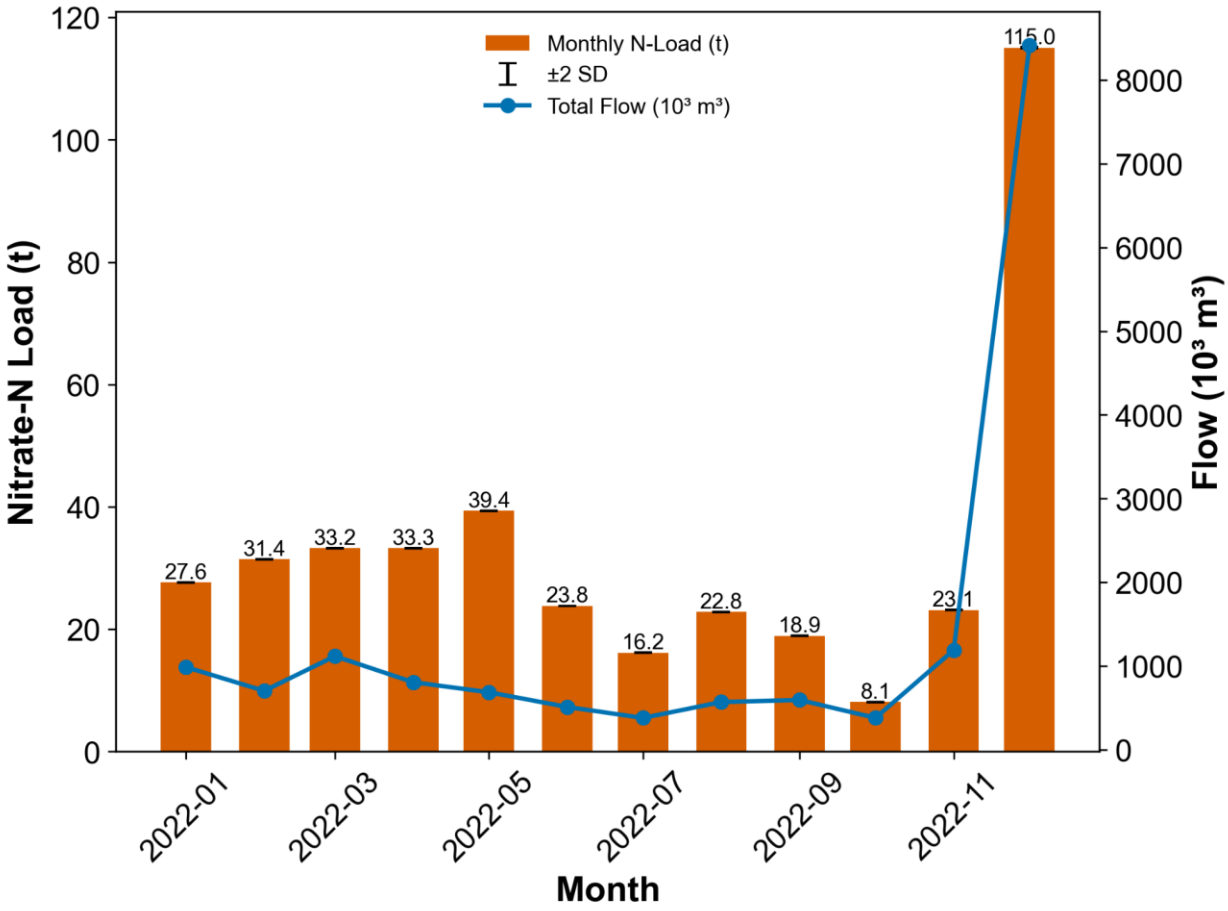

Figure D-2. Nitrate (t) load and flow (10^3 m^3) for each month in 2022 at the Tembladaro station. Values are total with error bars ∓ 2SD.

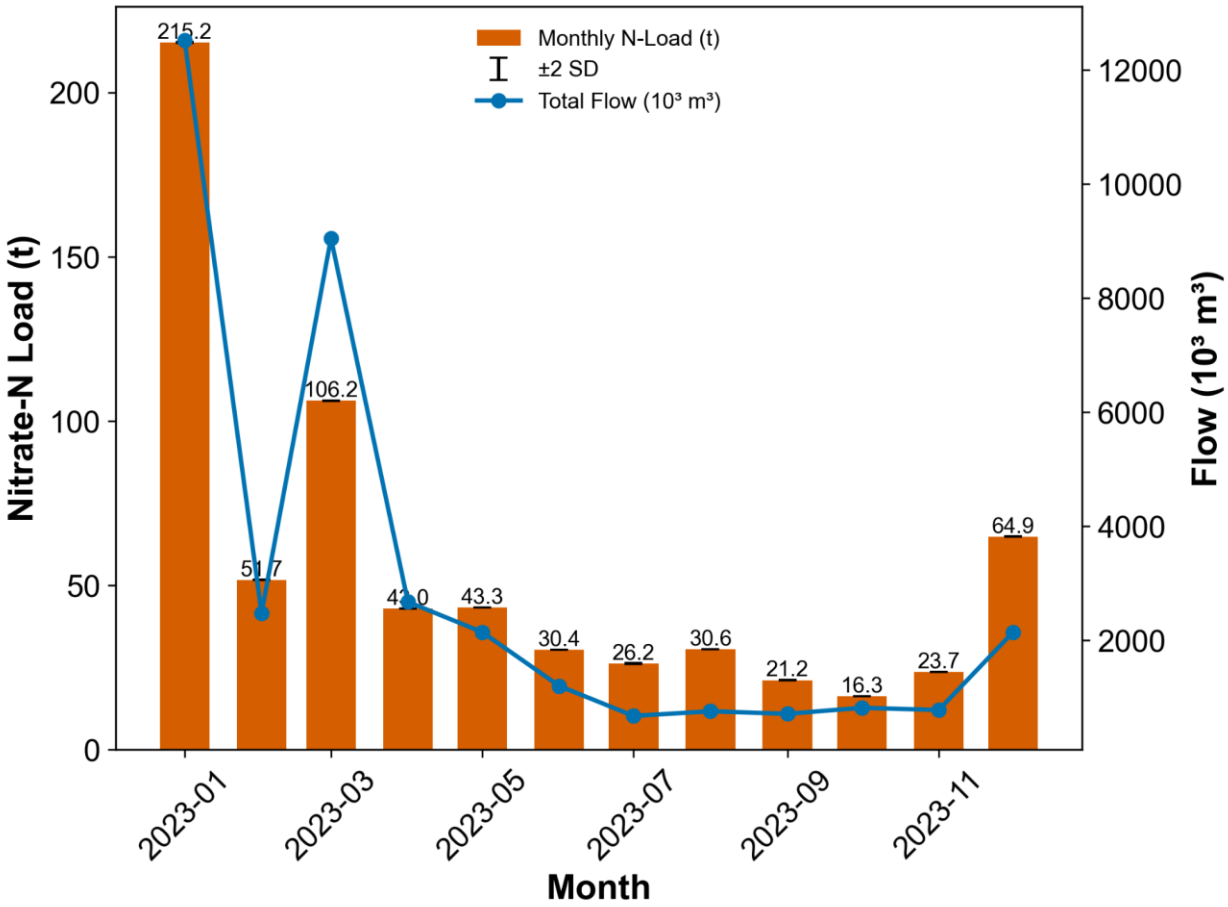

Figure D-3. Nitrate (t) load and flow (10^3 m^3) for each month in 2023 at the Tembladaro station. Values are total with error bars ∓ 2SD.

OSR Results

Table D-2: Summary of nitrate load, flow data, model performance (RMSE and R^2), and relative importance of model inputs for the Old Salinas River (OSR) station in 2022 and 2023. All values are reported annually. Nitrate data includes both measured and modeled data points.

Metric	2022	2023
Total Nitrate (t)	92.3	138.8
Total Nitrate (t)	408.7	614.9
Total Annual Flow (10^3 m^3)	3,196	6,879
Total Annual Flow (acre-ft)	2.6	5.6
Nitrate Samples - Measured	13245 (50.4%)	13829 (52.6%)
Nitrate Samples - Modeled	13059 (49.6%)	12475 (47.4%)
Flow Samples - Measured	12626 (53.1%)	15439 (60.2%)
Flow Samples - Modeled	11159 (46.9%)	10214 (39.8%)
Flow Model RMSE	0.0612	0.0932
Flow Model R^2	0.9663	0.9383
Relative Importance of Flow Model Inputs:	**2022**	**2023**
- **USGS Lag**	0.325	0.203
- **Rain_24h**	0.203	0.108
- **USGS Height (m)**	0.183	0.248
- **Tide height (m)**	0.138	0.223
- **Tide Lag1**	0.115	0.201
- **Rain_3h**	0.029	0.016
- **Rain2**	0.005	0.001

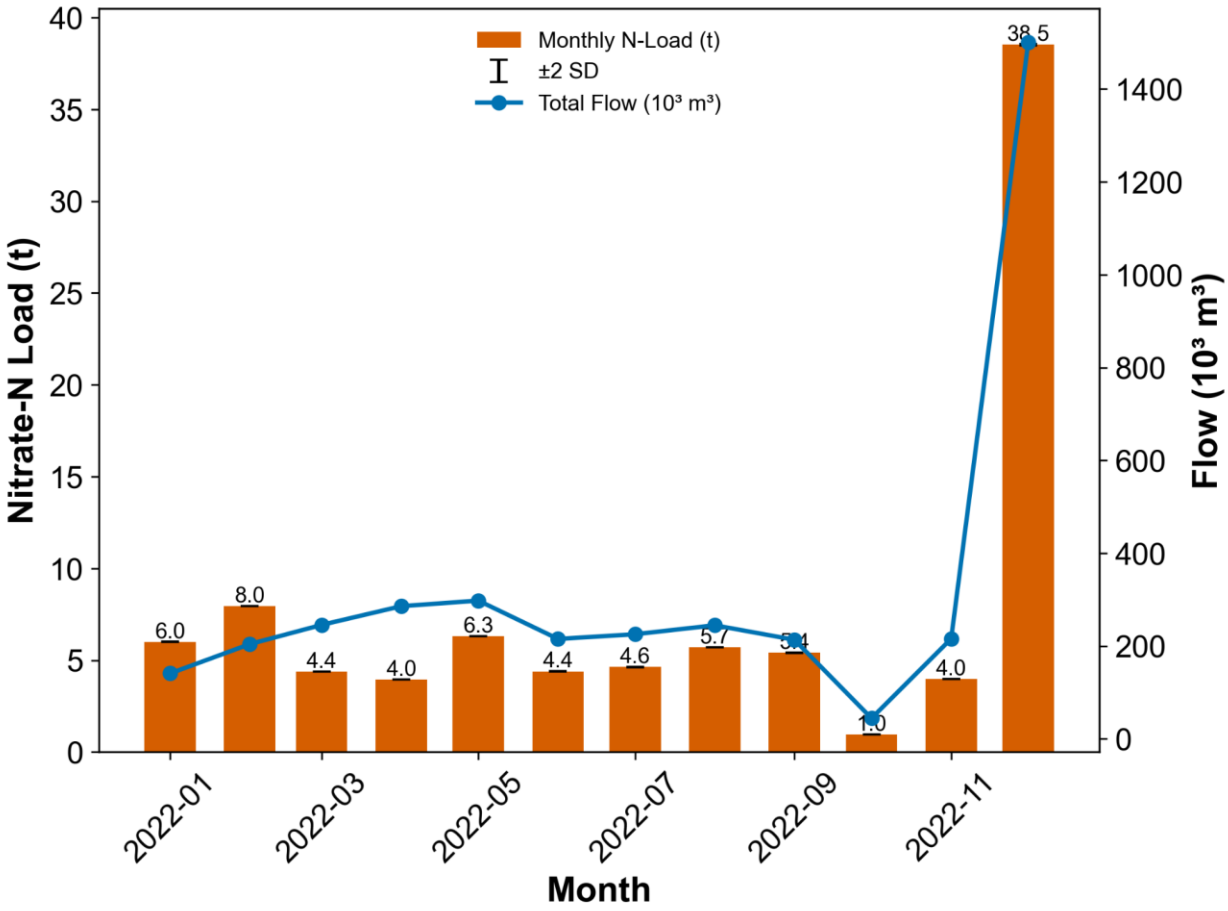

Figure D-4. Nitrate (t) load and flow (10^3 m^3) for each month in 2022 at the OSR station. Values are total with error bars ∓ 2SD.

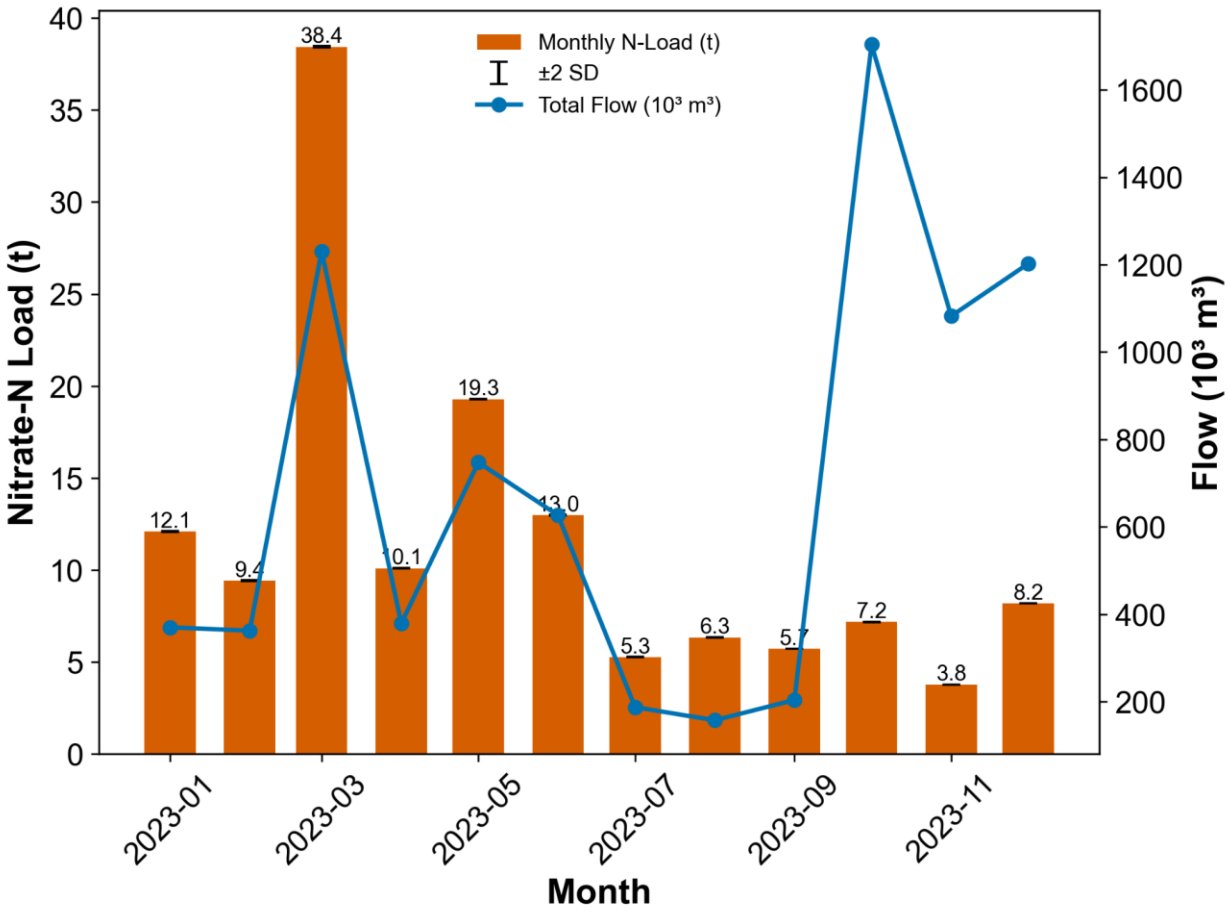

Figure D-5. Nitrate (t) load and flow (10^3 m^3) for each month in 2023 at the OSR station. Values are total with error bars ∓ 2SD.

Moro Cojo

Table D-3: Summary of nitrate load, flow data, model performance (RMSE and R^2), and relative importance of model inputs for the Moro Cojo station in 2022 and 2023. All values are reported annually. Nitrate data includes both measured and modeled data points.

Metric	2022	2023
Total Nitrate (t)	0.71	9.27
Total Nitrate (t)	3.16	41.08
Total Annual Flow (10^3 m^3)	659	4,008
Total Annual Flow (acre-feet)	0.53	3.25
Nitrate Samples - Measured	3,507 (13.3%)	8,898 (33.9%)
Nitrate Samples - Modeled	22,773 (86.7%)	17,382 (66.1%)
Flow Samples - Measured	19,906 (78.1%)	17,555 (66.8%)
Flow Samples - Modeled	5,593 (21.9%)	8,712 (33.2%)
Flow Model RMSE (m^3/s)	0.0407	0.1359
Flow Model R^2	0.9782	0.9749
Relative Importance of Flow Model Inputs:	**2022**	**2023**
Tide	0.441	0.692
Tide Lag1	0.220	0.077
USGS Lag1	0.170	0.110
USGS Height (m)	0.102	0.110
Rain_24h	0.044	0.008
Rain_3h	0.020	0.002
Rain2	0.002	0.001

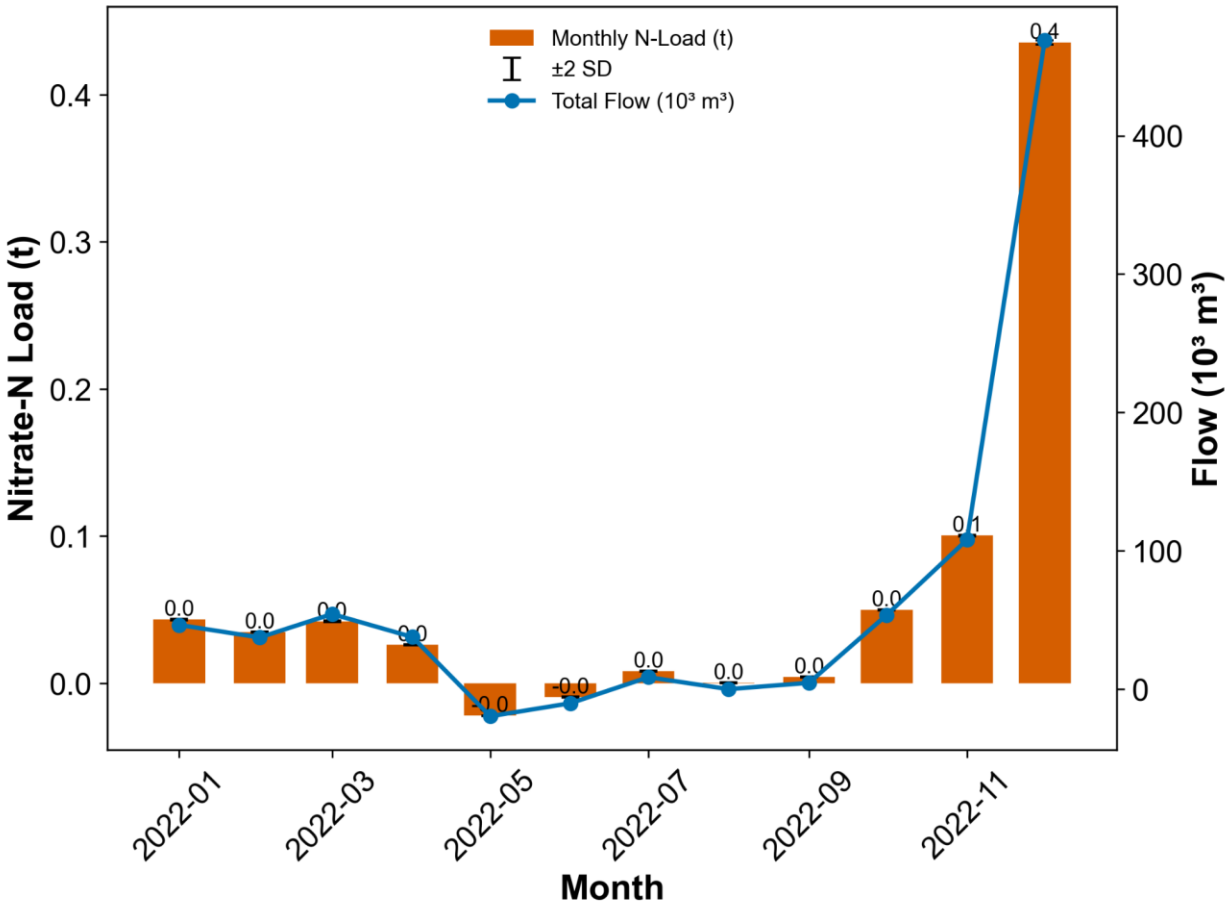

Figure D-6. Nitrate (t) load and flow (10^3 m^3) for each month in 2021 at the Moro Cojo station. Values are total with error bars ∓ 2SD.

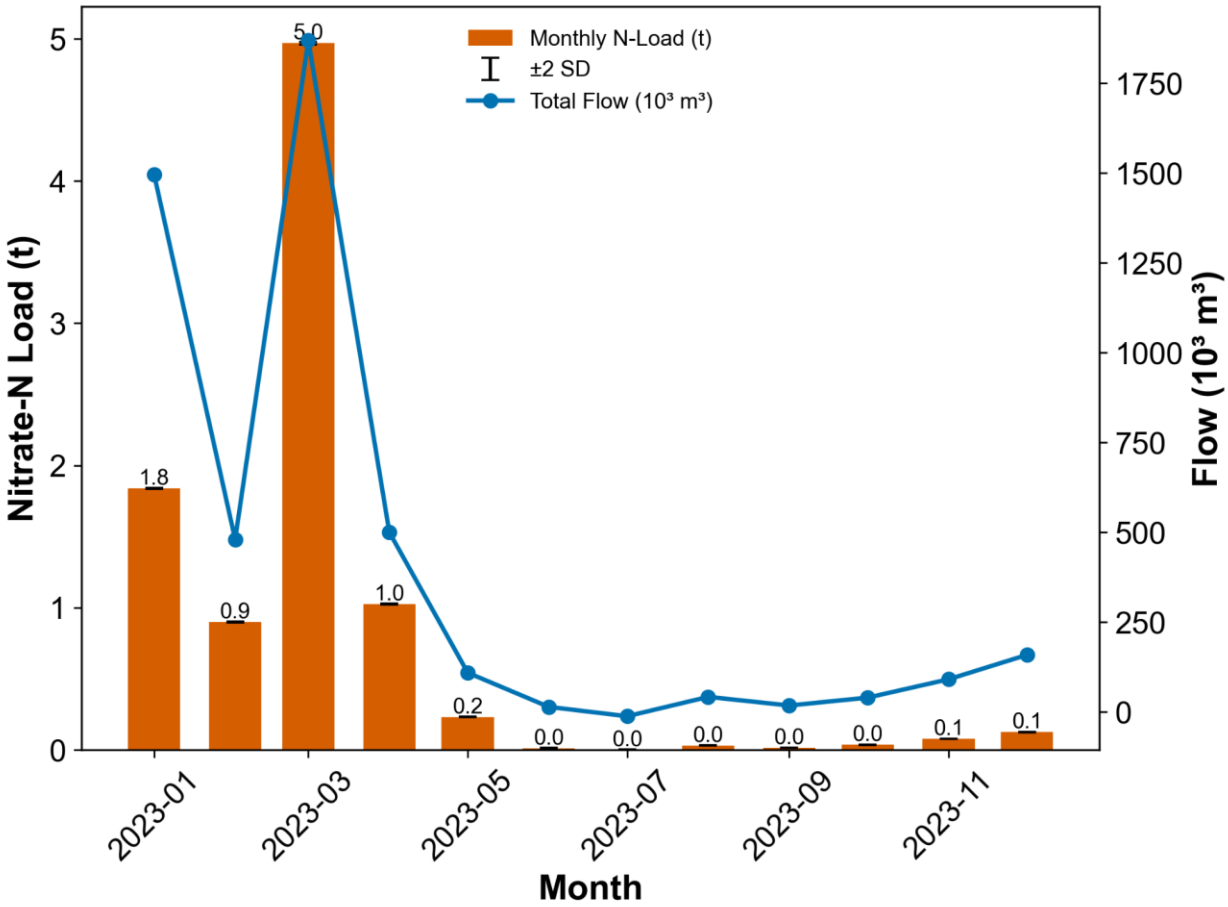

Figure D-7. Nitrate (t) load and flow (10^3 m^3) for each month in 2023 at the Moro Cojo station. Values are total with error bars ∓ 2SD.